Dynamics and Control of Quantum Statistics in Nano-Photonic Devices

---

vorgelegt von
Dipl.-Phys. Sven Moritz Hein
geb. in Stuttgart

von der Fakultät II – Mathematik und Naturwissenschaften
der Technischen Universität Berlin
zur Erlangung des akademischen Grades
Doktor der Naturwissenschaften – Dr. rer. nat. –

genehmigte Dissertation

Promotionsausschuss:

Vorsitzender: Prof. Dr. Mario Dähne
Gutachter: Prof. Dr. Andreas Knorr
Gutachter: Prof. Dr. Harald Giessen

Tag der wissenschaftlichen Aussprache: 25.01.2016

Berlin 2016

To my parents,
Rose and Hauke

Abstract

This thesis discusses the dynamics of quantum-optical systems located in complex, non-markovian photonic environments, using numerical simulations as well as analytical derivations. The main focus lies on time-delayed quantum-coherent feedback effects of the Pyragas type, in analogy to effects well-known in classical physics. Time-delayed feedback is treated as a specific kind of a non-markovian environment. Additionally, the control of qubit entanglement in optical cavities is studied.

The thesis consists of three main parts: After an overview of the important concepts of quantum optics, advanced methods for the description and numerical treatment of time-delayed quantum-coherent feedback are presented. The main focus lies on the development of a pseudomode-based approach, which describes time-delayed feedback as the coupling to a complex network of lossy harmonic oscillators. Additionally, further methods for numerical simplification are presented, in particular nonlinear expectation value dynamics for the treatment of arbitrary non-markovian reservoirs, as well as the use of input-output theory for time-delayed feedback. In the second part, applications of time-delayed feedback to control quantum statistics are discussed. First it is demonstrated that time-delayed feedback can be used to create and sustain entanglement between coupled qubits. This approach will then be extended to larger networks of qubits. Afterwards, feedback control is applied to nonlinear quantum-optical systems: It is shown how to use it for the stabilization of Fock states in a cavity containing a Kerr medium, and this analysis is expanded to a cavity containing a two-level system. Furthermore, it is shown how time-delayed feedback can be used to control and enhance the entanglement of photons emitted in a biexciton cascade. In the third and last part, the non-equilibrium dynamics of qubits coupled to a photonic environment consisting of high-Q cavities subject to periodic driving are discussed. First, the connection between bistability and entanglement in a cavity containing two qubits is analyzed. Next a setup of two coupled cavities, containing a qubit each, is examined. The influence of a third cavity in between the two other cavities, simulating a delay line, is analyzed. Furthermore, a protocol is developed on how to overcome dephasing between the two qubits, using a resonant Raman scattering process. It is shown that this protocol can create and sustain high values of entanglement, and is ready to be extended to systems of more than two qubits.

Zusammenfassung

Diese Arbeit behandelt die Dynamik quantenoptischer Systeme in komplexen, nichtmarkovschen photonischen Umgebungen mit Hilfe numerischer Simulationen und analytischer Rechnungen. Der Schwerpunkt liegt auf Effekten von zeitverzögerter quantenkoheränter Rückkopplung vom Pyragas-Typ, in Analogie zur Pyragas-Kontrolle in klassischen nichtlinearen Systemen. Zeitverzögerte Rückkopplung wird in dieser Arbeit als eine spezielle Art einer nicht-markovschen Umgebung behandelt. Am Ende der Arbeit wird außerdem die Kontrolle von Qubit-Verschränkung in optischen Kavitäten behandelt.

Diese Arbeit ist in drei Teile gegliedert: Nach einer Übersicht über die wichtigsten Konzepte der Quantenoptik werden neue fortgeschrittene Methoden zur Beschreibung und numerischen Simulation von zeitverzögerter Rückkopplung präsentiert. Ein Pseudomoden-basierter Ansatz wird entwickelt, der Rückkopplung als Kopplung zu einem Netzwerk von harmonischen Oszillatoren beschreibt. Zudem wird eine Methode präsentiert, mit der durch nichtlineare Terme die numerische Simulation nicht-markovscher Umgebungen vereinfacht werden kann. Auch die Verwendung der Input-Output-Theorie für zeitverzögerte Rückkopplung wird behandelt. Im zweiten Teil werden Anwendungen von zeitverzögerter Rückkopplung diskutiert. Zuerst wird die Erzeugung von Verschränkung in zwei gekoppelten Qubits analysiert. Diese Methode wird auf Qubit-Netzwerke verallgemeinert. Zeitverzögerte Rückkopplung wird daraufhin auf nichtlineare quantenoptische Systeme angewendet und die Stabilisierung von Fock-Zuständen in einer Kavität mit Kerr-Medium gezeigt. Die Resultate werden auf eine Kavität mit angekoppeltem Zweiniveausystem übertragen. Schließlich wird der Einfluss von zeitverzögerter Rückkopplung auf die Verschränkung von Photonen aus einer Biexzitonkaskade diskutiert. Im dritten Teil der Arbeit werden Qubits, die an eine oder mehrere Kavitäten gekoppelt sind, behandelt. Der Zusammenhang von Verschränkung und Bistabilität im Falle zweier Qubits in einer Kavität wird analysiert. Daraufhin wird ein System aus zwei gekoppelten Kavitäten, die je ein Qubit beinhalten und kohärent gepumpt werden, analysiert. Der Einfluss einer dritten Kavität, die eine verzögerte Kopplung modelliert, wird diskutiert. Schließlich wird ein Protokoll präsentiert, mit dem, basierend auf resonanter Raman-Streuung, die Dephasierung zwischen Qubits verringert werden kann. Es wird gezeigt, dass dieses Protokoll zu hohen Qubit-Verschränkungen führt und auch auf mehr als zwei Qubits erweitert werden kann.

Contents

List of Figures

1 Introduction

> *There is nothing new to be discovered in physics now. All that remains is more and more precise measurement.*
>
> — **William Thomson, 1st Baron Kelvin**
> Irish physicist (1900)

1.1 Taming Schrödinger's Cat

Every once in a while, even the most renowned scientists have gotten the feeling that everything important has been discovered. At the end of the 19th century, the world seemed to be perfectly describable using Isaac Newton's mechanics, James C. Maxwell's electrodynamics, Ludwig Boltzmann's thermodynamics, and all the other works based upon these theories. In 1900, William Thomson, better known as Lord Kelvin, is said to have produced above quote at a meeting of the British Association of the Advancement of Science [1].

He could not have been *more* wrong.

Only shortly afterwards, the works of Max Planck and Albert Einstein lead to maybe the largest paradigm shift in the history of physics: The formulation of *quantum physics*. It was first introduced by Planck in 1900, in what he later called an "act of despair" ("Akt der Verzweiflung") [2], in order to describe the radiation of so-called black bodies over the whole spectral range [3]. Five years later, in 1905, Einstein used the idea that light is quantized to explain the photoelectric effect [4]. In the decades afterwards, quantum mechanics made people re-think the very fundamentals of science: The concept of determinism had to be abandoned, instead it was only possible to calculate *probabilities* of certain outcomes of a measurement. It was also possible to prepare objects in *superpositions* of states, leading to Erwin Schrödinger's famous *gedankenexperiment* of a cat being dead *and* alive at the same time – as long as there is no measurement of the actual state of the cat [5]. The concept of *entanglement* [6] provided the possibility of instantaneous long-range statistical correlations, which cannot be explained by classical correlations [7–11].

Today, this world of quantum physics is not only interesting from a purely scientific point of view, but offers a completely new "toolbox" for applications – from secure communication [12, 13] to new ways of calculation using quantum computers [14, 15], or even a future "quantum internet" [16]. For all of this, it is important not only to understand, but also to *control* quantum-mechanical properties of nano-scale systems. This will be the topic of this thesis. In particular, *quantum-coherent time-delayed feedback control* [17] will be discussed, and the possibility to use this method to control quantum-statistical properties of light on the nano-scale will be studied. Additionally, in the last chapter, methods to create and control quantum-correlated states using cavity-based photonic bath engineering instead of time-delayed feedback, will be presented.

Feedback (or "closed loop" [17]) control has been a successful concept in classical mechanics and nonlinear dynamics for a long time and is still an area of active research [18]. There has been extensive work on feedback control of fundamental dynamical structures such as periodic orbits [19–21] and fixed points [22, 23] and also on applications such as lasers [24–30]. An important aspect in these control schemes is the active use of the *time delay* of the feedback, which renders the system infinite-dimensional [31]. One motivation for the research presented in this thesis is the question how this can be transferred to the quantum regime when the devices to be controlled are getting smaller.

Feedback control in the quantum regime can be divided into two different approaches: *measurement based* and *quantum-coherent* feedback control [17, 32–34]. In measurement based feedback control, a property of the quantum system is measured and afterwards a parameter of the system is changed according to the measurement. The *controller*, which decides on how to modify the parameters of the system after receiving the measurement results, can be fully classical. This provides the opportunity for large and complex controllers. Measurement based feedback control has been proposed and/or was experimentally implemented, e.g., to diminish decoherence [35, 36], control atomic motion [37], establish entanglement [38, 39] or Rabi oscillations [40], or to create Fock states [41]. The latter lead to a Nobel Prize for Serge Haroche in 2012.

A big disadvantage of the measurement based approach is the collapse of the wave function due to the measurement. The usual approach is to use "weak" measurements that disturb quantum coherence only slightly, however also lead to less information on the quantum state, and therefore less efficient control [34]. Thus, it is desirable to get rid of the measurement process and work with a quantum-coherent control mechanism. In that case, the information the controller works with, is *quantum information* [34]. Quantum-coherent feedback is usually implemented by partial outcoupling of the system's quantum state, a subsequent unitary transformation of this out-coupled signal, and finally transferring it back into the system coherently. This approach is especially suited for quantum optics, since photons can be controlled very easily. There exist proposals to use quantum-coherent feedback for the control of different quantum-statistical

properties, such as entanglement [42] or photon statistics [43]. These approaches usually treat the feedback as instantaneous, i.e. much shorter than the time-scale given by the system to be controlled. Vanishing feedback delay times can be advantageous since for short timescales dephasing can be neglected, which would reduce quantum coherence between system and controller. However this neglects the possibility to use the delay time as a control parameter. Only a few studies [44, 45] have been made on the effects of time-delayed quantum-coherent feedback in the quantum regime. In this thesis, it will be demonstrated that time-delayed quantum-coherent feedback is actually a very versatile approach to control quantum systems.

Finally, it will be shown that not only time-delayed feedback can provide the frequency-dependent photonic environment needed for the control of quantum statistics. Based on works of Aron *et al.* [46, 47], a protocol to diminish dephasing in entangled qubits will be developed.

1.2 Structure of this thesis

This thesis is structured as follows: First, an introduction to the important theoretical concepts used in the calculations will be given. In Chapter 2, core formulas of quantum statistics and quantum optics on the nanoscale will be presented, and time-delayed feedback will be introduced.

Chapter 3 covers methods developed to tackle the numerical complexity of time-delayed feedback and other non-Markovian reservoirs. A method to include complex reservoirs as nonlinear expectation value equations will be presented. Furthermore, it will be shown how pseudomodes can be used to model time-delayed feedback very efficiently, and also the use of input-output theory for time-delayed feedback will be discussed.

In Chapter 4, theoretical results on feedback control of coupled qubits are presented: The creation and stabilization of entanglement between nodes of a photonic quantum network will be presented.

Chapter 5 discusses nonlinear quantum-optical systems subject to time-delayed feedback. It will be shown that in a cavity containing a Kerr medium Fock states can be stabilized. In a direct analogy, oscillations within the n-excitation subspace can be stabilized in a Jaynes-Cummings system with feedback.

Photons emitted by a biexciton cascade can be polarization-entangled. In Chapter 6 it will be demonstrated that time-delayed feedback can enhance this entanglement by counteracting the detrimental effects of exciton fine-structure splitting.

In Chapter 7 the dynamics of qubits in coherently driven cavities is discussed. First, it will be analyzed if there is a connection between entanglement of two qubits in one cavity and bistability of the system. Then the system studied in Ref. [46], consisting of two coupled cavities containing a qubit each, will be examined in detail. The effect of long-distance coupling will be discussed. Then, a protocol on how to effectively counteract dephasing between these qubits by using a second drive and a resonant Raman transition will be developed.

This thesis will end with a conclusion and an outlook on interesting questions for further research which came up during the creation of this thesis.

2 Theoretical background

2.1 Quantum statistics

In this chapter, the concepts of quantum mechanics used in this thesis are introduced. After an overview on the different ways of calculating quantum dynamics and the introduction of statistical operators (density matrix theory), the concept of entanglement and measures to quantify it will be discussed. Afterwards, correlation functions $g^{(n)}$, which are important in photon statistics and give the possibility to identify non-classical light, will be introduced. For an extensive coverage of these topics, the reader is referred to standard textbooks on quantum mechanics and quantum optics, e.g. [48, 49], which this section is also strongly based upon.

2.1.1 Pure state dynamics

In quantum mechanics, classical variables become operators. The most important variable, describing the system, is the energy operator, the Hamiltonian $\hat{H}$. A system of which one has full knowledge about its quantum state (a *pure state*) can be described by a wave function $|\psi\rangle$, which is an object in an (extended) Hilbert space. Objects of the corresponding dual space are written as $\langle\phi|$ and the inner product is written as $\langle\phi|\psi\rangle$. The dynamic evolution of $|\psi\rangle$ is governed by the *Schrödinger equation*,

$$i\hbar\frac{\mathrm{d}}{\mathrm{d}t}|\psi\rangle = \hat{H}|\psi\rangle, \tag{2.1}$$

$\hbar$ being Planck's constant $\hbar = 6.626 \times 10^{-34}\,\mathrm{J\,s}$. The measurement of a quantity described by the operator $\hat{A}$ will always give one of the eigenvalues of $\hat{A}$ and "collapse" the state into the respective eigenstate. Since only real-valued measurement results are physically sensible, $\hat{A}$ must have a real-valued eigenvalue spectrum, which is guaranteed if $\hat{A}$ is a Hermitian operator. The Hermitian property also assures that the operator has a complete set of orthogonal eigenvectors.

If $|a\rangle$ is a particular eigenstate of $\hat{A}$, $\hat{A}|a\rangle = a|a\rangle$, the probability $p(a,\psi)$ of measuring a, given that the state of the system is $|\psi\rangle$, can be calculated as $p(a) = |\langle a|\psi\rangle|^2$. The

average value which is expected if one measures $\hat{A}$ is given by the *expectation value* $\langle\hat{A}\rangle$, calculated as

$$\langle\hat{A}\rangle = \sum_i p(a_i,\psi)a_i = \sum_i \langle\psi|a_i\rangle a_i \langle a_i|\psi\rangle = \langle\psi|\hat{A}|\psi\rangle. \tag{2.2}$$

The summation is over all eigenvalues a_i of $\hat{A}$.

The time evolution of expectation values is given by the *Ehrenfest theorem*,

$$\frac{\mathrm{d}}{\mathrm{d}t}\langle\hat{A}\rangle = \frac{-i}{\hbar}\left\langle[\hat{A},\hat{H}]\right\rangle + \left\langle\frac{\partial\hat{A}}{\partial t}\right\rangle, \tag{2.3}$$

which is also valid for explicitly time-dependent operators (hence the last term). The commutator $[\hat{A},\hat{B}]$ is defined as $[\hat{A},\hat{B}] = \hat{A}\hat{B} - \hat{B}\hat{A}$.

Although wave functions are a very useful concept, quantum mechanics offers no way to determine $|\psi\rangle$ unambiguously. It is also possible to apply all temporal dynamics to the operators and keep the wave function fixed, i.e. $|\psi(t)\rangle = |\psi(0)\rangle$. This is called the *Heisenberg picture* (in contrast to the *Schrödinger picture* using time-dependent wave functions). In this picture, the dynamics of operators obeys an equation very similar to the Ehrenfest theorem (Eq. 2.3), called the *Heisenberg equation of motion*:

$$\frac{\mathrm{d}}{\mathrm{d}t}\hat{A} = \frac{-i}{\hbar}[\hat{A},\hat{H}] + \frac{\partial\hat{A}}{\partial t}. \tag{2.4}$$

Both formulations are equivalent, however it is sometimes easier to work in one picture or the other. In this thesis,most of the time solve Eqs. 2.1 and 2.3 will be solved. However, in section 2.3, time-delayed feedback in the Heisenberg picture will be discussed.

2.1.2 The density matrix formalism

Often, the quantum state of the system is not fully known. Thus, it is necessary to have a theory that can incorporate imperfect knowledge and statistical ensembles. This theory is provided by the density matrix formalism.

Take a system which has the probability p_i to be in the quantum state $|\psi_i\rangle$. Then the "density matrix" ρ is given as

$$\rho = \sum_i p_i|\psi_i\rangle\langle\psi_i|. \tag{2.5}$$

The probabilities have to add up to one, $\sum_i p_i = 1$. However, the states $|\psi_i\rangle$ do not need to be orthogonal and do not need to form a basis of the full Hilbert space. The density matrix contains all the information available to an observer, which is why it was proposed recently [50] to view density matrices, and not quantum states, as the basic entities of quantum mechanics. Different ensembles can lead to equal density matrices, however there is no possibility to determine which ensemble is "correct" and therefore it makes

sense to see them as different "representations" of the same system state. As an example, take a "qubit", i.e., a quantum state that is an object of a 2-dimensional Hilbert space spanned by the two states $|0\rangle$ and $|1\rangle$. This qubit may now be prepared in a 1:1 "mixture" of $|0\rangle$ and $|1\rangle$, leading to the density matrix

$$\rho = \frac{1}{2}|0\rangle\langle 0| + \frac{1}{2}|1\rangle\langle 1| = \begin{pmatrix} 0.5 & 0 \\ 0 & 0.5 \end{pmatrix} \tag{2.6}$$

However, one could also prepare the system in a 1:1 mixture of the linear combinations $|+\rangle = \frac{1}{\sqrt{2}}(|0\rangle + |1\rangle)$ and $|-\rangle = \frac{1}{\sqrt{2}}(|0\rangle - |1\rangle)$. The states $|+\rangle$ and $|-\rangle$ are clearly distinct from the states $|0\rangle$ and $|1\rangle$, however, the density matrix of the mixture is still

$$\rho = \frac{1}{2}|+\rangle\langle +| + \frac{1}{2}|-\rangle\langle -| = \begin{pmatrix} 0.5 & 0 \\ 0 & 0.5 \end{pmatrix} \tag{2.7}$$

Therefore there exists no physical way to differentiate between the two mixtures and they have to be considered to represent the same object.

Expectation values in the density matrix formalism can be calculated using the *trace*,

$$\langle \hat{A} \rangle = \mathrm{tr}\left(\rho \hat{A}\right). \tag{2.8}$$

Setting $\hat{A} = \rho$ gives information whether the system is in a pure state or in a mixture of states: Only for pure states,

$$\mathrm{tr}\left(\rho^2\right) = 1. \tag{2.9}$$

The dynamics of a system given as a density matrix is governed by the *von Neumann equation*:

$$\frac{\mathrm{d}}{\mathrm{d}t}\rho = \frac{i}{\hbar}[\rho, \hat{H}]. \tag{2.10}$$

This equation is equal to the Heisenberg equation (Eq. 2.4) except for a different sign. However, ρ is an object in the Schrödinger picture, in which the implicit time dependence is contained in the states that build up ρ, and not in the operators.

The density matrix formalism also allows to analyze subsystems of more complex systems. Take a system that consists of a subsystem, described by ρ_S, and "everything else", described by ρ_B (in this thesis, ρ_B will usually be a "bath" to which the subsystem is connected, therefore the index B). If the density matrix of the full system ρ is known, the density matrix of the subsystem can be calculated using the *partial trace*

$$\rho_S = \mathrm{tr}_B \rho, \tag{2.11}$$

which is defined as

$$\mathrm{tr}_B \rho = \sum_i \langle b_i|\rho|b_i\rangle. \tag{2.12}$$

Here, $|b_i\rangle$ form a complete set of orthonormal states of the Hilbert space of the "bath" B. Any measurement result of properties of only the subsystem can be calculated using the reduced density matrix ρ_S.

2.1.3 Entanglement

For pure states, entanglement is defined as follows: Two systems A, B are called *entangled* if their wavefunction $|\Psi\rangle$ cannot be written as the direct product of the wave functions of the single systems, $|\Psi\rangle \neq |\psi_A\rangle \otimes |\psi_B\rangle$. Otherwise, they are called *separable*. As an example, take two qubits, described by the wave functions $|\psi_A\rangle$ and $|\psi_B\rangle$: The state

$$|\Psi\rangle = |0_A\rangle \otimes \frac{1}{\sqrt{2}}\Big(|0_B\rangle + |1_B\rangle\Big) \tag{2.13}$$

is separable, while the state

$$|\Psi'\rangle = \frac{1}{\sqrt{2}}\Big(|0_A\rangle \otimes |1_B\rangle + |1_A\rangle \otimes |0_B\rangle\Big) \tag{2.14}$$

is entangled. If two states are entangled, a measurement of the first state collapses the wave function of the second state as well, without any noticeable time delay. Historically, this made people think of quantum theory as incomplete [7], and that the correlation between entangled states were described by some "hidden variables". However, it was demonstrated subsequently that entanglement introduces statistical correlations which are not describable by classical ("local-realistic") ensembles, which was shown by the breakdown of the famous *Bell inequalities* [8–11]. In particular, the state $|\Psi'\rangle$ given in Eq. 2.14 is distinct from a 1:1 mixture of $|0_A\rangle \otimes |1_B\rangle$ and $|1_A\rangle \otimes |0_B\rangle$, or any other mixture. This can already be seen by the fact that the square of the density matrix given by $|\Psi'\rangle\langle\Psi'|$ will have a trace of 1, while any incoherent mixture would not (cf. Eq. 2.9)

For ensembles, there exists an equivalent definition of entanglement: An ensemble of bipartite systems described by the density matrix ρ is called separable, if ρ can be written as an ensemble of separable states. All other systems are (at least partly) entangled.

Although this definition of entanglement looks straightforward, there is actually not a "simple" way to define the amount of entanglement in an arbitrary mixed state [51, 52]. After all, entanglement is not a quantity that can be written as the eigenvalue of some (fictional) "entanglement operator $\hat{\mathscr{E}}$". It is rather a property of systems that can be "clearly" (which usually means "macroscopically") divided into two distinct subsystems. Handwavingly, the subsystems are entangled if their quantum state cannot be divided in this way. This idea leads to the definition of entanglement of *pure* states via the entropy of one subsystem while tracing out the other subsystem [53, 54]:

$$E(\rho) = -\mathrm{Tr}\left(\rho_A \log_2 \rho_A\right) = -\mathrm{Tr}\left(\rho_B \log_2 \rho_B\right). \tag{2.15}$$

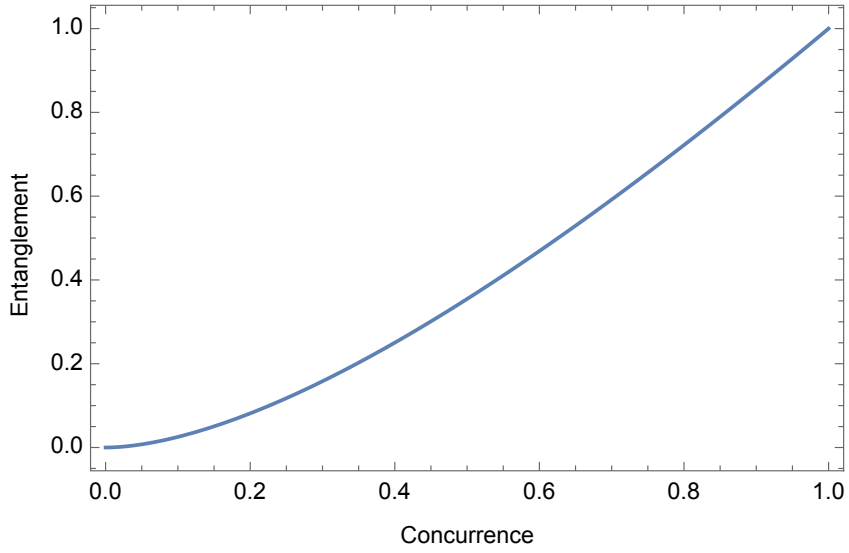

Fig. 2.1.: Entanglement of formation (E) vs concurrence (C). As it is a bijective relationship, that makes it possible to convert concurrence to entanglement and vice versa unambiguously. Since $E(C=0)=0$ and $E(C=1)=1$, concurrence itself can be seen as a valid entanglement measure and is widely used due to its easy computability.

Here, $\rho = |\psi\rangle\langle\psi|$ is the density matrix of a pure state $|\psi\rangle$, and $\rho_{A(B)}$ is the density matrix of subsystem A (B), acquired from ρ by tracing out subsystem $B(A)$. $E(\rho)$ is the entanglement of $|\psi\rangle$. Since a mixed state ρ can be seen as a collection of pure states, $\rho = \sum_i p_i |\psi_i\rangle\langle\psi_i|$, this definition can be generalized: The entanglement of a mixed state is the sum of the entanglements of the pure states that make up the mixed state, weighted by their probability p_i. There exists a complication since this decomposition into pure states is not unique. One therefore uses the decomposition which leads to the *smallest* entanglement:

$$E(\rho) = \min_D \sum_{i\in D} p_i E\left(|\psi_i\rangle\langle\psi_i|\right). \tag{2.16}$$

Here, D symbolizes the different decompositions of ρ into pure states. This entanglement measure is called *entanglement of formation*. While its definition is intuitive, it is hard to compute directly due to the necessary minimalization. However, it is possible to compute it from another entanglement measure, the *concurrence* C [6, 54], which will be defined below. Given the concurrence $C(\rho)$, the entanglement of formation can be calculated as [54]

$$E(\rho) = h\left(\frac{1+\sqrt{1-C(\rho)^2}}{2}\right), \tag{2.17}$$

using the function

$$h(x) = -x\log_2 x - (1-x)\log_2(1-x). \tag{2.18}$$

In Fig. 2.1, the relationship between concurrence and entanglement (of formation) is plotted. The bijective relationship between the two quantities makes it possible to convert concurrence to entanglement and vice versa. In particular, for a separable state ($E=0$) as

well as for a perfectly entangled state ($E = 1$), it is found that the concurrence is also 0 and 1, respectively. This makes the concurrence itself a valid measure of entanglement.

To calculate the concurrence for the case of two qubits, one needs the "spin flip" [54] operator

$$\Sigma := \sigma_y \otimes \sigma_y, \tag{2.19}$$

using the Pauli spin matrix σ_y. The matrix Σ can be expressed in the basis of two-qubit states ($|00\rangle, |10\rangle, |01\rangle, |11\rangle$):

$$\Sigma = \begin{pmatrix} 0 & 0 & 0 & -1 \\ 0 & 0 & 1 & 0 \\ 0 & 1 & 0 & 0 \\ -1 & 0 & 0 & 0 \end{pmatrix}. \tag{2.20}$$

Using Σ, one can calculate the eigenvalues $\lambda_1, \lambda_2, \lambda_3$ and λ_4 of the matrix $\rho\Sigma\rho^*\Sigma$, in which ρ is the density matrix of the bipartite system and ρ^* its complex conjugate. For a better understanding, it is interesting to note that the matrix $\Sigma\rho^*\Sigma$ gives the state directly opposite of ρ on the extended Bloch sphere [54] which is a Bloch sphere for two qubits. Therefore the term "spin flip" matrix for Σ [54]. The concurrence is then defined as [55]

$$C(\rho) := \max\left(0, \sqrt{\lambda_1} - \sqrt{\lambda_2} - \sqrt{\lambda_3} - \sqrt{\lambda_4}\right) \tag{2.21}$$

in which the eigenvalues are sorted in decreasing order. For pure states, the formula simplifies: Given the state

$$|\Psi\rangle = a|00\rangle + b|01\rangle + c|10\rangle + d|11\rangle, \tag{2.22}$$

the concurrence can be calculated as

$$C(|\Psi\rangle\langle\Psi|) = 2|ad - bc|. \tag{2.23}$$

While Eq. 2.21 is not very intuitive, this simpler formula demonstrates that entanglement is dependent on certain *off*-diagonal elements of the density matrix ρ.

There are ways to generalize the concept of concurrence to states more complex than qubits, in particular qutrits [56, 57].

One must bear in mind that concurrence is just one way to measure "entanglement" and always higher or equal to, e.g., the entanglement of formation. Which entanglement measure is the most suitable will usually depend on the task for which entangled states are needed. In the following usually the concurrence is taken directly as the entanglement measure, mainly due to its easy computability.

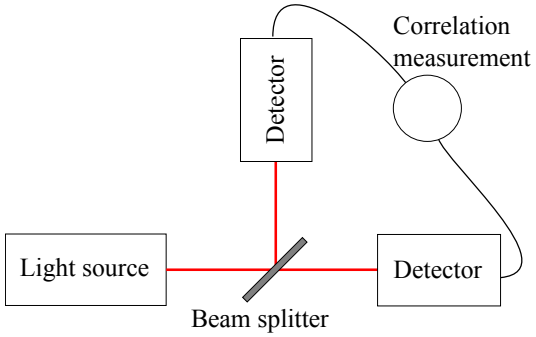

Fig. 2.2.: The setup of a Hanbury Brown and Twiss experiment to measure the second-order correlation function. A light beam is divided by a beam splitter and projected onto two detectors. Afterwards, the correlation between the two signals is computed.

Due to the "nonlinearity" of the definition of the concurrence, one cannot "simply" derive the concurrence of a mixture by only looking at the probability of the entangled constituent(s), even if there is only one. This shall be demonstrated by a simple example. For this, let us define the entangled state $|E\rangle = \big(|10\rangle + |01\rangle\big)/\sqrt{2}$. Now take a mixture, in which this entangled state has the (classical) probability of $1/2$, while the other $1/2$ is made up of the states $|11\rangle$ and $|00\rangle$:

$$\rho = \frac{1}{2}|E\rangle\langle E| + p_{00}|00\rangle\langle 00| + p_{11}|11\rangle\langle 11| \tag{2.24}$$

with $p_{00} + p_{11} + 1/2 = 1$. Intuition would say since all constituents but $|E\rangle$ are separable, the concurrence of this density matrix should be $1/2$. However, this is not correct – the concurrence crucially depends on p_{00} and p_{11} via $C = 0.5 - 2\sqrt{p_{00}p_{11}}$, which can take any value between 0.5 (for $p_{00} = 0$ or $p_{11} = 0$) and 0 (for $p_{00} = p_{11} = 0.25$). This is the reason behind "sudden death of entanglement" [58]: While all excitation in a system may decay exponentially, the entanglement in a system may actually become 0 after a finite amount of time due to the redistribution of probabilities.

2.1.4 Photon correlations: bunching and antibunching

Light of equal intensity and frequency can still have very different properties – compare, for example, the light emitted by a light bulb to that emitted by a laser. These differences become visible in the statistical properties of the light and its fluctuations. The most important experiment to examine light statistics is the *Hanbury Brown and Twiss* experiment [59], in which a beam of light is projected onto two photodetectors using a beam splitter, and the correlation between the two signals is examined (see Fig. 2.2). This measurement reveals the *second-order correlation function*, or $g^{(2)}(t, t')$ function,

using photodetection events at times t and t'. In terms of photon annihilation (creation) operators $c^{(\dagger)}$, the $g^{(2)}(t,t')$-function of a single photonic mode can be written as [48]

$$g^{(2)}(t,t') = \frac{\langle c^\dagger(t)c^\dagger(t')c(t')c(t)\rangle}{\langle c^\dagger(t)c(t)\rangle\langle c^\dagger(t')c(t')\rangle}. \tag{2.25}$$

Especially for $t' = t$, we get the *one-time second-order correlation function*

$$g^{(2)}(t) = \frac{\langle c^\dagger c^\dagger cc\rangle}{\langle c^\dagger c\rangle^2}(t). \tag{2.26}$$

An interpretation of this quantity is, that it measures the probability of having two photons at the same "place" in the light beam, normalized to the probability this happens for a completely random photon distribution. Different "types" of light show different values for the $g^{(2)}$-function. For coherent fields, such as laser light or Glauber states, one can factorize $\langle c^\dagger c^\dagger cc\rangle = \langle c^\dagger c\rangle^2$, which leads to $g^{(2)} = 1$. This is the value that one gets for a perfectly random distribution of photons within the light beam. For thermally emitted, incoherent light, one gets $g^{(2)} = 2$, i.e., the photons appear in "bunches" – this phenomenon is called "photon bunching". Light with $g^{(2)} > 2$ is called "super-bunched". For classical light fields, the $g^{(2)}$ function is bound, $g^{(2)} \geq 1$. The reason for this is the Cauchy-Schwartz inequality: In a classical theory, the field is not described by operators, but by complex numbers, which commute. Classically, one can therefore rewrite the second-order autocorrelation function in terms of the light intensity I as

$$g^{(2)}_{\text{class.}}(t) = \frac{\langle I^2\rangle}{\langle I\rangle^2}(t). \tag{2.27}$$

The brackets "$\langle\rangle$" denote statistical averages, since the intensity might as well be noisy. One can now express the classical intensity as a sum of its statistical average and a noise term, $I = \langle I\rangle + \eta$, with $\langle\eta\rangle = 0$ and $\langle\eta^2\rangle \geq 0$. With this, we find $g^{(2)}_{\text{class.}} = (\langle I\rangle^2 + \langle\eta^2\rangle)/\langle I\rangle^2 = 1 + \langle\eta^2\rangle/\langle I\rangle^2$. Since neither $\langle\eta^2\rangle$ nor $\langle I\rangle$ can be negative, we have $g^{(2)}_{\text{class.}} \geq 1$. This derivation however relies on the classical notion of $g^{(2)}$ (eq. 2.27) . Within quantum mechanics, all non-negative values are allowed. Light with $g^{(2)} < 1$ is called "anti-bunched", since the photons appear more separated than in a random distribution. In the special case of single-photon emission, $\langle c^\dagger c^\dagger cc\rangle = 0$, which leads to $g^{(2)} = 0$. For a Fock state with n photons, we get $g^{(2)} = (n-1)/n$, which is < 1 for all finite n.

One has to be careful, though, since different photon statistics can lead to the same $g^{(2)}$. It is often assumed that $g^{(2)} = 1$ means that the light is coherent; however one can create an infinite number of other photon statistics that lead to $g^{(2)} = 1$, and further measures, like higher order correlations, are necessary to determine the correct photon statistics. In fact, what "$g^{(2)} = 1$" says in terms of photon number distributions, is that the variance $V \equiv \langle(c^\dagger c)^2\rangle - \langle c^\dagger c\rangle^2$ is equal to the intensity $I \equiv \langle c^\dagger c\rangle$. This is the case for the Poisson distribution which one finds for coherent light, but this is not the only distribution with

this property. As an example on how to produce arbitrary large $g^{(2)}$ functions with highly non-classical states, take a photon state consisting of a 0-photon and a 2-photon part:

$$|\psi\rangle = c_0|0\rangle + c_2|2\rangle \tag{2.28}$$

For this state, we have $\langle c^\dagger c^\dagger c c\rangle = \langle c^\dagger c\rangle = 2|c_2|^2$. From this, we get $g^{(2)} = 1/(2|c_2|^2)$. Since $|c_2|^2$ can take any value between 0 and 1, the $g^{(2)}$ function can take any value between 0.5 and ∞. In particular, $g^{(2)} = 1$ can be reached without the state being a coherent state, for $c_0 = c_2 = 1/\sqrt{2}$. In order to test whether a photon field can be called "coherent"[1], one would need to check $g^{(N)} = 1$ for all higher correlations $N > 1$, with the higher-order autocorrelation defined as

$$g^{(N)} = \frac{\langle (c^\dagger)^N (c)^N\rangle}{\langle c^\dagger c\rangle^N}. \tag{2.29}$$

2.2 Open systems and dissipation

An "open" system is a system which is connected to another (mostly a lot larger) system. In such cases, the energy of the original system is not conserved, and its time evolution may be non-unitary. The second system is usually referred to as the "bath", and may be as small as a cavity mode (as it will be seen in Chapter 7) or as big as the "whole universe". Usually the bath dynamics are of no interest, and one only cares about system quantities which are acquired by tracing over the bath degrees of freedom.

2.2.1 Markovian dissipation and the Lindblad formalism

A lot of approximations can make the calculation of system properties much easier, most prominently the Born-Markov approximations. Here it will be shortly summarized, based upon Ref. [60], how to get to the well-known Lindblad equations which describe system-reservoir interaction in the second order Born-Markov approximation.The full formulas of the derivation are not given here since they can be found in Ref. [60] as well as in many other textbooks of quantum optics. A more detailed derivation is also given in Appendix A for sake of completeness. At this point, the basic concepts behind the approximations made are outlined, so that it becomes clear when the approximations are applicable.

The Hamiltonian H shall be written as the sum of a system Hamiltonian, H_S, a bath Hamiltonian H_B, and the system-bath interaction Hamiltonian H_{SB}: $H = H_S + H_B + H_{SB}$. We are interested in the dynamics of the density matrix of the system, ρ_S, which can

[1] Although this does not mean the system has to be in a Glauber state. The system could as well be in a mixed state with $\langle c\rangle = 0$. Such a mixed state would be $\rho = \frac{1}{2}\left(|+\alpha\rangle\langle+\alpha| + |-\alpha\rangle\langle-\alpha|\right)$, with $|\pm\alpha\rangle$ a Glauber state with $c|\pm\alpha\rangle = \pm\alpha|\pm\alpha\rangle$.

be acquired from the full density matrix ρ by tracing out the bath degrees of freedom: $\rho_S = \mathrm{tr}_B \rho$.

At the beginning, let us assume system and bath to be independent, and therefore factorizable: $\rho^0 = \rho_S^0 \rho_B^0$. This will no longer be the case for later times, though. This initial condition allows to write an integro-differential equation for $\partial_t \rho_S(t)$ depending on the full $\rho(t)$. As a first approximation, one writes $\rho(t) = \rho_S(t)\rho_B^0 + O(H_{SB})$, plugs this into the formula for $\partial_t \rho_S(t)$, and neglects terms of higher than second order in H_{SB}. This is the *Born approximation*. It states that the system-reservoir interaction is weak, and that the reservoir is virtually unchanged by the actions of the system. After the Born approximation, the integro-differential equation for $\partial_t \rho_S(t)$ only depends on $\rho_S(t' < t)$ and the initial reservoir state ρ_B^0.

The dependence on earlier states of the system, i.e., *memory*, still makes the equation hard to solve. Let us therefore assume that the reservoir introduces no memory effects into the system dynamics over the time scale studied. This coarse-graining is called the *Markov approximation*. With this approximation, we arrive at a differential equation for the system density matrix ρ_S of the form

$$\partial_t \rho_S = \frac{\kappa}{2}\left(2S\rho_S S^\dagger - S^\dagger S\rho_S - \rho_S S^\dagger S\right). \tag{2.30}$$

The operator S is the system operator with which the system couples to the reservoir in the form $H_{SB} = S\Gamma_B$, with Γ_B a reservoir operator. Note that if S is an annihilation operator, Eq. 2.30 leads to a decay of the system property $\langle S^\dagger S \rangle$. However, S can also be a creation operator, which then models incoherent driving of the system. This type of equation is called a Lindblad equation.

To summarize, the two important requirements to use the Lindblad approach are *weak system-reservoir coupling* and *no reservoir memory*.

The easiest type of reservoir that can exhibit these properties is a large collection of harmonic oscillators. It can be described by the Hamiltonian

$$H_B = \hbar \int_0^\infty \omega d_\omega^\dagger d_\omega \mathrm{d}\omega \tag{2.31}$$

and interact with the system via

$$H_{SB} = \hbar \int_0^\infty G(\omega)\left(d_\omega^\dagger S + S^\dagger d_\omega\right)\mathrm{d}\omega. \tag{2.32}$$

This coupling to an infinite set of harmonic oscillators can also be described in k-space as

$$H_{SB} = \hbar \int_{-\infty}^\infty \tilde{G}(k)\left(d_k^\dagger S + S^\dagger d_k\right)\mathrm{d}k. \tag{2.33}$$

This is the form for a $1D$ reservoir – for three-dimensional reservoirs, the integration has to be done over the whole set of $\vec{k}$-vectors.

Any memory of the reservoir will be reflected in a frequency-dependence of the system-reservoir coupling $G(\omega)$. In frequency space, the Markovian approximation is equivalent to choosing $G(\omega) = \text{const.}$ over the relevant frequency range of the system dynamics. We retrieve the exponential decay associated with Markovian dynamics if $G(\omega) = \text{const.}$ and the integral boundaries are expanded to $-\infty$. This is however not a "physical" situation (ω has to be positive), but it is a very useful approximation for large frequencies (i.e., when the frequency is much larger than any decay constant present in the system). Here we also see that the Markovian approximation breaks down at very short time scales, i.a. when calculating initial time dynamics. This breakdown of Markovianity is the mechanism behind the counter-intuitive "quantum Zeno effect" [61, 62], which says that a quantum state can be stabilized just by repeated measurements ("a watched pot never boils").

At this point it is appropriate to mention a very easy example of the breakdown of the Lindblad approach: The damped harmonic oscillator. If $c^{(\dagger)}$ is the annihilation (creation) operator of one excitation of the harmonic oscillator, the Hamiltonian takes the well-known form $H = \hbar\omega c^\dagger c$ (omitting the $+\hbar/2$ overall frequency shift). One can damp this system using the Lindblad equation (Eq. 2.30) with $S = c$. Now remember that the location expectation value $\langle x\rangle$ is proportional to $\langle c\rangle + \langle c^\dagger\rangle$, while the momentum expectation value $\langle p\rangle$ is proportional to $\langle c\rangle - \langle c^\dagger\rangle$. Within the Lindblad approach, *both* expectation values get damped with the damping constant $\kappa/2$. This is a clear contradiction to the classical case, in which the momentum is damped, but the position is *not*. This classical asymmetry in the damping leads to well-known phenomena like a damping-dependent frequency shift scaling with $O((\kappa/\omega)^2)$, as well as the complete disappearance of all oscillations for large enough damping. This "over-damped case" is not present in the quantum-mechanical model with Lindblad damping, and also the oscillation frequency is not shifted. These two discrepancies on the order of $O((\kappa/\omega)^2)$ alone show that Lindblad-type damping is invalid for strong damping ($\kappa \gg \omega$).

2.2.2 Non-Markovian dissipation

As soon as the coupling to the reservoir is frequency-dependent, the reservoir retains information of the system dynamics, at least for a finite amount of time. Such a reservoir is called non-Markovian. The simplest non-Markovian reservoir may be one photonic mode: If a two-level system is coupled to such a mode, the excitation oscillates between the two-level system and the mode in Rabi oscillations. This is obviously totally different to an exponential decay of the two level system excitation in a Markovian reservoir.

Besides the aforementioned quantum Zeno effect, non-Markovian reservoirs were shown to tremendously influence quantum statistics and dynamics, e.g., sudden "death"

and "re-birth" of entanglement [63, 64]. It was proposed that non-Markovian dynamics can be modeled by time-dependent Lindblad operators [65, 66], however such a description is only valid for linear systems, otherwise it is an approximation, as it will be discussed below.

One important non-Markovian reservoir which will be discussed in this thesis is a reservoir leading to time-delayed quantum-coherent feedback.

2.3 Time-delayed feedback

Parts of this section are submitted for publication as a conference paper for the SPIE Photonics West 2016 conference.

The main focus of this thesis is on control of quantum systems through time-delayed feedback, which shall be introduced in this section. Further elaboration on the different numerical implementations will be given in the subsequent chapter. On time-delayed feedback, a lot of research has already been done in classical and semi-classical physics, especially with respect to the control of chaotic dynamics (for an overview, see e.g. the book chapter of Schöll et al. [31] on *"Time-Delayed Feedback Control: From Simple Models to Lasers and Neural Systems"*). A notable application is the Lang-Kobayashi dynamics of lasers [24], which describe a laser with a time-delayed feedback of the laser radiation into the laser cavity. This feedback, i.a., modifies the light statistics by increasing the $g^{(2)}$-factor. We recently showed [45] theoretically that this behavior extends into the quantum regime for quantum dot lasers.

One can often think of time-delayed control as a very efficient frequency "filter": The time delay translates into a certain frequency in Fourier space. Generally, any dynamics that happens at this frequency (or multiples of it) will be influenced by the time-delayed feedback, while the influence of time-delayed feedback on other dynamics usually gets averaged out. This allows one to see time delay not just as something that needs to be avoided for "fast" control, but that can be actively used to steer the dynamics.

To derive the dynamics of systems with time delay, it is not only necessary to define initial conditions, but a whole initial dynamics spanning the delay time τ in the interval $-\tau < t < 0$. In this thesis, the system is usually treated to be in the ground state for $t < 0$ or to not interact with the environment until the "feedback is turned on" at $t = 0$.

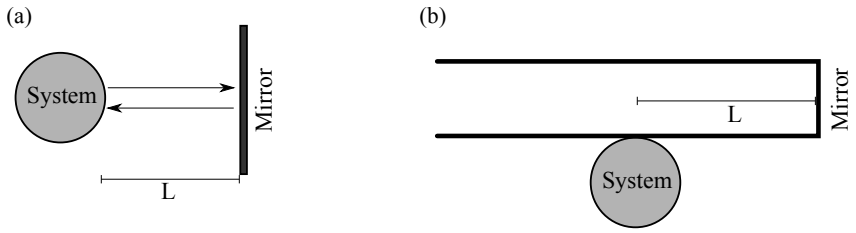

Fig. 2.3.: Simplified experimental implementations of Pyragas control in optical systems. (a) The system emits radiation towards a mirror at distance L, which is reflected back and interacts with the system again after the delay time $\tau = 2L/c$ (c being the speed of light). (b) The system is coupled to a waveguide with one closed end that acts as a mirror. The radiation emitted in this direction also interacts with the system again after the delay time $\tau = 2L/c$.

2.3.1 Pyragas control

A special kind of control was developed by Pyragas [19], which depends on the difference between the current system state and the system state at an earlier point of time: Say, the system dynamics can be described by the following differential equation:

$$\dot{x}(t) = f\big(x(t)\big). \tag{2.34}$$

With "Pyragas control", a control term of the form $-K \cdot \big(x(t) - x(t-\tau)\big)$ is introduced:

$$\dot{x}(t) = f\big(x(t)\big) - K \cdot \big(x(t) - x(t-\tau)\big). \tag{2.35}$$

K is the control strength, and τ the delay time. If now the dynamics given by Eq. 2.34 contain a limit cycle with periodicity τ, this limit cycle will also appear as a solution of the controlled equation 2.35. The reason is that the two terms in the control term perfectly cancel. Other dynamics which do not have the periodicity τ will however be strongly affected by the control term. This gives the possibility to change the stability properties of the limit cycle, without actually changing the limit cycle itself. Therefore, Pyragas control is called "non-invasive". The exact condition for a limit cycle with frequency ω_0 to be not affected by Pyragas control is

$$\omega_0 \tau = \mathbb{N} \cdot 2\pi, \tag{2.36}$$

with $\mathbb{N}$ any natural number.

Besides this peculiar property, Pyragas-type dynamics appear naturally in experimental setups where parts of the signal get re-emitted into the experimental setup, e.g. back-reflection of laser light into the laser through mirroring surfaces. Due to the single delay time, Pyragas control has the strongest influence on dynamics with frequencies around $1/\tau$. Note that Pyragas control does not include terms such as $x(t-2\tau), x(t-3\tau)\ldots$. This means that the system only interacts with itself after one delay time, and information is not stored in the feedback loop longer than τ.

In this thesis Pyragas control shall be used in the quantum limit, therefore a way to model it using the equations of quantum mechanics is needed. One way is to come from a direct experimental implementation and to demonstrate that the dynamics indeed show Pyragas-like terms. Two possible schemes for systems emitting light are presented in Fig. 2.3. In Fig. 2.3(a) we see a system in front of a mirror. Light which is reflected onto the mirror is transferred back into the system after the delay time $\tau = 2L/c$, with L the distance of the mirror and c the speed of light. What is not shown in the image, is that radiation can also be emitted to the other side, and can also pass the system after reflection without interaction. These loss channels make the whole setup open and allow for equilibration. This setup, sometimes equipped with a lens to collect the emitted radiation to project it onto the mirror, is discussed in literature [67, 68] mainly in the area of quantum optics of atoms. It is also discussed in Ref. [69] and compared to a hemispherical mirror geometry in Ref. [70]. This setup is however not suitable for all systems: It must be ensured that the radiation reflected back from the mirror will not be reflected from the system *without any interaction with the system*. Otherwise it will be stored in the area between system and mirror for longer than 1τ, which will lead to terms such as $x(t-2\tau)$ in the dynamics. "Interacting with the system" means that it excites the system and gets re-emitted, which is totally fine within Pyragas control. Of course this depends on how the system is modeled and simplified, and what is defined as "the system". In the end the interesting issue to be examined is Pyragas control on the system parameters that are interesting. It would not make sense to model, e.g., a mirror as a collection of atoms and include it into the "system", if we want to study the dynamics of a single mode contained between two of such mirrors. The Pyragas-like terms for the cavity mode would be hidden in the highly complex mode-mirror interaction. This problem is connected to the reason why the "mirror setup" is most suitable for atom-based quantum optics: The signal coming back from the mirror can either interact with the atom again, or pass right through it. In contrast, if the system is a cavity in itself (or something connected to a cavity mode), the setup is not suitable any more: The radiation may be reflected from the (system) cavity mirror without interacting with the cavity mode. To treat such systems, a setup as in Fig. 2.3(b) is necessary. Here, the system is coupled evanescently to a waveguide that is closed at one end and is supposed to be "infinite" (perfectly absorbing) at the other end. The closed end at distance L acts as a mirror. This setup is discussed in several publications [71–73] on semi-infinite waveguides. To model these quasi one-dimensional feedback environments, one needs the local photonic density of states (LDOS) at the position of the emitter. Since these environments are open, the LDOS will be a a continuous function depending on the wave vector k. Say, the different modes of the feedback environment are described by the ladder operators $d_k^{(\dagger)}$, and the system couples to this environment with the ladder operator $c^{(\dagger)}$ (which can be a bosonic

or fermionic operator). As it was shown in the last section on dissipation, the coupling to the environment can then be described by the interaction Hamiltonian H_I,

$$H_I = \int_{-\infty}^{\infty} dk\, G(k)\, c^\dagger d_k + \text{H.c.}. \tag{2.37}$$

Due to the assumed 1D geometry (induced by the waveguide or by collecting the emitted radiation by a lens to project it onto a mirror), the integral over k is just an integral from $-\infty$ to ∞. The density of states is included in the factor $G(k)$, which is the k-vector-dependent coupling between system and feedback loop. A k-*in*dependent coupling means that each mode has the same (relative) strength at the position of the system, which leads to exponential decay. In our case, the mirror (or the end of the waveguide) introduces a boundary for the electric fields: Every mode has to vanish at the position of the mirror (to be more precise, it's its field component parallel to the mirror). Any field distribution in the "feedback reservoir" that vanishes at the mirror can be expanded into sine functions with the origin set at the mirror surface. These sine functions describe the modes to which the system is coupled. The k-vector dependent coupling therefore reads [67]

$$G(k) = \hbar\gamma \sin(kL). \tag{2.38}$$

with a k-independent coupling strength γ. This is the case for perfect reflection at the feedback-inducing mirror. As described in Ref. [67], imperfect feedback can be incorporated by including another set of modes with a constant coupling factor $G'(k) = G'$.

This leads to Pyragas-like terms. To demonstrate this, let us investigate a system with the Hamiltonian

$$H = H_S + H_I + H_R \tag{2.39}$$

with an arbitrary system Hamiltonian H_S, the interaction Hamiltonian H_I (Eq. 2.37), and the "reservoir" Hamiltonian

$$H_R = \int_{-\infty}^{\infty} \mathrm{d}k\, \hbar\omega(k) d_k^\dagger d_k. \tag{2.40}$$

A linear dispersion relation $\omega(k) = c_0|k|$ is used. Let us now derive the equations of motion for the expectation value $\langle c \rangle$. If the operator c describes a photonic mode, the real part of this expectation value is proportional to the electric field. However, one has to keep in mind that in a fully quantum-mechanical simulation this value is usually *identically zero*, since the operator c is not bi-linear[2]. This issue has been covered in great detail by H. Wiseman [74], who demonstrates that the fundamental reason is that the phase of the (electric) field is not defined *a priori* in a full quantum-mechanical simulation without semiclassical terms. Averaging over all possible phase values creates a zero expectation

[2] This has nothing to do with c being non-hermitian – the electric field is proportional to the hermitian operator $c + c^\dagger$, which is also not bi-linear in the single operators.

value for the field operators [3]. One can therefore regard the dynamics of $\langle c \rangle$ as a look at the semiclassical properties of the system, since semi-classically it is no problem to introduce a phase through, e.g., an external ac drive. The derivation here is based on the derivation by Dorner and Zoller [67], and was also presented in Ref. [75].

Using the Ehrenfest theorem, we arrive at

$$\partial_t \langle c \rangle = \frac{i}{\hbar} \langle [H_S, c] \rangle - i \int_{-\infty}^{\infty} \mathrm{d}k \, G(k) \langle d_k \rangle \mathrm{e}^{-i\omega(k)t} \tag{2.41}$$

$$\partial_t \langle d_k \rangle = -iG^*(k) \langle c \rangle \mathrm{e}^{i\omega(k)t} \tag{2.42}$$

Here, the free oscillation of the external modes is already transformed away, which leads to the $e^{\pm i\omega(k)t}$ terms. One can formally integrate the differential equation for $\langle d_k \rangle$:

$$\langle d_k \rangle = -iG^*(k) \int_0^t \langle c \rangle(t') \mathrm{e}^{i\omega(k)t'} \, \mathrm{d}t'. \tag{2.43}$$

Here it is assumed that initially there is no excitation in the external reservoir: $\langle d_k \rangle(t = 0) = 0$. One can now put this into the equation for $\langle c \rangle$ to get

$$\partial_t \langle c \rangle = \frac{i}{\hbar} \langle [H_S, c] \rangle - \int_{-\infty}^{\infty} \mathrm{d}k \int_0^t \mathrm{d}t' |G(k)|^2 \langle c \rangle(t') \mathrm{e}^{-i\omega(k)(t-t')} \tag{2.44}$$

Let us now transform the integral to an integral over ω, which now only goes from 0 to ∞ – for symmetry reasons, this just leads to a factor of 2. Let us also put in $G(k) = \hbar\gamma \sin(kL) = \hbar\gamma \sin(2\omega\tau)$ with the delay time $\tau = 2L/c_0$, and rewrite the sine function in terms of exponential functions to get

$$\partial_t \langle c \rangle = \frac{i}{\hbar} \langle [H_S, c] \rangle - \frac{|\gamma|^2}{2c_0} \int_0^{\infty} \mathrm{d}\omega \int_0^t \mathrm{d}t' \langle c \rangle(t') \left(\mathrm{e}^{-i\omega(t-t'+\tau)} + \mathrm{e}^{-i\omega(t-t'-\tau)} - 2\mathrm{e}^{-i\omega(t-t')} \right). \tag{2.45}$$

Using the well-known formula

$$\int_0^{\infty} \mathrm{d}\omega \mathrm{e}^{i\omega T} = \pi\delta(T) + i\mathscr{P}\frac{1}{T}, \tag{2.46}$$

in which $\mathscr{P}$ symbolizes the Cauchy principal value, the integral can be simplified. In analogy to Wigner-Weisskopf decay [48], one can neglect the imaginary terms which lead to a (usually small) frequency renormalization which is part of the Lamb shift. Note that for positive τ, the integral over the part with $\mathrm{e}^{-i\omega(t-t'+\tau)}$ is zero since the integration boundaries are 0 and t. Also, in the term with $\mathrm{e}^{-i\omega(t-t')}$ the delta function is located directly at the integral boundary and therefore only contributes with a factor 1/2. One finally ends up with

$$\partial_t \langle c \rangle(t) = \frac{i}{\hbar} \langle [H_S, c] \rangle(t) - K\big(\langle c \rangle(t) - \langle c \rangle(t-\tau) \big). \tag{2.47}$$

[3] In some cases, such as electric fields, the phase can actually be measured, e.g. by magnetic fields [74], and is therefore a sensible quantity. This does not apply to all fields [74], in particular not to particle fields.

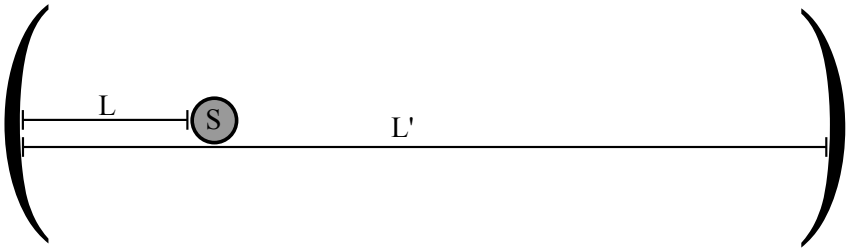

Fig. 2.4.: The large cavity interpretation of Pyragas control: The system (S) is located in a cavity of length L' at a distance L from one of the mirrors. The close mirror leads to Pyragas terms, while the reflection of the far mirror creates "un-wanted" feedback. This is the *actual* system simulated when the density of states $\sin(kL)$ is evenly discretized in frequency space for numerical simulations. "Pure" Pyragas control is achieved in the limit $L' \to \infty$.

For clarity, the t-dependence is included explicitly in this equation. The abbreviation $K = \frac{\pi|\gamma|^2}{2c_0}$ is used. One clearly recovers the Pyragas control terms. This shows that in the semiclassical limit, this description with modes leads to the Pyragas-type time-delayed differential equations. With only one excitation in the whole system-reservoir complex, one can derive an analogous equation for the probability amplitude of the system variable [67]. However, one has to note that for more complex quantities, like the bi-linear $\langle c^\dagger c\rangle$, one cannot derive such a simple expression [76]. The reason is that while $\langle c^\dagger c\rangle$ couples to $\{\langle c^\dagger d_k\rangle\}$,$\langle c^\dagger d_k\rangle$ itself couples to $\{\langle d_{k'}^\dagger d_k\rangle\}$. This dependence on k and k' makes it impossible to integrate out all the dependencies on the outer modes in analogy to the dynamics for $\langle c\rangle$ [76]. Simulating the whole external continuum (with a suitable discretization) is numerically very demanding. Recently however a proposal has been made to derive a time-delayed differential equation for whole density matrix propagators [77] which might be easier to solve for the first couple of delay times.

When simulating such a structured environment, usually the k-vector-dependent coupling $G(k)$ is discretized. This leads to a new interpretation, since *closed* systems can be described by discrete energy levels. In particular, evenly spaced energy levels are found for cavities with perfectly reflecting mirrors. One could therefore interpret Pyragas control as a system in a large cavity of length L', however with the system located only at distance L from one of the mirrors, and finally taking the limit $L' \to \infty$ (cf. Fig. 2.4). The electric field modes of such a cavity are evenly spaced in energy with an energy difference depending on L', while the intensity of each mode at the position L away from one mirror is $\sin^2(kL)$. Therefore, for finite discretization in numerical simulations, a "revival" of system quantities after approximately $t = 2L'/c_0$ is found, when the signal reflected from the far mirror returns back to the system. This defines a strict boundary for system dynamics after which any simulation breaks down. This already shows a big problem of simulating Pyragas control in the frequency space: In order to put this revival as late as possible, a very good frequency resolution of the feedback reservoir is needed,

in particular orders of magnitudes finer than the oscillation period of $\sin(kL)$. Later on it will be discussed how one can circumvent this problem by using "pseudomodes".

2.4 Matter–light interaction: The Jaynes-Cummings Hamiltonian

The simplest system to study fully quantum mechanical light-matter interaction is a two-level system coupled to one photon mode. Since this is one of the most important models of quantum optics, it shall be introduced here. The two-level system may represent, e.g., two distinct energy levels $|g\rangle$ and $|e\rangle$ (ground state and excited state) of an atom. Let us define the lowering- and raising operators $\sigma^+ = |e\rangle\langle g|$ and $\sigma^- = |g\rangle\langle e|$. The *polarization* of the two-level system can then be described by the operator $P \propto (\sigma^+ + \sigma^-)$. The electric field of the photon mode will be described by the photon creation and annihilation operators $c^{(\dagger)}$. The electric field E will then be proportional to $(c + c^\dagger)$. One can write the simplest bi-linear atom-field interaction with the Hamiltonian

$$H_{\text{atom-field}} = \hbar(\omega_e - \omega_g)\frac{\sigma^z}{2} + \hbar\omega_0 c^\dagger c + \hbar\frac{g}{2}(E \cdot p). \tag{2.48}$$

Here, the energy of the ground (excited) state of the two-level system is defined as $\hbar\omega_g$ ($\hbar\omega_e$). The angular frequency of the photon mode is ω_0, and the atom-field coupling is g. The operator σ^z is defined as $\sigma^z = |e\rangle\langle e| - |g\rangle\langle g|$.

At this point, let us approximate the Hamiltonian by removing all operators that do not conserve excitation number, namely $c^\dagger\sigma^+$ and $c\sigma^-$. For small coupling g (compared to the intrinsic frequencies), these terms will only lead to fast oscillations of the order of $\omega_e + \omega_0 - \omega_g$, which can be averaged out. This is called the *rotating wave approximation*. One then gets the famous *Jaynes-Cummings Hamiltonian*:

$$H_{\text{JC}} = \hbar\omega_q\frac{\sigma^z}{2} + \hbar\omega_0 c^\dagger c + \hbar\frac{g}{2}\left(\sigma^+ c + \sigma^- c^\dagger\right). \tag{2.49}$$

The abbreviation $\omega_e - \omega_g = \omega_q$ is used. In the following, let us also abbreviate $\Delta = \omega_q - \omega_c$. The eigenenergies of this Hamiltonian are

$$E_\pm(n) = \hbar\omega_c\left(n + \frac{1}{2}\right) \pm \hbar\frac{1}{2}\sqrt{\Delta^2 + g^2(n+1)}. \tag{2.50}$$

Here, n is a natural number (including 0). It can be directly seen that this is a nonlinear system by the square-root dependence of the energy on n. If the system is prepared in the $|e\rangle$ state with n photons in the cavity mode, it will exhibit oscillations between this state (let's call it $|e,n\rangle$) and the state $|g,n+1\rangle$ with frequency $\Omega(n) = \sqrt{\Delta^2 + g^2(n+1)}$. This frequency is called the *Rabi frequency* and the oscillations *Rabi oscillations*.

A typical system is also lossy: The two-level system may decay with the rate γ without emitting a photon into the mode, and the cavity may experience losses with the rate κ. Both rates not only lead to a decay of the excitation number of the system, but also change the Rabi frequency. For very strong losses, no Rabi oscillations will be visible, in a direct analogy of the over-damped classical harmonic oscillator. This parameter region is called the "weak coupling" regime. If Rabi oscillations are present, the system is in the "strong coupling" regime. Note, however, that the system only enters this "weak coupling" state, if the *difference* between κ and γ, $|\kappa - \gamma|$, is much larger than the coupling g. In contrast to intuition, the Jaynes-Cummings system can be in the region of "strong coupling" for *arbitrarily large* cavity losses, as long as the direct two-level system losses γ are equally large. Experimentally it might still be very hard to see the Rabi oscillations in this region, though.

3 Advanced methods for the numerical treatment of time-delayed feedback

While the calculation of Pyragas control (and other non-markovian reservoirs) using a full calculation of the outer modes is straightforward, it is also numerically very demanding. On a Schrödinger equation approach, $O(K^n)$ terms are needed, with K the number of external modes and n the number of excitations. Including dissipation in a density matrix- or expectation value approach even leads to a scaling of $O(K^{2n})$. This becomes unsolvable already for very low n. Usually during the numerical simulations presented in this thesis it is found that K is in the order of several hundred to thousands, in order to make sure no unwanted revivals (see last chapter) occur until the system has equilibrated.

Very recently some progress has been made to tackle this problem: It was suggested by Grimsmo [77] to create time-delayed propagator equations. It is still a matter of current research how broadly this approach can be applied – especially since it becomes exponentially more demanding the more delay times τ shall be covered – and if it may be combined with other methods, such as non-markovian dynamical maps [78].

In this chapter advanced methods to tackle the issue will be presented. They are mainly based on simplifying the full calculation of the external bath by introducing suitable approximations.

3.1 Calculation of non-markovian reservoirs by nonlinear equations of motion

Calculating non-markovian dynamics in an equation-of-motion (EOM) framework for expectation values makes it easy to include other markovian dissipative effects via the Lindblad formalism. In particular, this will be used later on when we introduce the pseudomode approach to time-delayed feedback. However, due to the scaling with $O(K^{2n})$, full calculations of a non-markovian reservoir become numerically unfeasible very quickly. Calculations can be done, however, in a Schrödinger equation approach. Dissipative effects may then be introduced by Monte Carlo methods [79] that simulate quantum trajectories and average over them to receive expectation values.If one does not want to make stochastic simulations, the presented method will be suitable.

We start from a Hamiltonian of the form

$$H = H_{\text{system}}(c, c^\dagger) + \hbar \int_{-\infty}^{\infty} \left(G(k) c^\dagger d_k + \text{H.c.} \right) \mathrm{d}k + \hbar \int_{-\infty}^{\infty} \omega_k d_k^\dagger d_k \mathrm{d}k. \tag{3.1}$$

The presented method will use the remaining coherence that often stays in lossy systems to reduce the number of terms to calculate substantially – which, in a way, combines the benefits of a (fully coherent) Schrödinger equation simulation with (some of the) flexibility of expectation value EOMs. The basic idea is the following: It is much easier to compute quantities such as $\langle c^\dagger d_k \rangle$ than quantities such as $\langle d_{k'}^\dagger d_k \rangle$ since the latter leads to a double summation over the k-modes. The new method is to approximate in first order of $d_k^{(\dagger)}$ quantities in the following nonlinear way:

$$\langle \mathcal{O} d_{k'}^\dagger d_k \rangle \approx \frac{\langle \mathcal{O} d_{k'}^\dagger c \rangle \langle c^\dagger d_k \rangle}{\langle c^\dagger c \rangle}. \tag{3.2}$$

$\mathcal{O}$ is an arbitrary operator (which can as well be the unit matrix). This approximation saves memory storage as well as computational power: First of all, one does not need to store the K^2 values of $\langle \mathcal{O} d_{k'}^\dagger d_k \rangle$. Second, when calculating EOM for $\langle \mathcal{O} d_{k'}^\dagger c \rangle$, the equations become much simpler. Without the approximation, the equations read

$$\partial_t \langle \mathcal{O} d_{k'}^\dagger c \rangle = \ldots + \int_{-\infty}^{\infty} \mathrm{d}k\, G(k) \langle \mathcal{O} d_{k'}^\dagger d_k \rangle \tag{3.3}$$

which creates a *different* sum over k for each of the K elements $\langle \mathcal{O} d_{k'}^\dagger c \rangle$. With above approximation however, one can once evaluate

$$\Omega \equiv \int_{-\infty}^{\infty} \mathrm{d}k\, G(k) \frac{\langle c^\dagger d_k \rangle}{\langle c^\dagger c \rangle} \tag{3.4}$$

and then approximate Eq. 3.3 by

$$\partial_t \langle \mathcal{O} d_{k'}^\dagger c \rangle \approx \ldots + \Omega \langle \mathcal{O} d_{k'}^\dagger c \rangle. \tag{3.5}$$

This removes the sum and leaves us with a simple multiplication. The important issue is that Ω is independent of k' as well as of $\mathcal{O}$. It can be seen as a environment-induced frequency shift and dissipation: While the imaginary part of Ω shifts the frequency, the real part acts like a dissipative term. If $\mathrm{Re}(\Omega)$ is negative, it is usual dissipation, while if it is positive, it is "negative dissipation" – a common feature of non-markovian dynamics [80, 81]. While this approximation apparently decreases the numerical complexity of the problem, how good is it as an approximation? In fact, it is *exact* in the case of one excitation, with or without included markovian decay. It can also be extended to systems with higher number of excitations. Let us treat this at the example of a Jaynes-Cummings model (JCM) with time-delayed feedback, as it was presented by Carmele *et al.* [44].

The Hamiltonian of this system is given as [44]

$$\begin{aligned} H =& \hbar\omega_c a_c^\dagger a_c + \hbar\omega_v a_v^\dagger a_v + \hbar\omega_0 c^\dagger c - \hbar M\left(a_v^\dagger a_c c^\dagger + a_c^\dagger a_v c\right) \\ & - \hbar\sum_k \left(G(k) c^\dagger d_k + G^*(k) d_k^\dagger c + \omega(k) d_k^\dagger d_k\right). \end{aligned} \tag{3.6}$$

The first line of Eq. 3.6 is the Hamiltonian of a standard JCM with a two-level system given by the valence band ($\hbar\omega_v$) and conduction band ($\hbar\omega_c$) energies and a cavity mode of angular frequency ω_0. The fermionic annihilation (creation) operators of the valence/conduction band are $a_{v/c}^{(\dagger)}$, the photonic annihilation (creation) operators are $c^{(\dagger)}$. Cavity and two-level system are coupled by the strength M. The second line gives the coupling to the external feedback reservoir. Note that here the integral over k was already replaced by a sum, since this is how it will be simulated numerically. The coupling is $G(k) = \gamma \sin(kL)$ as before. In the one-excitation limit, the corresponding Schrödinger equation can be solved using the state [82]

$$|\psi\rangle = c_e|e,0,\{0\}\rangle + c_g|g,1,\{0\}\rangle + \sum_k c_{g,k}|g,0,\{k\}\rangle. \tag{3.7}$$

Here, g (e) denotes whether the two-level system is in its excited or ground state, the first number denotes the number of photons in the cavity, and the second number $\{k\}$ denotes that there is a photon in mode k, or not (in which case it is written $\{0\}$). The only quantity that has a double k-dependence is $\langle d_{k'}^\dagger d_k\rangle$ [44], which, expressed in this state, is $\langle d_{k'}^\dagger d_k\rangle = c_{g,k'}^* c_{g,k}$. Therefore Eq. 3.2 exactly holds:

$$\langle d_{k'}^\dagger d_k\rangle = c_{g,k'}^* c_{g,k} = \frac{c_{g,k'}^* c_g c_g^* c_{g,k}}{c_g^* c_g} = \frac{\langle d_{k'}^\dagger c\rangle\langle c^\dagger d_k\rangle}{\langle c^\dagger c\rangle} \tag{3.8}$$

This argument can straightforwardly be extended to any 1-excitation dynamics that is fully coherent. It is not surprising that dynamics that can be described by a Schrödinger equation can be calculated in an expectation value EOM ansatz with comparable numerical complexity. However the approximation is still exact if the cavity mode as well as the two-level system is damped via the Lindblad formalism. The important ingredients will be that

1. No pure dephasing is present, i.e. all decay lowers the number of excitations, and
2. the initial state is a pure state and can therefore be described by a single wave function.

Let us now derive the dynamics of the error, $\frac{\langle d_k^\dagger c\rangle\langle c^\dagger d_{k'}\rangle}{\langle c^\dagger c\rangle} - \langle d_k^\dagger d_{k'}\rangle$. The equations of motion will be taken from Ref. [44], where also the names of the quantities are listed in detail. Let

us introduce an additional damping of the photonic mode with γ_c and a damping of the two level system excitation with γ_{TLS}.

$$\begin{aligned}
&\partial_t \left(\frac{\langle d_k^\dagger c\rangle \langle c^\dagger d_{k'}\rangle}{\langle c^\dagger c\rangle} - \langle d_k^\dagger d_{k'}\rangle \right) \\
&= \frac{1}{\langle c^\dagger c\rangle^2} \Big(\langle c^\dagger c\rangle \big(\langle \dot{d_k^\dagger} c\rangle \langle c^\dagger d_{k'}\rangle + \langle d_k^\dagger c\rangle \langle c^\dagger \dot{d}_{k'}\rangle \big) - \langle d_k^\dagger c\rangle \langle c^\dagger d_{k'}\rangle \langle \dot{c^\dagger} c\rangle \Big) - \langle \dot{d_k^\dagger} d_{k'}\rangle
\end{aligned} \tag{3.9}$$

It can already be seen here that γ_c will not have any influence on the error, since it will affect the first three terms such that any contribution cancels. One can now plug in the dynamics from Ref. [44]:

$$\begin{aligned}
\text{[Eq. (3.9)]} = &\frac{1}{\langle c^\dagger c\rangle} \Big(iM\langle T d_k^\dagger\rangle \langle c^\dagger d_{k'}\rangle + i\sum_{k''} G(k'')\langle d_k^\dagger d_{k''}\rangle \langle c^\dagger d_{k'}\rangle - iG(k)\langle c^\dagger c\rangle \langle c^\dagger d_{k'}\rangle \\
&- iM\langle T^\dagger d_{k'}\rangle \langle d_k^\dagger c\rangle - i\sum_{k''} G^*(k'')\langle d_{k''}^\dagger d_{k'}\rangle \langle d_k^\dagger c\rangle - iG^*(k)\langle c^\dagger c\rangle \langle d_k^\dagger c\rangle \Big) \\
&- \frac{\langle d_k^\dagger c\rangle \langle c^\dagger d_{k'}\rangle}{\langle c^\dagger c\rangle^2} \Big(iM\langle T c^\dagger\rangle - iM\langle T^\dagger c\rangle + i\sum_{k''} \Big(G(k'')\langle c^\dagger d_{k''}\rangle - G^*(k'')\langle d_{k''}^\dagger c\rangle \Big) \Big) \\
&- \langle \dot{d_k^\dagger} d_{k'}\rangle
\end{aligned} \tag{3.10}$$

The abbreviation $T = a_v^\dagger a_c$ was used here. Upon closer look one discovers the time derivative of $\langle d_k^\dagger d_{k'}\rangle$ contained in the first three lines, which cancels with the fourth line, revealing

$$\begin{aligned}
\text{[Eq. (3.9)]} = &\frac{1}{\langle c^\dagger c\rangle} \left(\sum_{k''} iG(k'')\langle c^\dagger d_{k'}\rangle \left(\langle d_k^\dagger d_{k''}\rangle - \frac{\langle d_k^\dagger c\rangle \langle c^\dagger d_{k''}\rangle}{\langle c^\dagger c\rangle} \right) \right) \\
&- \frac{1}{\langle c^\dagger c\rangle} \left(\sum_{k''} iG^*(k'')\langle d_k^\dagger c\rangle \left(\langle d_{k''}^\dagger d_{k'}\rangle - \frac{\langle d_{k''}^\dagger c\rangle \langle c^\dagger d_{k'}\rangle}{\langle c^\dagger c\rangle} \right) \right) \\
&+ iM \frac{\langle c^\dagger d_{k'}\rangle}{\langle c^\dagger c\rangle} \left(\langle T d_k^\dagger\rangle - \frac{\langle T c^\dagger\rangle \langle d_k^\dagger c\rangle}{\langle c^\dagger c\rangle} \right) \\
&- iM \frac{\langle d_k^\dagger c\rangle}{\langle c^\dagger c\rangle} \left(\langle T^\dagger d_{k'}\rangle - \frac{\langle T^\dagger c\rangle \langle c^\dagger d_{k'}\rangle}{\langle c^\dagger c\rangle} \right).
\end{aligned} \tag{3.11}$$

One finds that the error only couples to other error terms of the same $(\langle d_{k''}^\dagger d_{k'}\rangle - \frac{\langle d_{k''}^\dagger c\rangle \langle c^\dagger d_{k'}\rangle}{\langle c^\dagger c\rangle})$ or similar $(\langle T^\dagger d_{k'}\rangle - \frac{\langle T^\dagger c\rangle \langle c^\dagger d_{k'}\rangle}{\langle c^\dagger c\rangle})$ structure. Following the same kind of analysis one finds that this will also be the case for any new error-like terms. Therefore the dynamics of the error stays in "error space" and does not couple to "bare" quantities. In particular, when the error was 0 at $t = 0$, it stays zero.

Also, the error terms are not affected by decay, as long as it affects the "real" and "approximate" part (i.e. the nonlinear part) of the error term in the same way. This

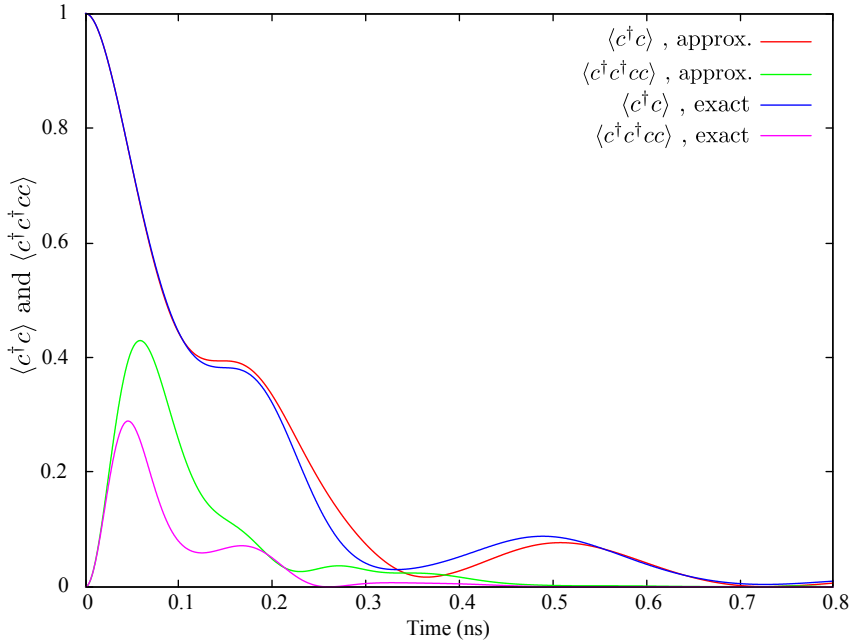

Fig. 3.1.: Comparison of the dynamics of a JCM in a structured background: Nonlinear approximation vs. full numerical simulation. Plotted are the photon density $\langle c^\dagger c\rangle$ as well as the second order correlation $\langle c^\dagger c^\dagger cc\rangle$. Good agreement is found for $\langle c^\dagger c\rangle$ but stronger deviations are present for $\langle c^\dagger c^\dagger cc\rangle$.

is not the case for pure dephasing however, since it affects $\frac{\langle T^\dagger c\rangle\langle c^\dagger T\rangle}{\langle c^\dagger c\rangle}$ while it does not affect $\langle a_c^\dagger a_c\rangle$. The difference between these terms is however coupled to the dynamics of $\langle T^\dagger d_{k'}\rangle - \frac{\langle T^\dagger c\rangle\langle c^\dagger d_{k'}\rangle}{\langle c^\dagger c\rangle}$. As soon as pure dephasing plays a role, the "approximation" becomes a real approximation and is not exact any more. Note that a *decay* of the two-level system with γ_{TLS} does not affect these terms differently and therefore does not diminish the quality of the approximation.

All above analysis is done for a system with only one excitation. For more than one excitation, it may still be a sensible approximation to describe the non-markovian effects of the external continuum by Ω. To check the approximation in the two-photon excitation limit, a JCM coupled to a structured continuum was simulated. Instead of the sine-modulated density of states from Pyragas control, a simpler structuring by two Lorentz functions was chosen. The simulated density of states was

$$\mathscr{D}(\omega) = |G(\omega)|^2 = \frac{\Theta}{\alpha(\omega-\omega_0-\delta/2)^2+1} + \frac{\Theta}{\alpha(\omega-\omega_0+\delta/2)^2+1}, \tag{3.12}$$

with $\Theta = 0.0018\,\mathrm{fs}^{-2}$, $\alpha = 10^{10}\mathrm{fs}^2$, $\delta = 50\,\mathrm{ns}^{-1}$, and $\omega_0 = 1\,\mathrm{fs}^{-1}$. Furthermore, the coupling strength $M = 10\,\mathrm{ns}^{-1}$ was used. $G(k)$ was simply computed as $\sqrt{\mathscr{D}(c_0 k)}$. No further decay channels additional to the coupling to the structured continuum are introduced. The initial state is an excited two-level system and one photon in the cavity. In Fig. 3.1, the results for the photon density $\langle c^\dagger c\rangle$ as well as the second order correlation $\langle c^\dagger c^\dagger cc\rangle$

are displayed. For the photon density, the results agree very well, while the second order corellation is only reproduced qualitatively by the approximation. Another problem is that the numerical implementation becomes unstable for $\langle c^\dagger c\rangle \to 0$, since then the denominator of Ω becomes zero.

There is a straightforward way to extend the approximation to two excitations, making it exact again while still keeping a large numerical advantage compared to a full simulation. Instead of the substitution of Eq. 3.2, one has to approximate triple k-sums by

$$\langle d_k^\dagger d_{k'}^\dagger \mathcal{O} d_{k''}\rangle \approx \frac{\langle d_k^\dagger d_{k'}^\dagger c c\rangle \langle c^\dagger c^\dagger \mathcal{O} d_{k''}\rangle}{\langle c^\dagger c^\dagger c c\rangle}. \tag{3.13}$$

Using a Schrödinger equation approach, one can straightforwardly derive that this equation is exact for fully coherent dynamics with maximally two excitations. Due to the symmetry of the substitution, again decay can be included. This makes this approach very versatile: It allows the study of non-linear effects since it is not bound by the one-excitation limit, it also has the flexibility of expectation-value based EOMs, what is needed e.g. for pseudomode approaches, but it only needs the computational power of a Schrödinger approach. This idea can be extended to include even higher numbers of excitations exactly, using the following substitution on the *highest* level of excitations:

$$\left\langle \left(\prod_{i=1}^{n} d_i^\dagger\right) \mathcal{O} d_k \right\rangle \approx \frac{\left\langle \left(\prod_{i=1}^{n} d_i^\dagger\right) c\right\rangle \left\langle \left(\prod_{i=1}^{n} c^\dagger\right) \mathcal{O} d_k\right\rangle}{\left\langle \left(\prod_{i=1}^{n} c^\dagger\right)\left(\prod_{i=1}^{n} c\right)\right\rangle} \tag{3.14}$$

Note that this can only be used exactly if n is the maximal number of excitations in the system. This shows that for higher excitation numbers one does not gain much – it only reduces the numerical complexity from n excitations to $n-1$ excitations. However it may still make a big enough difference to actually calculate dynamics which would otherwise be too complicated (e.g. go from a 2-excitation manifold to a 3-excitation manifold with a large number of external modes).

3.2 Time-delayed operator equations

Input-output theory, as developed by Gardiner and Collett [83] has become a standard way for the treatment of cascaded dissipative systems [79]. It tackles the issue of dissipation in quantum-mechanical systems on the basis of time-dependent operators (i.e., in the "Heisenberg picture"). Since Pyragas-type feedback can be written as a (dissipative) system-bath interaction, input-output theory is suitable to address systems with Pyragas-type feedback. To derive the appropriate Langevin equations, let us start at the

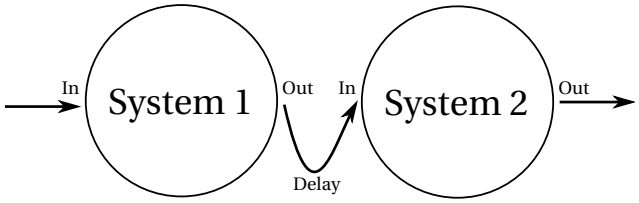

Fig. 3.2.: The textbook case of a cascaded system: The output of system 1 drives system 2 with a finite delay, while the output of system 2 does not drive system 1.

usual Hamiltonian of a system coupled to a reservoir of external modes via the system operator c,

$$H = H_{\text{sys}} + \hbar \int_{-\infty}^{\infty} \left[G(k) c^\dagger d_k + \text{H.c.} \right] \mathrm{d}k + \hbar \int_{-\infty}^{\infty} \omega(k) d_k^\dagger d_k \mathrm{d}k. \tag{3.15}$$

Setting $G(k) = \gamma \sin(kL)$, as usual for Pyragas-type feedback, leads to the Langevin equation for c [76]

$$\partial_t c = -\frac{i}{\hbar}[c, H_{\text{sys}}] - \kappa c + e^{i\omega_0 \tau} c(t-\tau) + F(t). \tag{3.16}$$

Again, $\tau = 2L/c_0$. The derivation, which was presented, e.g., in Ref. [76], is similar to the derivation for expectation values presented in the last chapter. However, one now needs to include "noise" terms $F(t)$, since one cannot put $d_k^{(\dagger)}(t=0) = 0$ on an operator level. These noise terms are crucial in keeping the commutation relation $[c(t), c^\dagger(t)] = 1$. Otherwise, the commutator of $c^\dagger$ and c would decay in time. For Pyragas-type feedback, one gets

$$F(t) = \int_{-\infty}^{\infty} G(k) d_k^\dagger(t=0) e^{-i\omega t} \mathrm{d}k, \tag{3.17}$$

using $\omega = c_0 k$. While this $F(t)$ has some similarities to the definition of an "input field", it does not look like the input field defined in Ref. [83] as

$$d_{\text{in}} \equiv \frac{1}{\sqrt{2\pi}} \int_{-\infty}^{\infty} e^{-i\omega t} d_\omega^\dagger(t=0) \mathrm{d}\omega. \tag{3.18}$$

Note that this definition does not have the k-vector-dependent coupling constant $G(k)$ under the integral. In the original derivation [83], it could be moved outside the integral in a Markov approximation. To directly adapt input-output formalism to time-delayed feedback and to find the exact input (and output) operators, let us go a different way:

Let us start from the textbook case [79] of a cascade of two systems, in which the output of system 1 drives the input of system 2, however not the other way round (cf. Fig. 3.2). The drive is mediated by a markovian reservoir, i.e., system 1 decays in a markovian reservoir, and system 2 gets the excitation from a markovian reservoir. Let us describe the interactions of these systems with the reservoir via the Hamiltonians

$$H_{I_1} = i\hbar \int_{-\infty}^{\infty} G_1(\omega) \left(d_\omega^\dagger c_1 - \text{h.c.} \right) \mathrm{d}\omega \tag{3.19}$$

and

$$H_{I_2} = i\hbar \int_{-\infty}^{\infty} G_2(\omega)\left(d_\omega^\dagger c_2 e^{i\omega\tau} e^{i\phi} - \text{h.c.}\right)\mathrm{d}\omega. \tag{3.20}$$

$c_{1,2}$ are the system operators of system 1 and 2 that couple to the reservoir. Note that system 2 couples to the reservoir with a time delay τ. Let us also allow the signal to acquire an additional phase ϕ on its way from system 1 to system 2. Note that the reservoir shall be markovian, therefore one can set $G_{1,2}(\omega) = \sqrt{\frac{\gamma_{1,2}}{2\pi}}$ for $\omega \geq 0$ with a time-independent $\gamma_{1,2}$. In order to allow only forward propagating signals, and no driving of system 1 by system 2, one needs to set $G_{1,2}(\omega) = 0$ for $\omega < 0$. Using this, one can derive the differential equation for any operator X as [79]

$$\begin{aligned}
\partial_t X = &-\frac{i}{\hbar}[X, H_{\text{sys1}} + H_{\text{sys2}}] \\
&- [X, c_1^\dagger]\left(\frac{\gamma_1}{2} c_1 + \sqrt{\gamma_1} d_{\text{in}}\right) + \left(\frac{\gamma_1}{2} c_1^\dagger + \sqrt{\gamma_1} d_{\text{in}}^\dagger +\right)[X, c_1] \\
&- [X, c_2^\dagger]\left(\frac{\gamma_2}{2} c_2 + \sqrt{\gamma_1\gamma_2}\, c_1(t-\tau)e^{i\phi} + \sqrt{\gamma_2} d_{\text{in}}(t-\tau)e^{i\phi}\right) \\
&+ \left(\frac{\gamma_2}{2} c_2^\dagger + \sqrt{\gamma_1\gamma_2}\, c_1^\dagger(t-\tau)e^{i\phi} + \sqrt{\gamma_2} d_{\text{in}}^\dagger(t-\tau)e^{i\phi}\right)[X, c_2]
\end{aligned} \tag{3.21}$$

This equation is known as the quantum-mechanical Langevin equation for two cascaded systems. Starting from the input operator d_{in}, one can also define the output operator

$$d_{\text{out}} = d_{\text{in}} + \sqrt{\gamma}\, c(t). \tag{3.22}$$

This can be understood as a boundary condition [83], stating that "what goes out is what comes in, plus a signal from the system scaled by the square root of the system-reservoir coupling".

Let us now modify this system to match Pyragas control: Instead of the signal of system 1 driving system 2, it will now drive system 1 again. It will, at this second point of interaction, however have the delay τ and the additional phase ϕ. From the point of system 2, system 1 is not a different system, but "system 2 at time $t-\tau$". This has important implications: For two different systems 1 and 2, the time delay and extra phase may always be transformed away in a linear transformation of the system operators. This will no longer be possible in case of the Pyragas setup.

One can formulate the Langevin equation for Pyragas-type feedback from Eq. 3.21 by putting $c_1 = c_2 \equiv c$. For simplicity, the interaction strength between the system and the feedback reservoir for the signal going "out" (γ_1) shall be the same as the interaction strength with the delayed signal coming back $\gamma_2 = \gamma_1 \equiv \gamma$. Since only the dynamics of *one* system are calculated, one has to change $H_{\text{sys1}} + H_{\text{sys2}} = H_{\text{sys}}$.

From this, one can derive the equation of motion for the system operator c as

$$\partial_t c(t) = -\frac{i}{\hbar}[c(t), H_{\text{sys}}] - \gamma c(t) + e^{i\phi}\gamma c(t-\tau) - \sqrt{\gamma}\left(d_{\text{in}}(t) + e^{i\phi} d_{\text{in}}(t-\tau)\right). \tag{3.23}$$

With this, one can express the "noise term" F using input operators:

$$F(t) = -\sqrt{\gamma}\big(d_{\text{in}}(t) + e^{i\phi} d_{\text{in}}(t-\tau)\big). \tag{3.24}$$

It can be shown explicitly that these equations are equivalent to a description with a sin-modulated reservoir density function. Let us therefore add Eqs. 3.19 and 3.20, and also make the substitution that the system operators c_1 and c_2 are actually the same system operator c. This leads to

$$H_I = i\hbar \int_0^\infty \sqrt{\frac{\gamma}{2\pi}} \big(d_\omega^\dagger c + d_\omega^\dagger c e^{i\omega\tau} e^{i\phi} - \text{h.c.}\big) \mathrm{d}\omega \tag{3.25}$$

Let us put $\phi = \pi$, since the reflection at the mirror creates an additional π phase jump. Let us then use $1 - e^{i\omega\tau} = 2ie^{i\omega\tau/2}\sin(\omega\tau/2)$ to arrive at

$$H_I = -\hbar \int_0^\infty \sqrt{\frac{2\gamma}{\pi}} \big(\sin(\omega\tau/2) e^{i\omega\tau/2} d_\omega^\dagger c + \text{h.c.}\big) \mathrm{d}\omega. \tag{3.26}$$

Defining $\widetilde{d}_\omega^\dagger \equiv e^{i\omega\tau/2} d_\omega^\dagger$, which is a unitary transformation, one arrives at

$$H_I = -\hbar \int_0^\infty \sqrt{\frac{2\gamma}{\pi}} \big(\sin(\omega\tau/2) \widetilde{d}_\omega^\dagger c + \text{h.c.}\big) \mathrm{d}\omega. \tag{3.27}$$

This is the equation of motion of coupling c to a sin-structured bath.

In this approach, time-dependent operator equations are introduced. Time-dependent operator equations lead to multi-time expectation values, when the expectation value dynamics are calculated. Since $c(t)$ couples to $c(t-\tau)$, the expectation value $\langle c^\dagger c\rangle(t)$ couples to quantities like $\langle c^\dagger(t)c(t-\tau)\rangle$. For linear systems subject to Pyragas control, this allows the formulation of expectation value dynamics without the need to calculate the dynamics of the reservoir. The reason is that, whenever an operator equation of motion for normally ordered quantities of the form $\langle A(\partial_t c)B\rangle$ is put up, the solution also contains only operators in normal order. For such operators, the noise terms can be shown to show no influence on the system dynamics, if the noise is white noise [79]. They can therefore be excluded from the simulation.

A problem arises as soon as nonlinear system dynamics shall be considered. To derive the respective equations of motion, one needs commutators such as $[c^\dagger(t), c(t-\tau)]$ to bring the system into normal order. These commutators can generally not be calculated without relying on the noise terms. Without noise, the same-time commutator $[c^\dagger, c]$ would decay in time, which is incorrect. Only the noise terms keep it at 1. This is usually referred to as the "fluctuation-dissipation theorem": If dissipation is present (here: a decay with κ), fluctuations (noise) also have to be present. Whether there is a way to include the noise terms in a multi-time expectation-value based approach without having to calculate them explicitly via integrals in k-space is still a matter of current research.

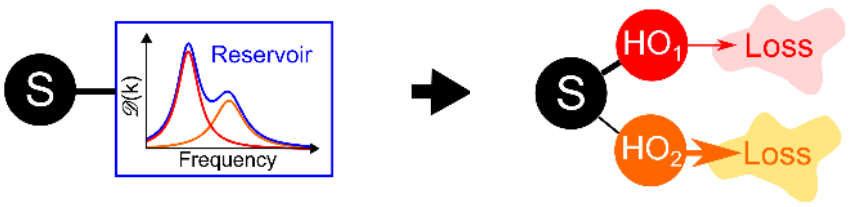

Fig. 3.3.: The idea behind pseudomode theory: Take a system (S) which is coupled to a structured reservoir (left, blue reservoir structure function). In case the structure function can be approximated by a sum of Lorentz functions (red and orange peaks), the reservoir can be modeled as a set of lossy harmonic oscillators (HO_1 and HO_2).

3.3 Pseudomode approach to time-delayed feedback

If a density of states $|G(k)|^2 \equiv \mathscr{D}(k)$ (which is proportional to the so-called reservoir structure function or density function, which is why these terms will be used interchangably in this section) of a non-markovian reservoir can be written as the superposition of Lorentz functions, it is possible to substitute the reservoir by a collection of harmonic oscillators, the so-called pseudomodes [84–87] (cf. Fig. 3.3). Such densities of states are fully determined by their poles and the respective residues, which can then be used to calculate the coupling strength and (markovian) decay rates of the pseudomodes. Such an approach leads to a tremendous decrease of numerical complexity: While, when modeling a density of states as a sum over k-modes the resolution Δk must be very high to eliminate spurious revivals – they appear on the timescale $t \propto (c_0 \cdot \Delta k)^{-1}$ –, with pseudomodes it may be sufficient to use approximately one pseudomode per peak. The intrinsic "open-ness" of pseudomodes, in contrast to a simple discretization of the reservoir, also removes the revivals completely. It is therefore especially suitable for long-term dynamics.

In addition to this numerical advantage, pseudomodes offer an intuitive way to implement the discussed non-markovian reservoir in an actual quantum-optical setup, since pseudomodes can easily be realized through coupled cavities. Pseudomodes provide a "network realization" of the non-markovian reservoir – independent of how the reservoir structure was derived in the first place. In case of time-delayed feedback, it may lead to a realization of Pyragas control without the need of long delay lines. This will certainly help to create integrated structures that use Pyragas control.

The pseudomode theory is closely related to the theory of quasimodes which are derived from the Helmholtz equations of the actual reservoir [88, 89] – however for pseudomodes the approach does not come from a direct modeling of the actual reservoir, but from an analysis of the reservoir structure function. It is of no importance *how* the structure function is created.

Obviously, for certain reservoir structure functions, a lot of information can be gained by looking solely at the poles of the function. This is the motivation for using the pseudomode method to study the structure function of time-delayed feedback. Unfortunately, the function $\sin^2(kL)$ is not a simple superposition of Lorentz functions, and it also does not show any poles one could analyze. Therefore, an extension of the pseudomode method is needed. As we will see, it is possible to approximate $\sin^2(kL)$ with Lorentz functions as soon as one allows *negative* Lorentz peaks.

First the pseudomode method will be introduced for standard examples, as it is done in literature [86, 87, 90], also discussing negative Lorentz peaks. Then, the applicability on time-delayed quantum-coherent feedback will be demonstrated.

Let us start again with the usual Hamiltonian of a system (H_{sys}) coupled to a set of external modes:

$$H = H_{\mathrm{sys}} + \hbar \int_{-\infty}^{\infty} \left[G(k) c^\dagger d_k + \mathrm{H.c.} \right] \mathrm{d}k + \hbar \int_{-\infty}^{\infty} \omega(k) d_k^\dagger d_k \mathrm{d}k. \tag{3.28}$$

It is easy to show that the dynamics do not depend on the full coupling constant $G(k)$, but only on the reservoir structure function $\mathscr{D}(k) = |G(k)|^2$. For this, let us substitute [87]

$$d_k = G^*(k) b_k. \tag{3.29}$$

The new operators obey the commutation relation

$$[b_k, b_{k'}^\dagger] = \frac{1}{G^*(k)G(k')} [d_k, d_{k'}^\dagger] = \frac{1}{\mathscr{D}(k)} \delta(k-k'). \tag{3.30}$$

The Hamiltonian reads as

$$H = H_{\mathrm{sys}} + \hbar \int_{-\infty}^{\infty} \left[\mathscr{D}(k) c^\dagger b_k + \mathrm{H.c.} \right] \mathrm{d}k + \hbar \int_{-\infty}^{\infty} \omega(k) \mathscr{D}(k) b_k^\dagger b_k \mathrm{d}k. \tag{3.31}$$

It is apparent that the commutation relations as well as the Hamiltonian only depend on $\mathscr{D}(k)$.

The pseudomode method was originally derived for the one-excitation subspace [86], in which the substitution $d \to b$ was done not on the operator level, but on the level of probability amplitudes of the wave function. There, b is called "reduced probability amplitude" [87].

In the pseudomode method, the coupling to the reservoir described by $\mathscr{D}(k)$ will be replaced by the coupling to a finite set of lossy bosonic modes (cf. Fig. 3.3), usually one for each pole in $\mathscr{D}(k)$ [86]. Let us now derive the properties of these bosonic modes, given a reservoir structure function $\mathscr{D}(k)$. We shall describe the j-th pseudomode with the operators $\zeta_j^{(\dagger)}$, coupling to the system with the coupling strength $\sqrt{D_j}$. The pseudomode has angular frequency ω_j and decay rate κ_j.

In a master equation, the pseudomodes can be described by the Hamiltonian

$$H_{\mathrm{pm}} = \hbar \sum_j \left[\sqrt{D_j} \left(c^\dagger \zeta_j + \zeta_j^\dagger c \right) + \omega_j \zeta_j^\dagger \zeta_j \right] \tag{3.32}$$

and Lindblad terms for the dissipation, coupled to ζ_j with strength κ_j, leading to the master equation for the density matrix ρ

$$\frac{\mathrm{d}}{\mathrm{d}t}\rho = \frac{i}{\hbar}[\rho, H_{\mathrm{sys}} + H_{\mathrm{pm}}] + \sum_j \mathscr{L}_j \rho. \tag{3.33}$$

Here, the Lindblad operators are defined as

$$\mathscr{L}_j \rho = \kappa_j \left(2\zeta_j \rho \zeta_j^\dagger - \zeta_j^\dagger \zeta_j \rho - \rho \zeta_j^\dagger \zeta_j \right). \tag{3.34}$$

Note that the pseudomodes are not coupled amongst themselves. This is a severe limitation which needs to be lifted for the description of time-delayed Pyragas-type feedback – however it is sufficient for modeling a spectrum consisting of Lorentz peaks.

On the one-excitation subspace, the equations of motion for probability amplitudes usually look like

$$\begin{aligned} \partial_t c(t) &= f(c(t)) - i \sum_j D_j \xi_j(t) \\ \partial_t \xi_j(t) &= -(\kappa_j + i\omega_j)\xi_j(t) - i c(t) \end{aligned} \tag{3.35}$$

Here, $c(t)$ is the probability amplitude of finding the excitation in the system. The coupling from the system to the j-th pseudomode is D_j. $\xi_j(t)$ is the *reduced* probability amplitude of finding the excitation in the j-th pseudomode, coming from a substitution of ζ_j equivalent to Eq. 3.29, using $\sqrt{D_j}$ instead of $G(k)$. Note that the equation is thus written such that D_j only appears in the equation of c and not of ξ_j, by writing it in terms of reduced probability amplitudes of the reservoir. This is just a notational issue that will make it easier to include negative Lorentz peaks later on. The system dynamics are abbreviated by the function $f(c(t))$, and can be arbitrarily complex – in fact, there might even be more system variables than just $c(t)$. Due to the decay, the probability of having one excitation is decreasing, Eqs. 3.35 are therefore not the full solution of a Schrödinger equation. One could interpret Eqs. 3.35 as the solutions of a Schrödinger equation after carrying out a Wigner-Weisskopf approximation for the Markovian reservoirs coupled to the pseudomodes.

To connect the pseudomode ansatz (Eq. 3.32) to the original problem (Eq. 3.28), the parameters D_j, ω_j, and κ_j can be directly read [85] from the structure function, if the structure function is written as a sum of Lorentz peaks of the form

$$\mathscr{D}(k) = ... + \frac{A_j \kappa_j^2}{\kappa_j^2 + \big(\omega(k) - \omega_j\big)^2}. \tag{3.36}$$

One finds $D_j = \frac{\pi}{c_0} A_j \kappa_j$ when a linear dispersion relation is assumed, $\omega(k) = c_0|k|$. Additional *constant* terms in the structure function of the form $\mathscr{D}(k) = ... + K + ...$ shall be included in the system+pseudomodes master equation as a *Markovian* decay of the respective system variable with decay constant $\kappa_0 = \frac{\pi}{c_0} K$, using the standard Lindblad approach.

Eq. 3.36 also demonstrates a straightforward way to include negative Lorentz functions: One just has to put a minus sign in front of any D_j appearing in the equations. However this leads to a non-Hermitian Hamiltonian (Eq. 3.32), which is unphysical. There has to be a different explanation if negative Lorentz terms are in themselves physical. This explanation can be provided by a coordinate transform. Let us discuss this on the example of a simple reservoir structure function:

$$\mathscr{D}(k) = K - \frac{A_1 \kappa_1^2}{\kappa_1^2 + \big(\omega(k) - \omega_1\big)^2}. \tag{3.37}$$

This structure function describes a markovian decay (via K), which at ω_1 has a Lorentz-type dip. In order to make the situation physical, it is necessary that $\mathscr{D}(k) > 0$ for all k, in particular for $\omega(k) = \omega_1$, i.e., in the center of the dip. This condition leads to

$$K \geq A_1. \tag{3.38}$$

For $K = A_1$, the reservoir should not introduce any decay in the long-time limit to a system oscillating with ω_1. Translated into pseudomodes, this reservoir creates a markovian decay with decay rate $\kappa_0 = \frac{\pi}{c_0} K$ and additionally a coupling to a pseudomode with frequency ω_1, decay rate κ_1, and (unphysical) coupling constant to the system $-D_1 = -\frac{\pi}{c_0} A_1 \kappa_1$. Suppose now a harmonic oscillator with angular frequency ω_0 is coupled to this reservoir. We restrict ourselves to the one-excitation limit and describe the probability amplitude of the one-excitation state of this harmonic oscillator with c. This leads to the following differential equations:

$$\begin{aligned} \partial_t c(t) &= -(\kappa_0 + i\omega_0) c(t) + i \frac{\pi}{c_0} A_1 \kappa_1 \xi_1(t) \\ \partial_t \xi_1(t) &= -(\kappa_1 + i\omega_1) \xi_1(t) - i c(t) \end{aligned} \tag{3.39}$$

Note the different signs in the coupling from c to ξ_1 compared to the coupling from ξ_1 to c. To get physical dynamics, let us now substitute

$$\tilde{\xi}_1 := -i\sqrt{\frac{\pi}{c_0}\kappa_1 A_1}\,\xi_1 = -i\sqrt{D_1}\,\xi_1. \tag{3.40}$$

This gives

$$\begin{aligned}\partial_t c(t) &= -(\kappa_0 + i\omega_0)c(t) - \sqrt{D_1}\,\tilde{\xi}_1(t)\\ \partial_t \tilde{\xi}_1(t) &= -(\kappa_1 + i\omega_1)\tilde{\xi}_1(t) - \sqrt{D_1}\,c(t)\end{aligned} \tag{3.41}$$

Note that the pseudomode leads to a term that looks like a collective decay. This becomes even clearer after re-writing Eq. 3.41 as

$$\begin{aligned}\partial_t c(t) &= -\big((\kappa_0 - \sqrt{D_1}) + i\omega_0\big)c(t) - \sqrt{D_1}\big(c(t) + \tilde{\xi}_1(t)\big)\\ \partial_t \tilde{\xi}_1(t) &= -\big((\kappa_1 - \sqrt{D_1}) + i\omega_1\big)\tilde{\xi}_1(t) - \sqrt{D_1}\big(c(t) + \tilde{\xi}_1(t)\big)\end{aligned} \tag{3.42}$$

These equations describe a system as well as a pseudomode, which show individual decays as well as a decay into a common reservoir. The individual decay rates are $\kappa_0 - \sqrt{D_1}$ and $\kappa_1 - \sqrt{D_1}$, respectively, while the decay rate into the collective reservoir is $\sqrt{D_1}$. This choice of substitutions leads to a physical scenario as long as $\kappa_{0,1} \geq \sqrt{D_1}$. For other values, there also exist other physical scenarios derivable through substitutions. Necessary condition is that the real part of the eigenvalues of the matrix relating $\partial_t(c, \{\xi_j\})$ to $(c, \{\xi_j\})$ is zero or negative, which means that there is no mode that gains energy through dissipation. In above case, using Eq. 3.41, this leads to the equation

$$D_1 = \frac{\pi}{c_0}\kappa_1 A_1 \leq \kappa_0\kappa_1 = \frac{\pi}{c_0}K\kappa_1. \tag{3.43}$$

From this, we recover Eq. 3.38, $K \geq A_1$. All this demonstrates that a negative Lorentzian peak in the reservoir density function $\mathscr{D}(k)$ can be interpreted in the pseudomode formalism as a pseudomode *dissipatively* coupled to the system via a common reservoir (cf. Fig. 3.4).

One can also derive the pseudomode "network" of a density consisting of a sharp Lorentzian centered within a broad Lorentzian peak [90]. The result is that the system and a "low-loss" pseudomode are both connected to a common "high-loss" pseudomode. Interestingly, the properties of these effective pseudomodes are not the same as the properties of the sharp and broad peak, so one cannot straightforwardly derive the effective network by reading their parameters. However, the structure is the same as above: Peaks are coherently coupled harmonic oscillators, dips are dissipatively coupled harmonic oscillators.

These examples show that negative Lorentz dips can be interpreted physically within the pseudomode formalism if common reservoirs and coupling between pseudomodes

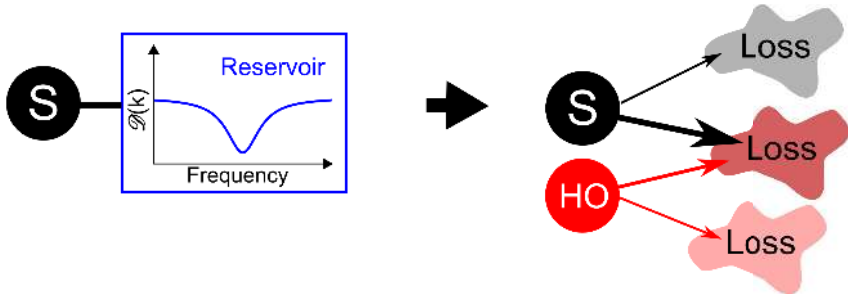

Fig. 3.4.: Within the pseudomode formalism, a dip in the density function can be interpreted as a harmonic oscillator coupled dissipatively to the system via a common Markovian reservoir. The system as well as this pseudomode may also have further Markovian decay channels.

are allowed. For a numerical treatment however, such an explanation is not needed. One can simply add negative Lorentz peaks via a minus sign in front of D_j and make sure the final density of states stays positive.

Let us now transfer the method to time-delayed Pyragas-like feedback. For this, let us model the density function $\mathscr{D}(k) = \gamma^2 \sin^2(kL)$ (cf. chapter 2.3).

One can write $\sin^2(x)$ as an infinite sum of infinitely wide Lorentz peaks:

$$\sin^2(x) = \lim_{a\to\infty}\left[\frac{1}{2} - \frac{1}{4\sqrt{a}\,\mathrm{csch}\left(2\sqrt{a}\right)} \sum_{n=-\infty}^{\infty} \frac{(-1)^n}{1+\frac{1}{a}\left(x-\frac{n\pi}{2}\right)^2}\right] \tag{3.44}$$

We see that $\sqrt{a}$ is proportional to the Lorentz peak width. Furthermore, as one could expect, negative and positive Lorentz functions alternate. Finally, there is an offset of $1/2$ to make the whole function positive – this is a first hint that a Markovian decay channel directly connected to the system will be needed.

First, it looks like we did not gain anything. Even worse, one infinite sum (cf. chapter 2.3) was replaced by two infinities. However this also offers a way to approximate: One only needs to cover the $\sin^2(kL)$ function over the frequency range in which the system shows interesting dynamics. The markovian initial dynamics of Pyragas control (for times $t < \tau$) is even exactly included, and only one Lorentz peak is needed per "sinus bump" or "dip". As an approximation, one therefore will usually only need a few to a few dozen Lorentz peaks to approximate Pyragas-type feedback sufficiently. In that case, the infinite width also needs to be replaced by a finite width. In practice, widths of the order of $\pi/2$ will be used, because they lead to good approximations in the desired frequency range, tested by numerical simulations (see below).

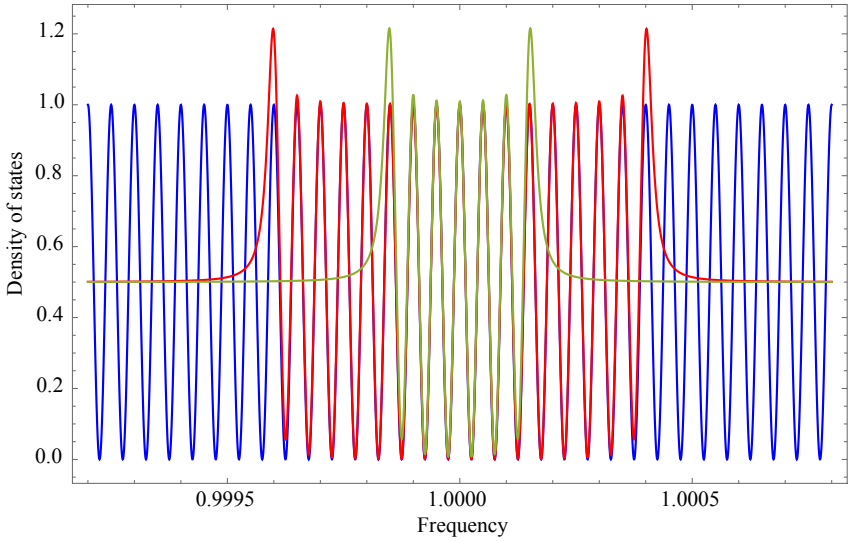

Fig. 3.5.: Approximation of a $\sin^2$-modulated density of states by a set of Lorentzians centered around $\omega_0 = 1$, as discussed in the text. Blue: $\sin^2(\omega)$, red (green): Approximation using 33 (13) Lorentz functions around the central frequency ω_0. Here, $A = 0.908$ was used (cf. Eq. 3.45) which is slightly too low for the 13 mode case and therefore makes the oscillation not reach 0. Such a deviation leads to an additional decay compared to the "exact" case of a $\sin^2$ modulation.

As an example, let us calculate the mode structure for Pyragas-type time-delayed feedback around $\omega_0 = 1$ (in units of 1/time, cf. Fig. 3.5). The approximate density of states which shall approximate $\sin^2(\omega L/c)$ is written as

$$\mathscr{D}(\omega) = \frac{1}{2} + A \sum_{n=0}^{N} \frac{(-1)^n}{\left[(\omega - \omega_0)\,\frac{L}{c_0} - \left(n - \frac{N}{2}\right)\frac{\pi}{2}\right]^2 + 1}. \tag{3.45}$$

Let us choose two different mirror distances, which lead to two opposite phases of the feedback signal. For "positive feedback" the mirror distance L is chosen such that $\frac{\omega_0 L}{c_0} = 10000 \cdot 2\pi$, leading to $\exp(2\omega_0 L/c_0) = +1$. For "negative feedback", let us set L such that $\frac{\omega_0 L}{c_0} = 10000.25 \cdot 2\pi$, leading to $\exp(2\omega_0 L/c_0) = -1$. The number of Lorentz peaks, $(N+1)$ has to be odd with one more positive than negative peak in order to keep $\mathscr{D}(\omega)$ positive. For positive feedback, N has to be an integer multiple of 4. A is a scaling factor, which is approximately 1. It has to be chosen appropriately for a given number of Lorentz peaks such that the density function is never below zero. For feedback-induced stabilization, it is crucial that A is chosen such that the dip in the sinus function around the frequency that is to be stabilized is actually very close to zero – otherwise an additional decay is visible. In Fig. 3.5, the density function for 33 and 13 modes is plotted and compared to the $\sin^2$ function. "Overshoot" effects are present at the end of the modulated region, where it transforms into a flat density of states. In the center, the $\sin^2$ function is well approximated.

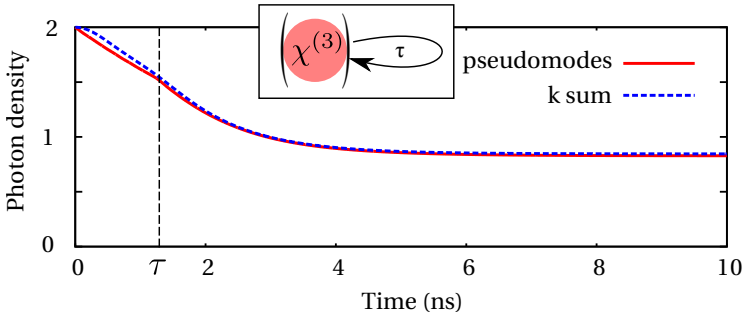

Fig. 3.6.: Comparison of the photon density dynamics calculated by a k-sum and calculated via 33 pseudomodes. The system consists of a cavity containing a $\chi^{(3)}$ medium and subject to time-delayed Pyragas-type feedback with delay time τ (see inset). There is excellent agreement between the two results. For short times, the pseudomode approach even better reproduces the expected exponential decay, while the k-sum over-estimates the photon density.

From Eq. 3.45 we find that the decay rate of the individual pseudomodes is $\frac{c_0}{L}$. This is actually an approximate value: In the full formula to express $\sin^2(x)$ (cf. Eq. 3.44) this value is taken in its limit to infinity. However for a finite number of pseudomodes, above value leads to a very good agreement, as it is visible in Fig. 3.5. However, there is some flexibility in this value: Doubling it, and correcting the peak heights by choosing a different A, does not change the mode structure much. The coupling of the pseudomodes is found to be $A\frac{\pi}{L}$.

At this point it must be mentioned that a pseudomode approach contains actually two steps: First, the modeling of the density function via Lorentz functions, and second the representation of Lorentz functions by harmonic oscillators. The first step contains – especially in the case of Pyragas-type feedback – large approximations, since one has to deal with the infinities of Eq. 3.44. The second step demands that the pseudomode method in itself is valid. There does not seem to be an explicit proof of the pseudomode theory in literature for arbitrary systems. The method will break down as soon as the frequency of the system is no longer much larger than any other rate of the system, since at that point the infinite tails of Lorentz peaks will create unphysical results when they reach into the "negative frequency realm". However it is remarkable that in all simulations performed for this thesis deviations from the "full external mode simulation" ansatz could always be attributed to imperfect approximations of the density function by Lorentz peaks or inaccuracies of the full simulation itself (especially for small times). A breakdown of the pseudomode theory itself was never observed, even when multiple excitations and nonlinearities were included.

It is necessary to test the validity of the pseudomode method for time-delayed feedback numerically, in order to evaluate its usefulness for time-delayed feedback. Since it shall be applied to more complex systems, it needs to be checked for a *nonlinear* system with *more than one excitation*. The system chosen for this task will be discussed in detail

later in Chapter 5: It is a single mode cavity including a Kerr nonlinearity coupled to time-delayed feedback. The initial state of the cavity mode is a two-photon Fock state. For a certain choice of the delay τ, a stabilization of the one-photon Fock state within the cavity is expected, as presented in section 5.1.

In Fig. 3.6, the dynamics of the photon density of such a system are plotted, calculated by including the "k-sum", i.e., directly modeling the external feedback reservoir, and in comparison by using the pseudomode method with 33 modes. The number of external modes for the full calculation is 4 000 with a mode distance of $10^{-7}\,\mathrm{fs}^{-1}$. The coupling γ to the reservoir (cf. Eq. 2.38) is $0.01\sqrt{2}\,\mathrm{fs}^{-1}$.

There is an excellent agreement for long times between the two methods, in particular the pseudomode approach reproduces the stabilization. This is interesting in so far that there are actually lossy modes coupled to the system in the pseudomode approach – in particular, the system experiences markovian decay through the $1/2$-term in Eq. 3.45. The negative Lorentz peaks however counterbalance these processes. The stabilization crucially depends on the choice of A. If A is chosen slightly smaller, so that the modulation of the density function does not reach 0, a slow decay in the pseudomode-modeled dynamics is present.

It is remarkable that for short time scales, the pseudomode approach even seems to better recreate the expected exponential decay of the photon density. The k-sum ansatz overestimates the photon density due to the finite bandwidth of the covered frequency range. In the pseudomode approach, the built-in markovian decay circumvents this problem, since the frequency range is in fact infinite.

The performance of the pseudomode method was also checked on a Jaynes-Cummings system. For this, the $\chi^{(3)}$-medium was replaced by a two-level system which coupled to the cavity mode with a coupling constant $M = 5.0 \cdot 10^{-5}\,\mathrm{fs}^{-1}$. Further details of this system will be discussed later on in section 5.2. The photon density dynamics is plotted in Fig. 3.7. The initial state is again a 2-photon Fock state of the cavity mode. The pseudomode calculations are done with 21 pseudomodes. Again there is excellent agreement, for the overall dynamics as well as for the single Rabi oscillations.

Even when using pseudomodes, it is advisable to not use more modes than needed to keep the numerical load low. To check the dependence of feedback dynamics on the number of pseudomodes, the dynamics of above system *without* any nonlinearity was calculated with different numbers of pseudomodes. In those simulations, the coupling to the reservoir was increased by a factor of 4 in order to see stronger feedback effects. The results are displayed in Fig. 3.8 for 11, 23, 31, and 43 pseudomodes. Only small deviations are present even down to the 11 mode case. In the inset, a zoom into the region where the feedback sets in is presented. In theory, this should be a infinitely sharp kink. For 11

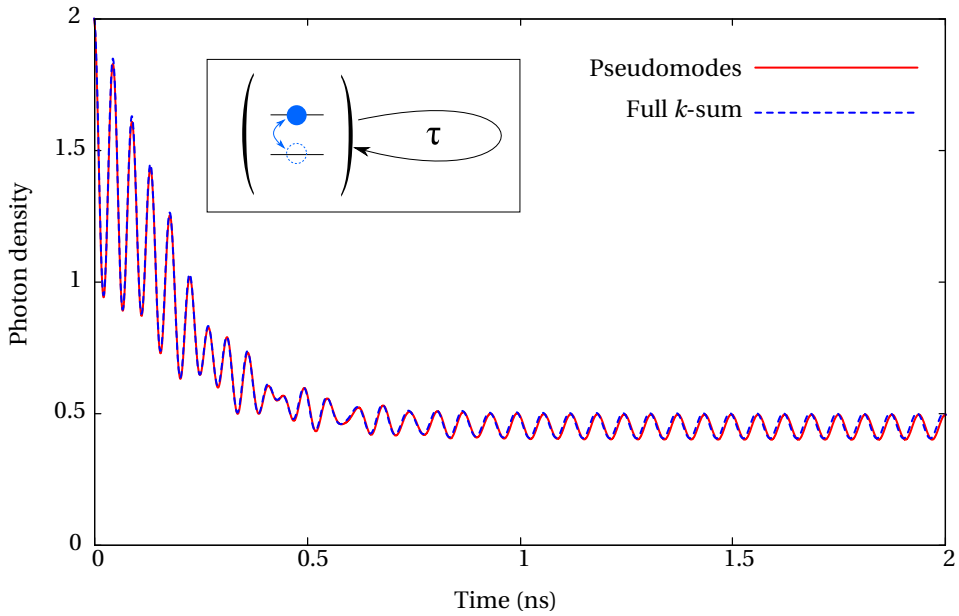

Fig. 3.7.: Dynamics of a Jaynes-Cummings model (i.e., a two-level system coupled to a cavity mode, cf. inset) subject to time-delayed feedback. The plot demonstrates how well the dynamics (blue curve) can be approximated with pseudomodes (red curve).

modes there is a quite strong deviation, but the more modes one takes the sharper it gets. However there does not seem to be much gain by extending the system beyond 23 modes. The reason for this is that the outer pseudomodes are already too off-resonant from the cavity mode, so that they barely get excited.

Besides the numerical advantages, pseudomodes could also point towards a network representation of Pyragas control: In simple systems, as it was presented above, on can interpret positive and negative Lorentz peaks as a network of coupled harmonic oscillators. In the delayed feedback case, such an interpretation is not straightforward, since a large number of modes has to be treated and the necessary transformation becomes very complex. This is clearly an interesting topic of future research. It should be expected that such a representation exists as long as the mode structure is physical. If such a network representation is found, it will pave the way for integration of Pyragas control without the need of long delay lines, since it would only require the *local* coupling of several harmonic oscillator modes (e.g., provided by photonic cavities) to the system. In analogy to the discussed simple cases, here it shall be conjectured that the network structure will consist of $(N/2+1)$ harmonic oscillators coupled to the system, as well as a markovian reservoir coupled to the system. Additionally, there should be $N/2$ harmonic oscillators coupled to the system dissipatively by sharing this network as a common dissipation channel.

To summarize the benefits and drawbacks of the pseudomode method when it is applied to Pyragas-like time-delayed feedback, we found the following benefits:

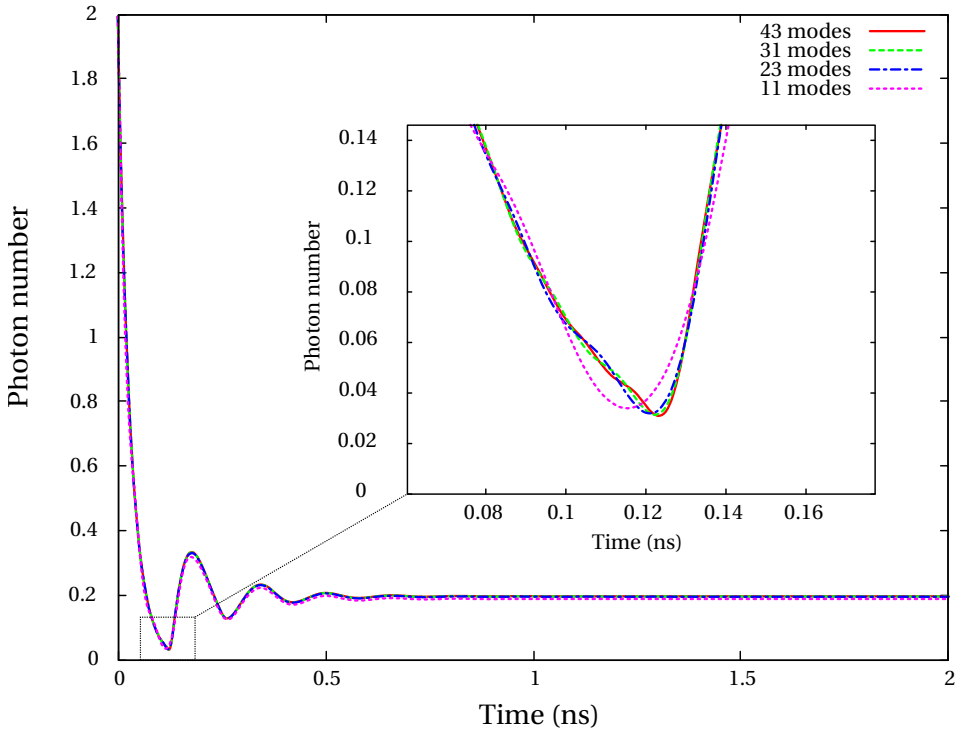

Fig. 3.8.: Comparison of results calculated with different numbers of pseudomodes (11, 23, 31, and 43). Shown is the dynamics of a cavity mode subject to Pyragas-type feedback. The initial state is a 2-photon Fock state. The simulations give almost identical results. The inset shows a zoom to the region where the feedback first sets in. The higher number of pseudomodes better recreates the sharp kink, however it does not make a strong difference for mode numbers larger than 23.

1. Pseudomodes drastically reduce the number of modes needed,
2. pseudomodes show a real equilibration of the system in the long term, without the appearance of spurious revivals,
3. pseudomodes reproduce the initial markovian decay better than the direct k-sum calculation,
4. pseudomodes do not increase the numerical load if the calculation runs for a longer time span, in contrast to other approaches [77],
5. pseudomodes may point towards a "network-like" implementation of Pyragas control without the need for long delay lines.

However, it also has its drawbacks:

1. The accuracy of the calculation is hard to estimate beforehand, and strongly depends on parameters such as A and κ,
2. still a quite large number of modes is needed, which limits the number of excitations that can be calculated,
3. dissipation is crucial, which rules out Schrödinger equation based calculations – however stochastic Schrödinger equation solutions might be possible,
4. there is no formal proof of the validity of the approach.

3.4 Further methods

In this section methods will be discussed which were studied during the preparation of this thesis, which however proved to be not very successful in improving the modeling of time-delayed feedback.

3.4.1 Time-dependent Lindblad operators

It has been proposed by An et al. [66], that non-markovian effects can be included by a time-dependent, and in some cases negative decay rate (modeled via Lindblad operators), in tandem with a time-dependent phase shift. As it was shown in section 3.1, within the one-excitation limit it is possible to construct this time-dependence by calculating Ω. However, this approach only works for linear systems or in the one-excitation limit. For non-linear systems, the non-markovian reservoir might, e.g., affect $\langle c^\dagger c^\dagger cc\rangle$ differently than $\langle c^\dagger c\rangle^2$, e.g. decreasing the photon intensity but increasing the $\langle c^\dagger c^\dagger cc\rangle$ term. This is exactly what will be presented in the discussion of the behavior of a system with $\chi^{(3)}$-nonlinearity under time-delayed feedback (section 5.1). Lindblad terms, however, will affect both of these terms in the same manner. As we have seen in section 3.1, it might however be a first approximation to analyze the dynamics.

3.4.2 Equations of motion for the full k-sum

Instead of calculating the dynamics of each of the external modes, one could also calculate the dynamics only of the *coherent sum* as it appears in the equations of motion for the system parameters. This will lead to an infinite hierarchy of equations, which has to be cut at a certain order. This shall now be discussed using the example of a cavity with angular frequency ω_0 coupled to a structured bath. It is described by the Interaction Hamiltonian

$$H = \hbar c^\dagger \sum_k G(k) d_k \mathrm{e}^{i(\omega_0-\omega_k)t} + \mathrm{H.c.}. \tag{3.46}$$

Let us define

$$K_n \equiv \sum_k G(k)\big(i(\omega_0-\omega_k)\big)^n d_k \mathrm{e}^{i(\omega_0-\omega_k)t} \tag{3.47}$$

as well as

$$\Gamma_n \equiv \sum_k |G(k)|^2 \big(i(\omega_0-\omega_k)\big)^n. \tag{3.48}$$

One can then rewrite

$$H = \hbar c^\dagger K_0 + \hbar K_0^\dagger c. \tag{3.49}$$

One finds that the newly defined K_n operators commute in the following way:

$$[K_n, K_m^\dagger] = (-1)^m \Gamma_{m+n}. \tag{3.50}$$

Using this, one can now calculate the infinite hierarchy of equations of motion for a single bosonic mode coupled to a reservoir of modes:

$$\partial_t \langle c^\dagger c\rangle = 2\,\mathrm{Im}\big(\langle c^\dagger K_0\rangle\big) \tag{3.51}$$

$$\partial_t \langle c^\dagger K_n\rangle = -i\Gamma_n \langle c^\dagger c\rangle + i\langle K_0^\dagger K_n\rangle + \langle c^\dagger K_{n+1}\rangle \tag{3.52}$$

$$\partial_t \langle K_m^\dagger K_n\rangle = -i\Gamma_n \langle K_m^\dagger c\rangle + i(-1)^m \Gamma_m \langle c^\dagger K_n\rangle + \langle K_{m+1}^\dagger K_n\rangle + \langle K_m^\dagger K_{n+1}\rangle. \tag{3.53}$$

The equations of motions are now developed in $(\omega_0-\omega_k)$, which means that it is necessary to restrict the bath to a finite frequency window in order to achieve convergence. The whole information on the reservoir structure is now contained in the factors Γ_n. They have to be calculated very precisely. A numerical implementation showed that the whole approach is numerically very unstable. A switch from `double` to `long double` precision in the C code almost doubled the time until the numerics gave "unphysical" values. There was also a strong dependence of the stability on the exactness of the integration when calculating Γ_n. Using a smaller frequency range led to greater stability, however also highly unprecise results. This is expectable due to the factors of $(\omega_0-\omega_k)^n$ appearing in K_n and Γ_n. While it was not possible to make the method outperform a direct integration of the k-sums, the fact that it is still bounded by numerical accuracy rather than by a breakdown of a "physical" approximation gives hope that there might be

a more sophisticated way to express Γ_n. This might lead to higher stability and make the method useful.

4 Control of modes in a quantum network by time-delayed feedback

Parts of the results discussed in this chapter have been published in Physical Review A [91]. Parts of this chapter are also submitted for publication as a conference paper for the SPIE Photonics West 2016 conference.

In this chapter, it is proposed to use time-delayed feedback on nodes of a quantum network is to selectively stabilize certain network states. Since these states can be highly non-local and entangled, this gives the ability to create an entangled state in the network, even starting from a fully separable initial state.

Quantum networks, as any network, consist of a number of *nodes* coupled together via *links*. In contrast to classical networks, the nodes are objects which show highly quantum-mechanical behavior and therefore allow for non-classical correlations between the nodes. The interconnects also need to be able to carry quantum information. A very suitable carrier is the photon [92]. A possible realization of a quantum network would be photonic cavities, possibly containing single atoms [92], coupled via waveguides, optical fibers [16, 93], or, for close nodes, directly via photon tunneling.

In the presented case, the coherent evolution of the quantum network is described using a Hamiltonian of the form

$$\hat{H} = \sum_i \left[\hat{H}_i(\hat{c}_i^{(\dagger)}) + \sum_{j \neq i} M_{ij} \hat{c}_i^\dagger \hat{c}_j \right]. \tag{4.1}$$

$\hat{H}_i$ is a (sub-)Hamiltonian which describes the dynamics at node i – examples would be the Hamiltonian of a cavity or a Jaynes-Cummings model. The excitation of node i is described by the ladder operators $\hat{c}_i^{(\dagger)}$. The coupling is done directly via the coupling matrix M_{ij}, which models photon tunneling, but can also be realized effectively via fiber coupling [94]. For the Hamiltonian to be Hermitian, the coupling matrix M must obey $M_{ij} = M_{ji}^*$. M gives the network *topology*, of which there are many different types [95]. Even for the most simple topology, next-neighbor coupling, complex dynamics can be observed, e.g. a Mott-insulator – superfluid transition [96] in case of coupled Jaynes-Cummings systems. Networks with only next-neighbor coupling are often called "X-Hubbard models", where X characterizes the node type, e.g. "Jaynes-Cummings".

A more complex network geometry, the Appolonian network, has also recently been investigated [97].

Hamiltonians of the type described in Eq. 4.1 usually have complex eigenstates with delocalized excitation distributions. The aim of the method proposed in this chapter is to single out one of these eigenstates (or "eigenmodes") by coupling one or several nodes to structured reservoirs that provide time-delayed feedback. The idea is that the different eigenmodes react differently to the additional feedback loop – in the best case scenario, one of the modes is fully unaffected while all the others experience a strong decay channel. This dynamics then automatically drives the network in a state mainly consisting of this unaffected mode. The subspace spanned by the unaffected modes is called a "decoherence-free subspace". It is well-known that decoherence-free subspaces arise when several nodes are coupled to the same reservoir [98–100], in which case decay paths interfere destructively. Decoherence-free subspaces are used for the creation of entanglement in bipartite systems [101, 102].

A problem with the creation of decoherence-free subspaces via *common* reservoirs is that one has to make sure the two decay paths can actually interfere. This imposes profound limitations on the quantum nodes: They must not be too far away from each other, and they must decay in the same way into the reservoir. For example, the emission of photons of orthogonal polarization would not create a decoherence-free subspace. These limitations may be met by close, identical atoms in an optical lattice, for which the terms "sub-radiant state" (a state with suppressed decay due to the coupling to a common reservoir) and "super-radiant state" (a state with enhanced decay into a common reservoir) are typically used. Even there, the problem arises that the sub-radiant state is usually pre-defined by symmetry conditions.

It would therefore be desirable to have a mechanism to create decoherence-free subspaces by only coupling network nodes to individual reservoirs. In order to address the different modes, one cannot utilize their symmetry to differentiate between them: symmetry is not defined on the single node level, but as a property of the whole mode. Instead, one can use the different frequencies that arise due to the coupling with M. This however means that the coupling to the reservoir has to be frequency-dependent: the reservoir needs to be *non-Markovian*.

Non-Markovian reservoirs are well-known in literature for their effects on entanglement. They can lead to faster-than-exponential entanglement decay ("sudden death"), but also "revivals" [58, 63–65]. They can also be used to stabilize [62] or create [103, 104] entanglement. As time-delayed feedback can be seen as the coupling to a highly controllable non-Markovian reservoir, strong effects on entanglement can be assumed. In the following it will be shown that one can tune the reservoir, using the delay time τ, to single out the "entangled network mode of our choice" and thereby create entanglement.

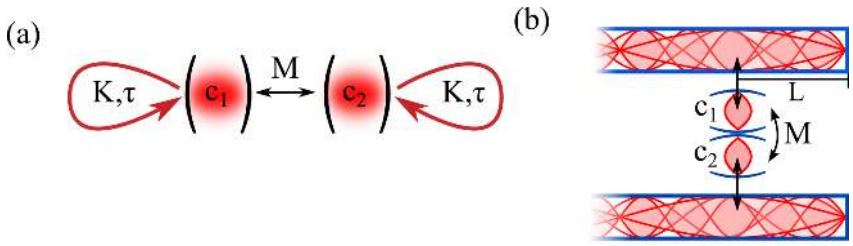

Fig. 4.1.: The simplest realization of a network, discussed first, consisting of two coupled nodes (coupling constant M) that are both subject to time-delayed feedback. (a): Schematic drawing of the full system. For both nodes, the time-delayed feedback will have the same delay time τ and strength K. (b): A possible realization, using coupled cavities. Each cavity is coupled to a waveguide that that provides time-delayed feedback. One end of the waveguide is at distance L which leads to a feedback delay time $\tau = 2L/c_0$.

4.1 Simple two-node network

For simplicity, the analysis will start by discussing the simplest of all possible networks, consisting of two coupled nodes (see Fig. 4.1). The nodes will be modeled as harmonic oscillators, realizable e.g. via single-mode cavities. Let us stick to the subspace of maximally one excitation quantum, which enables us later to discuss the system using time-delayed differential equations for the probability amplitudes. Due to that constraint, there is no difference between fermionic and bosonic nodes, so that one can also describe networks consisting of quantum dots, atoms [68], or superconducting artificial atoms [73]. The mechanism described here is therefore quite general.

For this System, the node Hamiltonians (cf. Eq. 4.1) simply read as

$$\hat{H}_i = \hbar\omega_i \hat{c}_i^\dagger \hat{c}_i, \; i = 1,2. \tag{4.2}$$

Let us further simplify the system by putting $\omega_1 = \omega_2 := \omega_0$. The coupling between the two nodes will be mediated by $M_{12} = M_{21} := M$. Both nodes couple separately to reservoirs that provide time-delayed feedback. A possible experimental setup is depicted in Fig. 4.1(b): The two coupled cavities could each be connected to a waveguide, that has one end at a distance L which determines the feedback delay time. The coupling strength K and the feedback delay time τ shall be equal for both nodes. Solving the Schrödinger equation with a state $|\psi\rangle$, one can derive time-delayed differential equations for the probability amplitudes $c_1 := \langle 10|\psi\rangle$ and $c_2 := \langle 01|\psi\rangle$. Here, the states $|10\rangle$ ($|01\rangle$) describe the situation in which one photon is in the left (right) cavity and none is in the right (left). The differential equations read as (cf. section 2.3):

$$\begin{aligned}
\frac{\mathrm{d}}{\mathrm{d}t}c_1(t) &= -i\omega_0 c_1(t) - iMc_2(t) - Kc_1(t) + Kc_1(t-\tau) \\
\frac{\mathrm{d}}{\mathrm{d}t}c_2(t) &= -i\omega_0 c_2(t) - iMc_1(t) - Kc_2(t) + Kc_2(t-\tau).
\end{aligned} \tag{4.3}$$

This set of differential equations can easily be decoupled by switching to the states $|\pm\rangle := (|10\rangle \pm |01\rangle)/\sqrt{2}$. In contrast to the original states, these states $|\pm\rangle$ show entanglement between the nodes. They also oscillate at different angular frequencies $\omega_0 \pm M := \omega_\pm$, therefore time-delayed feedback will have a different effect on the two states. In the following the abbreviation $c_\pm = \langle\pm|\psi\rangle$ will be used.

In particular, one can use this frequency difference to give the two entangled states different stability. If τ is chosen such that, e.g., $\omega_+\tau$ is an integer multiple of 2π, the oscillation of c_+ would not see any influence of the decay and feedback terms, since they cancel each other due to the fulfillment of the Pyragas condition (cf. Eq. 2.36). After an initial equilibration period, the probability to be in $|+\rangle$ would then no longer decrease. In contrast, for c_-, the oscillation does not fulfill the Pyragas condition, and the probability to be in $|-\rangle$ will decay to zero in the long term. Depending on the value of $\omega_-\tau$, this decay can even be faster than without feedback. The exact decay rate will be derived below.

All of this provides the possibility to create entanglement from a disentangled state: The two separable states $|10\rangle$ and $|01\rangle$ can be written as a linear combination of $|+\rangle$ and $|-\rangle$. If only the $|+\rangle$-subspace is stabilized, this component will be singled out. The final entanglement can then be calculated via the concurrence (see Eq. 2.21). In the presented case, since we are restricted to the one- and zero-excitation space, the concurrence is simply given by

$$C = 2|c_1^* c_2|. \tag{4.4}$$

From this, an upper bound on the achievable entanglement can be derived: The best one can do is separate one of the states $|+\rangle$ or $|-\rangle$ with negligible loss for that state. Since the separable states consist of equal amounts of $|+\rangle$ and $|-\rangle$ one can maximally reach an entanglement of only 50% when starting from a fully separable state.

One can calculate the exact value of the entanglement as well as the timescale needed to reach this value using Laplace transforms. As an example, take the case that τ is chosen such that the $|+\rangle$-state is stabilized, while the probability to be in the $|-\rangle$-state will decay to 0 in the long-term limit. The derivation for the opposite case is analogous. Defining $c_+ := \langle+|\psi\rangle$ and $c_- := \langle-|\psi\rangle$, let us rewrite Eq. 4.4 as

$$C = |c_+^* c_+ - c_-^* c_- + c_-^* c_+ - c_+^* c_-|. \tag{4.5}$$

Given that one will end up in a state with $c_- = 0$, the concurrence in the long-term limit is then simply $C = c_+^* c_+$. For further analysis, it is necessary to switch to Laplace space. Let us therefore rewrite the differential equation for $c_\pm$,

$$\frac{\mathrm{d}}{\mathrm{d}t} c_\pm(t) = -i\omega_0 c_\pm(t) \mp iMc_\pm(t) - Kc_\pm(t) + Kc_\pm(t-\tau), \tag{4.6}$$

using

$$\tilde{c}_{\pm}(s) = \int_0^{\infty} \mathrm{d}t\, c_{\pm}(t) \mathrm{e}^{-st} \tag{4.7}$$

into

$$s\tilde{c}_{\pm} = c_{\pm}(t=0) + \left(-i(\omega_0 \pm M) - K + K\mathrm{e}^{-s\tau}\right)\tilde{c}_{\pm}. \tag{4.8}$$

Substituting $s' = s - i(\omega_0 + M)$, one can solve Eq. 4.8 for $\tilde{c}_+$ to get

$$\tilde{c}_+ = \frac{c_+(t=0)}{s' + K - K\exp(-s'\tau + i(\omega_0 + M)\tau)}. \tag{4.9}$$

To fulfill the Pyragas condition for c_+, it is necessary to choose $(\omega_0 + M)\tau$ to be an integer multiple of 2π, which then simplifies the equation to

$$\tilde{c}_+ = \frac{c_+(t=0)}{s' + K - K\exp(-s'\tau)}. \tag{4.10}$$

The dynamics of c_+ in the long term limit are given by the residue of the pole of $\tilde{c}_+$, which lies at $s' = 0$. The residue can be calculated as

$$\lim_{t\to\infty} c_+(t) = \lim_{s'\to 0} s' \frac{c_+(t=0)}{s' + K - K\exp(-s'\tau)} = \frac{c_+(t=0)}{1 + K\tau} \tag{4.11}$$

which finally leads us to the equilibrium concurrence of

$$C_{t\to\infty} = \frac{c_+^* c_+(t=0)}{(1+K\tau)^2} \tag{4.12}$$

For a fully separable initial state, $c_+^* c_+(t=0) = 1/2$, one will reach a concurrence of $\frac{1}{2(1+K\tau)^2}$. We re-discover the previously discussed value of $C_{t\to\infty} \leq 0.5$ and it also seems like the coupling to the feedback bath K as well as the delay time τ should be kept as small as possible. This seems counter-intuitive, since that would mean that non-Markovianity as well as the coupling to baths itself were rather detrimental to the creation of entanglement. However, in the limit of $K \to 0$, one would not have any equilibration of the system, and would see infinite oscillations between the states $|10\rangle$ and $|01\rangle$. On the other hand, in the limit $\tau \to 0$, the terms $-Kc_{1,2}(t)$ and $+Kc_{1,2}(t-\tau)$ in Eq. 4.3 would fully cancel, and one would also get a dissipation-less system which would never equilibrate. This demonstrates that *some* non-Markovian dissipation must be present. To find the optimal value, one needs to analyze the dynamics of the unstable component – in this example, c_-. The faster this component decays, the faster a stable (partly) entangled steady state is reached. Let us use Eq. 4.8 to get the dynamics of c_-, however this time substitute $s' = s - i(\omega_0 - M)$ to get

$$\tilde{c}_- = \frac{c_-(t=0)}{s' + K - K\exp(-s'\tau + i(\omega_0 - M)\tau)}. \tag{4.13}$$

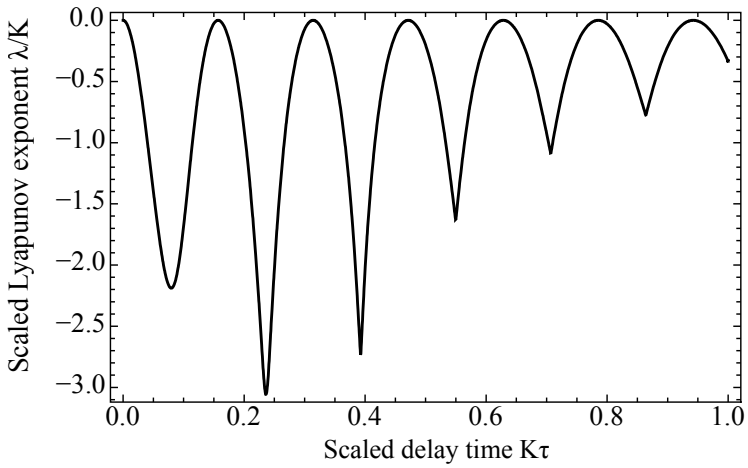

Fig. 4.2.: A plot of Eq. 4.17 for strong coupling $M = 20K$. A series of dips can be seen. At the largest dip of λ/K, there is a fast separation between the two components described by c_- and c_+, which is needed for efficient entanglement generation and stabilization. When $\lambda/K = 0$, one will never see stable entanglement, since both components will be finally stabilized. This will lead to oscillations of the excitation probability between the two network nodes, analogous to two coupled undamped harmonic oscillators.

Let us eliminate ω_0 using the Pyragas condition $\exp(i(\omega_0 + M)\tau) = 1$ to get

$$\tilde{c}_- = \frac{c_-(t=0)}{s' + K - K\exp(-s'\tau - 2iM\tau)}. \tag{4.14}$$

For the long-time dynamics, the poles of $\tilde{c}_-$ are needed. The decay rate of c_- is then simply given by the real part of the pole. The poles are calculated via

$$s' + K - K\exp(-s'\tau - 2iM\tau) = 0. \tag{4.15}$$

This equation can be solved using the Lambert-$\mathcal{W}$ function [22]

$$s'\tau = \mathcal{W}\left(K\tau e^{K\tau - 2iM\tau}\right) - K\tau. \tag{4.16}$$

One can therefore formulate a scaled decay constant λ/K of the unstable component, using the real part of s' at the pole,

$$\frac{\lambda}{K} = \frac{1}{K\tau}\mathrm{Re}\left(\mathcal{W}\left(K\tau e^{K\tau - 2iM\tau}\right) - K\tau\right). \tag{4.17}$$

Apparently, the achievable decay constant – which is also the Lyapunov exponent of the entanglement stabilization – does not depend on τ itself, but rather on the dimensionless values $K\tau$ and $M\tau$. In Fig. 4.2, the scaled Lyapunov exponent for strong coupling $M = 20K$ is plotted. A series of oscillations can be found: For certain values, λ/K reaches 0. At these values, both components, c_+ and c_-, will eventually be stabilized. When starting in a superposition, such as $|\psi\rangle = |10\rangle$, the system will then show oscillations between the state where the excitation is in the first node, and the state where the excitation is in the

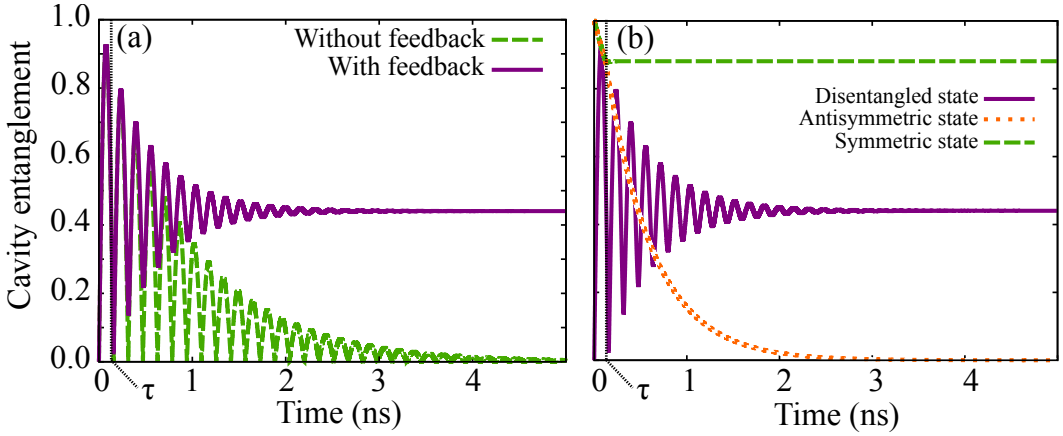

Fig. 4.3.: Concurrence dynamics. Feedback delay is chosen such that the anti-symmetric component fulfills the Pyragas condition. (a) Without feedback (orange), the concurrence decreases in a set of oscillations, while with feedback (purple), it gets stabilized to a finite value. In both simulations, the initial state was fully separable. The dotted black line marks the feedback delay time. (b) Concurrence dynamics, depending on initial state. Purple: Initial state is $|10\rangle$ (cf sub-figure a). Orange: Initially antisymmetric state $|-\rangle$, which oscillates with a frequency that does not fulfill the Pyragas condition and decays even faster after τ. Green: Initial state is the symmetric state $|+\rangle$, which is stabilized shortly after τ since its frequency fulfills the Pyragas condition.

second node, in direct analogy to two coupled undamped oscillators. One will however never reach a stable equilibrium. On the other hand, for large negative values of λ/K, one can achieve a strong decay of the unstable component c_-. This leads to a fast separation between the c_- and c_+ components, and therefore a fast creation of entanglement. This demonstrates that a finite value of τ is needed for such a separation, and in fact, it might be advisable to chose the value of $K\tau$ slightly above 0.2 to work at the second negative peak. However, this has to be balanced with the achievable entanglement (cf. Eq. 4.12).

Let us will now continue to examine this system using numerical simulations, using $\omega_0 = 1\,\mathrm{fs}^{-1}$, $M = 10\,\mathrm{ns}^{-1}$, and $K = 0.52\,\mathrm{ns}^{-1}$. Since $M \gg K$, these values are in the region of strong coupling between the network nodes. Strong coupling remains an experimental challenge, however it was achieved e.g. in coupled photonic crystal cavities [105, 106] or microdisc resonators [107]. The time-delayed feedback is simulated by including the full dynamics of 2000 external modes (a non-Markovian reservoir) for each node with a sine-modulated coupling constant (cf. section 2.3). Let us choose $\tau = 4\pi \cdot 10^4/(\omega_0 + M) \approx 126\,\mathrm{ps}$, which makes the angular frequency of the symmetric mode $|+\rangle$ fulfill the Pyragas condition.

The concurrence dynamics are shown in Fig. 4.3. In Fig. 4.3(a), the decay dynamics with and without feedback terms present are compared. For the simulations without feedback, the sine modulation of the node-reservoir coupling was removed and the coupling strength was adjusted by a factor of $\sqrt{2}$ such that the dynamics are identical up to $t = \tau$ [76].

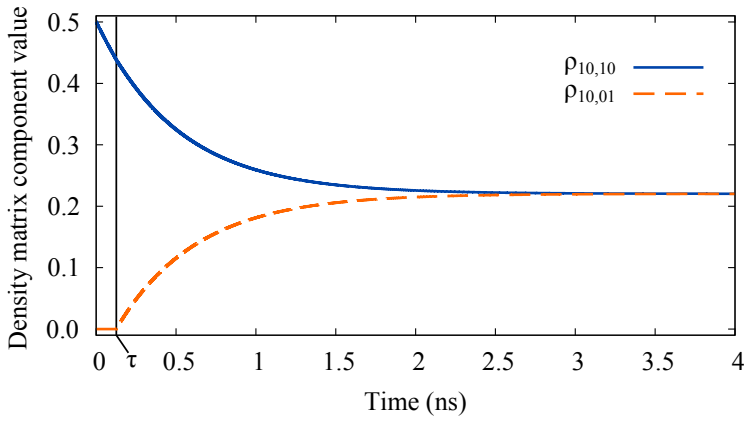

Fig. 4.4.: Density matrix component dynamics with time-delayed feedback. The initial density matrix $\rho(0)$ is given by Eq. 4.18. The diagonal element $\rho_{10,10}$ shows an exponential decay that finally stabilizes at a finite value. In contrast, the off-diagonal element $\rho_{10,01}$ stays exactly 0 until the feedback sets in. Afterwards, it rises strongly and finally equilibrates at about 0.2.

The initial state of the system is the fully separable state $|10\rangle$. Strong oscillations in the concurrence are present in both plots. However, without feedback, the overall concurrence decays to zero, while with feedback, it gets stabilized at a value slightly above 0.4. In the equilibrium, it does not show oscillations any more. This demonstrates a creation and stabilization of entanglement by time-delayed feedback.

Fig. 4.3(b) compares the concurrence dynamics for different initial states. The purple curve is the same as in Fig. 4.3(a) and displays the dynamics starting from $|10\rangle$. The green, dashed line shows the dynamics starting from $|+\rangle$, which shows a quick stabilization after the feedback delay time τ. Since the frequency of $|+\rangle$ fulfills the Pyragas condition, this can be expected. On the other hand, starting from $|-\rangle$ will not lead to any non-zero stable entanglement in the long run: The feedback even leads to a faster decay. The different effects that time-delayed feedback has on the two states is clearly observable, which is the reason why we can get entanglement creation.

A close look at the purple curves in Fig. 4.3 reveals that there is already a peak in the concurrence for $t < \tau$, which can not be attributed to time-delayed feedback. This peak solely comes from the coupling of the two nodes, which leads to a coherent exchange of the excitation. The full potential of time-delayed feedback is visible when the initial state is not a pure state, but a mixture of $|10\rangle$ and $|01\rangle$. For a $1:1$ mixture, the initial density matrix of our system is given by

$$\rho(t=0) = \frac{1}{2}|10\rangle\langle 10| + \frac{1}{2}|01\rangle\langle 01|. \tag{4.18}$$

The concurrence depends on the off-diagonal elements such as $\rho_{10,01} = \langle 10|\rho|01\rangle$, and in the highly symmetric case discussed here it is given by $C = 2|\rho_{10,01}|$.

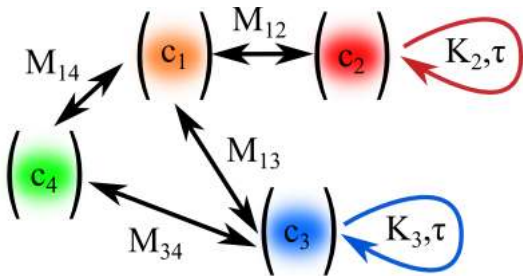

Fig. 4.5.: Many-node network with oscillators of different frequency, some of them subject to time-delayed feedback. In such a system, one can also use the feedback delay time to single out a certain network mode.
(This figure is already published in Ref.[91], Copyright 2015 American Physical Society, used with permission)

The dynamics of the density matrix elements $\rho_{10,10}$ and $\rho_{10,01}$ are shown in Fig. 4.4. The diagonal element shows an exponential decay to a finite value of slightly above 0.2, and is not affected visibly by the onset of time-delayed feedback. The behavior of the off-diagonal element is totally different: It stays exactly zero up to the feedback delay time, and then abruptly rises up and finally equilibrates at the same level as $\rho_{10,10}$. Since the concurrence only depends on this value, we see that in this case time-delayed feedback is the crucial ingredient for the creation of entanglement.

4.2 Extension to larger networks

The system discussed until now was very symmetric. The question to be answered in the following section is: Can the concept be transferred to less symmetric situations? Especially in large networks one can expect a plethora of network modes [100], which show strong correlations between the single nodes.

For this the approach will be generalized to a whole network of nodes (see Fig. 4.5). These nodes are connected with each other with different strengths, and some of them are also subject to time-delayed feedback. The feedback delay time will be kept equal for all of these nodes – at the end of the section, it will be derived that this is necessary for the approach to work. Let us stick to the one excitation limit so that time-delayed differential equations can be used for the description. Let us describe the probability amplitude of the state with the excitation at node i, $\langle 0...1_i...0|\psi\rangle$, by the quantity c_i and collect all of them in the vector $\vec{c}$. The coupling between the nodes is described using the matrix $\mathbf{M}$, which means that modes i and j are coupled with strength $M_{ij} = M_{ji}$. The nodes may have different angular frequencies ω_i, which are described using the diagonal matrix Ω with $\Omega_i = \omega_i$. These frequencies should however all be quite similar to allow for efficient coupling. The coupling strength of the individual nodes to feedback reservoirs is

given by the matrix **K**. If some nodes are coupled to the *same* reservoir, this matrix will have off-diagonal elements [100]. One can then write the differential equation for $\vec{c}$ as

$$\frac{\mathrm{d}}{\mathrm{d}t}\vec{c} = -i\Omega\vec{c}(t) - i\mathbf{M}\vec{c}(t) - \mathbf{K}\Big(\vec{c}(t) - \vec{c}(t-\tau)\Big). \tag{4.19}$$

As a sidenote, if the kernel of **K** is not empty, there exist decoherence-free subspaces independent of the feedback delay. This is however only the case if several nodes of the network couple to the same reservoir. Let us simplify Eq. 4.19 by introducing the matrix **T** that diagonalizes $\Omega + \mathbf{M}$ into Ξ:

$$\mathbf{T}\big(\Omega + \mathbf{M}\big)\mathbf{T}^{-1} := \Xi \tag{4.20}$$

The differential equation of the transformed vector $\mathbf{T}\vec{c} = \vec{\xi}$ is

$$\frac{\mathrm{d}}{\mathrm{d}t}\vec{\xi} = -i\Xi\vec{\xi} - \mathbf{T}\mathbf{K}\mathbf{T}^{-1}\left(\vec{\xi}(t) - \vec{\xi}(t-\tau)\right) \tag{4.21}$$

The frequencies of the network eigenmodes are given by the diagonal matrix elements of Ξ, Ξ_{ii}. If one of these frequencies fulfills the Pyragas condition, the respective mode will be stabilized, because the terms $\left(\vec{\xi}(t) - \vec{\xi}(t-\tau)\right)$ vanish for finite intensity. For all the other modes, their eigenfrequency normally does not fulfill the Pyragas condition and thus these modes decay to zero.This demonstrates that one can also single out certain network nodes in more complex networks. The important insight is, that this does not depend on the matrix $\mathbf{T}\mathbf{K}\mathbf{T}^{-1}$, i.e., how exactly the delayed feedback is brought into the system. In particular, this means that one does not need to have feedback at each node – one feedback reservoir is enough to filter out the desired mode. However, this only works if the delay time is equal in all existing feedback reservoirs. Otherwise, one would not be able to write Eq. 4.19 and Eq. 4.21. Different delay times impose different Pyragas conditions – only a mode that happens to fulfill *all* of them would remain unaffected by the feedback, and therefore stable.

4.3 Conclusion

It was shown, that in the one-excitation limit, time-delayed feedback can be used in quantum networks to create and stabilize entanglement. There were however several assumptions made during the derivation which need to be discussed to assess the applicability of the approach.

First, the dynamics were always calculated with maximally one excitation, starting from a Fock state. This also means, that the system is inherently "quantum-like". For classical systems, the stabilized states would not be highly entangled, but just (anti-)correlated. It is possible to directly transfer our approach to the classical world – instead of (anti-) symmetrically entangled states, one would stabilize (anti-)symmetrical oscillations of

coupled harmonic oscillators. The “quantum” nature of our system can be achieved e.g. by feeding one of the nodes with a single photon emitter such as a quantum dot.

Second, feedback was treated with the strength of 100%, i.e, all losses go into the feedback bath and will be reflected into the system. This, of course, will not happen in a real setup where there are always different decay channels, and where also the feedback mirror will not reflect all the light. As a result, the entanglement will not be stable, but also decay since the Pyragas condition will not be met perfectly. However, the feedback control will still be able to differentiate between the two components, if the coupling is strong enough, which will still lead to the creation of entanglement. One important experimental goal would be to make the feedback as efficient as possible. Losses can also be counteracted by pumping the system – however then one would need a nonlinearity to bring the system in a one-excitation state and not in a semiclassical coherent state, such as a Glauber state. The interplay of nonlinearities and feedback will be discussed in the next chapter.

5 Feedback control of photon statistics in nonlinear optical devices

The dynamics of *linear* systems subject to time-delayed feedback is rather simple, since it can be described exactly by time-delayed equations [44, 67, 82, 91, 108]. As soon as the system becomes nonlinear, one can expect a plethora of new phenomena due to the interaction of feedback with the nonlinearity. In quantum optics, this demands more than one excitation in the system. Due to feedback, these excitations may interact in the system, then get separated, and interact with each other again after the delay time τ. This leads to interference effects which can be used to stabilize non-classical states, as it will be shown in this chapter. There is only few literature of nonlinear *quantum* systems subject to feedback, discussing, e.g., Rabi oscillations [67, 77], lasers [45], optomechanical systems [75] or a Dicke model [109]. Many of those [45, 75, 109] rely on semiclassical approximations which might hide purely quantum-mechanical behavior.

In the following, two situations will be discussed in which a nonlinear medium is put into a cavity subject to time-delayed feedback, an demonstrate that it can be used to single out and stabilize non-classical states such as Fock states.

5.1 Kerr nonlinearity – control of photon number states

The creation of single- or multiple photon Fock states is a task currently approached from different directions, using systems ranging from atoms and ions to semiconductor nanostructures [110, 111]. For single photon emitters, quantum dots [112, 113] have been proven to be a very effective source. There have also been feedback-based experiments [41, 114] to stabilize single Fock states, using a complicated measurement-based feedback system, which in the end led to a Nobel prize in 2012 for Serge Haroche. A nonlinearity that changes optical properties of a material inside a cavity depending of the number of photons in the cavity will be a suitable tool for the creation of a Fock state: In this section it shall be presented that feedback will in that case enable to modify decay dynamics depending on the Fock state. The decay dynamics can be tuned such that the desired Fock state has a distinctively lower decay rate than any other state and can therefore be separated. A Kerr medium can offer such a nonlinearity. A Kerr nonlinearity (also called a $\chi^{(3)}$ nonlinearity) describes an intensity-dependent refractive index of an

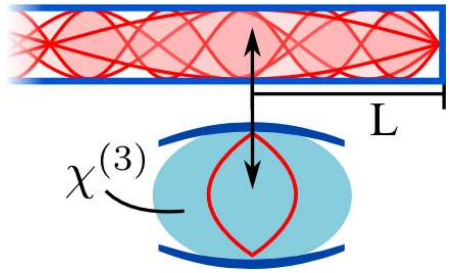

Fig. 5.1.: A possible setup to combine Pyragas control with a Kerr medium: A cavity containing the Kerr medium (light blue) is coupled to a waveguide which is closed at one end at distance L to provide feedback.

optical material. Quantum-mechanically, a single mode cavity enclosing a Kerr medium can be modeled with the following Hamiltonian [115]:

$$H_{\text{Kerr}} = \hbar\omega_0 c^\dagger c + \hbar\chi c^\dagger c^\dagger cc. \tag{5.1}$$

Here, χ is the strength of the Kerr effect, ω_0 the angular frequency of the mode, and $c^{(\dagger)}$ the annihilation (creation) operator of the mode. Usually, χ is much smaller than the decay rate of a mode, which made Kerr effects not visible on the single photon level. However, with the development of superconductor-based quantum optics [116], a single photon Kerr effect is in the reach of current experiments. In that case, the Kerr medium is implemented as a strongly detuned superconducting "artificial atom" [116] coupled to a cavity. The nonlinearity introduced by the atom leads to an effective Hamiltonian for the cavity mode containing terms as in Eq. 5.1.

Interestingly, the photon number operator $c^\dagger c$ commutes with H_{Kerr} – the Kerr effect therefore only influences the *phase*, but not the *intensity* of the electric field in the cavity. This is however only the case as long as the cavity is not coupled to another system, in which case interference effects can convert the phase change into an intensity change.

In the following, Pyragas control will be added to a system described by Eq. 5.1, and the dynamics of different Fock states in the cavity will be examined. The idea is that different Fock states acquire different phases due to the Kerr effect, which will then lead to different interference effects with the timed-delayed signal. It will be shown that this can be used to single out and stabilize a 1-photon Fock state, as well as to create other non-classical states of light.

The dynamics will be modeled by including the calculations for the full feedback reservoir (full k-sum calculations). They can however be solved much faster by using the pseudomode method (cf. section 3.3). The equations of motion for the pseudomode approach, combined with the nonlinear equations-of-motions approach of section 3.1 are presented in the appendix B.

First, the stabilization of a 1-photon Fock state in the cavity is discussed. Let us choose $\chi = 1.0 \cdot 10^{-5}\,\mathrm{fs}^{-1}$ and the coupling to the feedback reservoir as $\gamma = 0.01\sqrt{2}\,\mathrm{fs}^{-1}$ (cf. the definition of γ in Eq. 2.38). These values are just for demonstration of the general effect and need to be adapted to different experimental conditions. These parameters assume a strong single photon Kerr effect with the relation between χ and the decay rate into the feedback reservoir on the order of 30, which is however in the same order of magnitude as recent experiments [116]. The cavity angular frequency is set as $\omega_0 = 1\mathrm{fs}^{-1}$. A single photon Fock state is not affected by the Kerr effect, since the Kerr effect works on the level of two-photon operators, which give zero when working on the 1-photon state: $\chi c^\dagger c^\dagger c c|n=1\rangle = 0$. One can therefore calculate the conditions for stabilization of a single photon state by using the one photon limit and as a first stage forget about the nonlinearity. This stabilization appears as soon as the Pyragas condition for the oscillation with ω_0 is fulfilled, i.e., if $\exp(i\omega_0\tau) = 1$. The feedback mirror distance was chosen as $L = 10000.00\,\mathrm{fs} \cdot 2\pi \cdot c_0$, with c_0 the speed of light. Outside of the single-photon subspace, e.g. for the two-photon state, the Pyragas condition will generally not be fulfilled, which therefore leads to a decay of this state. In our numerical simulations, the initial state is a 2-photon Fock state. We simulate the system by solving the Schrödinger equation acting on the Hamiltonian of Eq. 5.1 with added feedback (Eqs. 2.37 and 2.38). The dynamics of the 2-, 1-, and 0-photon Fock state probabilities are displayed in Fig. 5.2. For comparison, the dynamics *without* any feedback are also plotted. Before the feedback sets in, a strong exponential decay of the 2-photon state is present, creating a non-vanishing probability of the 1-photon state. Without feedback, this probability would build up but very soon it would also decay, finally leading to zero photons in the cavity.

Including the feedback, the situation changes: After the delay time τ, the 2-photon states decays even stronger, while a stabilization of the 1-photon state is found. The buildup of the 0-photon state is blocked and the system equilibrates at about a 80% : 20% distribution between the 1-photon state and the empty cavity. It is remarkable that the single photon state ideally gets perfectly stabilized, although there are two photons in the calculation.

In Fig. 5.3, the dynamics of the $g^{(2)}$-function of the photon field is plotted, which demonstrates the influence of time-delayed feedback on the photon statistics more clearly. Up to the delay time τ, the $g^{(2)}$ function is 0.5 – the same value as for the initial 2-photon state, although there is no pure Fock state in the cavity any more, and the probability of finding a 1-photon state at the time the feedback sets in is about the same as finding a 2-photon state. After τ, a rapid decrease of the $g^{(2)}$-function down to zero is observed, which demonstrates that a single photon Fock state is created in the cavity.

One can change the feedback phase to try to stabilize other states. As an example, the situation of $L = 10000.25\,\mathrm{fs} \cdot 2\pi \cdot c_0$ is simulated, which creates a maximal decay of the 1-photon state, since $exp(i\omega_0\tau) = -1$.

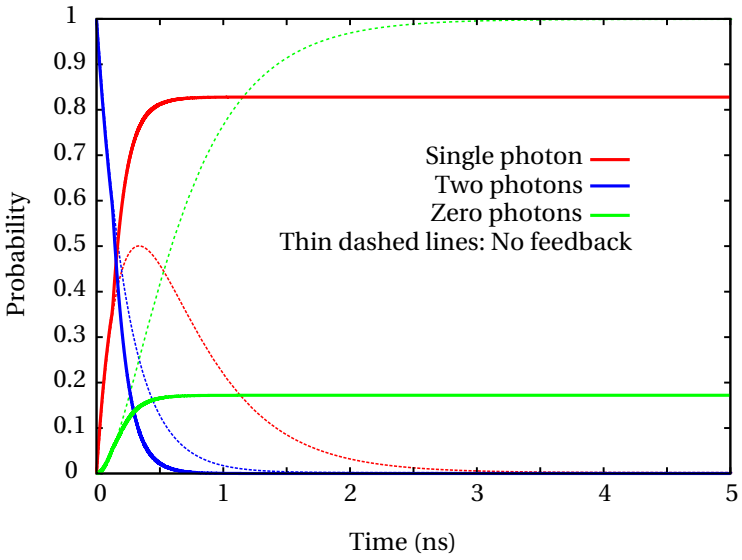

Fig. 5.2.: Feedback control of the photon statistics inside a cavity containing a Kerr medium. Dynamics of the stabilization of $n = 1$ Fock state by time-delayed feedback control. Parameters see text. The dynamics without feedback are included as thin dashed lines. Red: Probability $n = 1$, blue: probability $n = 2$, green: probability $n = 0$. Stabilization of $n = 1$ is found and a even more rapid decrease of $n = 2$ after the delay time (the delay time is visible as the time where the thick solid curves and the thin dashed curves differ first).

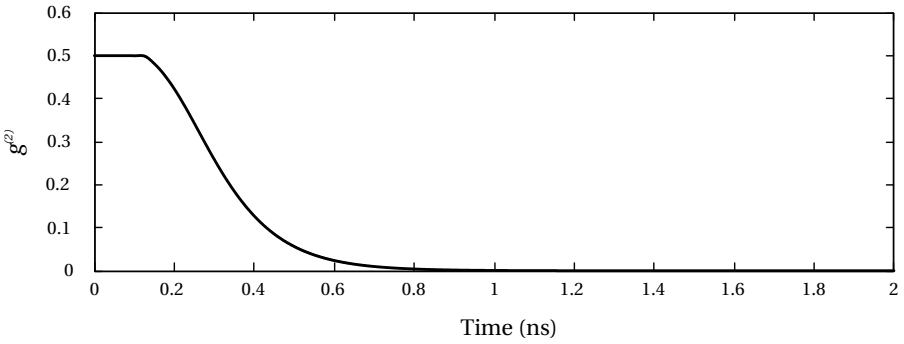

Fig. 5.3.: Feedback control of the photon statistics inside a cavity containing a Kerr medium. Dynamics of the $g^{(2)}$-function in the case of stabilization of the 1-photon Fock state. $g^{(2)} = 0.5$ is maintained until the feedback sets in. Afterwards a rapid decrease to $g^{(2)} = 0$ is visible, which demonstrates that indeed a 1-photon Fock state is stabilized.

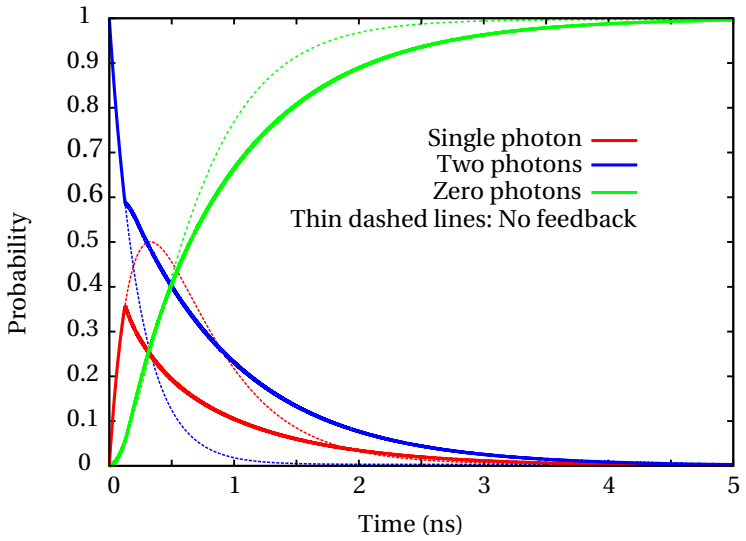

Fig. 5.4.: Feedback control of the photon statistics inside a cavity containing a Kerr medium. Dynamics of the different Fock state probabilities if the feedback is chosen such that the 1-photon probability decays the fastest. A feedback-induced slowing down of the 2-photon decay rate is observed, which makes the 2-photon probability always higher than the 1-photon probability. The situation without feedback is again included for comparison (thin dashed lines).

The results (cf. Fig. 5.4) show that while the 1-photon state decays rapidly after the delay time, the 2-photon state decay rate is decreased. While there is no stabilization of the 2-photon state, for the whole time the probability of finding 2 photons is higher than the probability of finding 1. This choice of L was also the one that gave one of the highest ratios of the 2-photon state to the 1-photon state in the region of $L/(2\pi c_0) \in [10000.00, 10001.00]$ fs. Slower decay rates for the 2-photon state can be achieved in the setting described by Fig. 5.2, if the cavity angular frequency is switched from ω_0 to $\omega_0 - 2\chi$, however perfect stabilization is not observed. This leads to the conclusion that unfortunately a perfect stabilization of the 2-photon state does not seem to be achievable. The problem might be counteracted by a pumping mechanism or by starting with a higher Fock state. One would not expect a perfect stabilization of the 2-photon state in that case as well, but it can also not be totally ruled out. The larger amount of photons might lead to a higher overall probability for the 2-photon state. This is certainly a point worth further investigation. Including more photons will also allow to investigate whether higher n-photon states can be selectively stabilized by Pyragas-type time-delayed feedback. However such a calculation is numerically very demanding due to the high number of external modes used to model the feedback.

5.2 Jaynes-Cummings model – control of excitation number

The Jaynes-Cummings system subject to time-delayed feedback was already studied in the one-excitation limit [44], and a stabilization of vacuum Rabi oscillations was

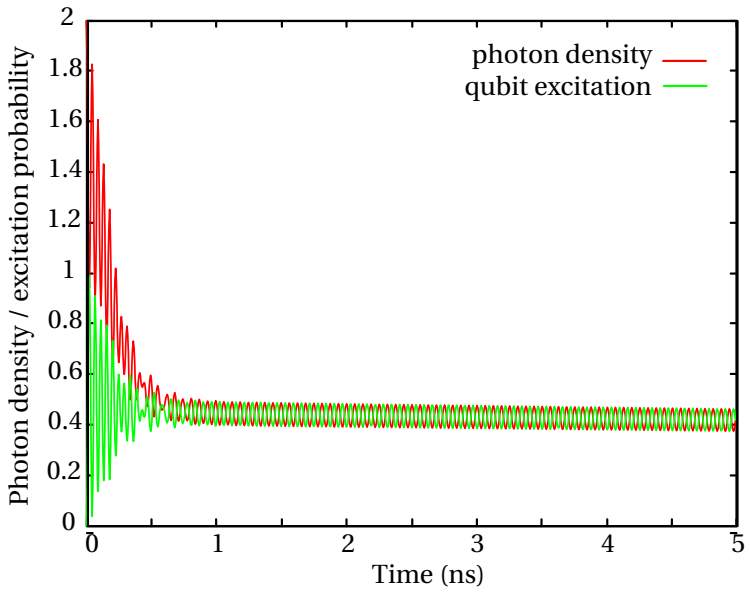

Fig. 5.5.: Dynamics of a Jaynes-Cummings system subject to time-delayed feedback. The initial state is a two-photon Fock state of the cavity mode, while the two-level system is in its ground state. Plotted are the photon density (red) and the probability of the two level system to be in the excited state (green). It is found that the system equilibrates and shows prolonged Rabi oscillations with the vacuum Rabi frequency. However, in contrast to the single excitation dynamics described in Ref. [44], the Rabi oscillations are only weak.

reported. In the following, what happens as soon as you have more than one excitation will be investigated. The Jaynes-Cummings energy spectrum shows a distinct set of lines, that can always be grouped in pairs depending on the "excitation number", i.e., the expectation value of $c^\dagger c + |e\rangle\langle e|$, with $|e\rangle$ being the excited state of the involved two-level system. What will be shown is that Pyragas-type feedback has different implications for different excitation numbers, which can be used to separate one excitation-number subspace. This analysis can not only be seen as an extension of Ref. [44], but also as a different view on the Kerr effect dynamics described above. While a Kerr effect can be created by a highly off-resonant two-level system in a cavity, here it will be investigated what happens as soon as the two level system and the cavity are in resonance. The Jaynes-Cummings model is modeled with the Hamiltonian in the frame rotating with the cavity angular frequency, leading to

$$H_{\mathrm{JCM}} = -\hbar M\left(\sigma^- c^\dagger + \sigma^+ c\right) \tag{5.2}$$

with $\sigma^\pm$ the fermionic ladder operators of a two-level system. The coupling between cavity and two-level system is set to $M = 5.0 \cdot 10^{-5}\mathrm{fs}^{-1}$ and all other parameters are left identical to the first case discussed for the Kerr medium, for the cavity as well as for the feedback. The initial state is again a 2-photon Fock state in the cavity. In Fig. 5.5, the dynamics of the photon density $\langle c^\dagger c\rangle$ and the probability to be in the excited state, $\left\langle |e\rangle\langle e| \right\rangle$, are displayed. The feedback is chosen such that in the 1-excitation case vacuum

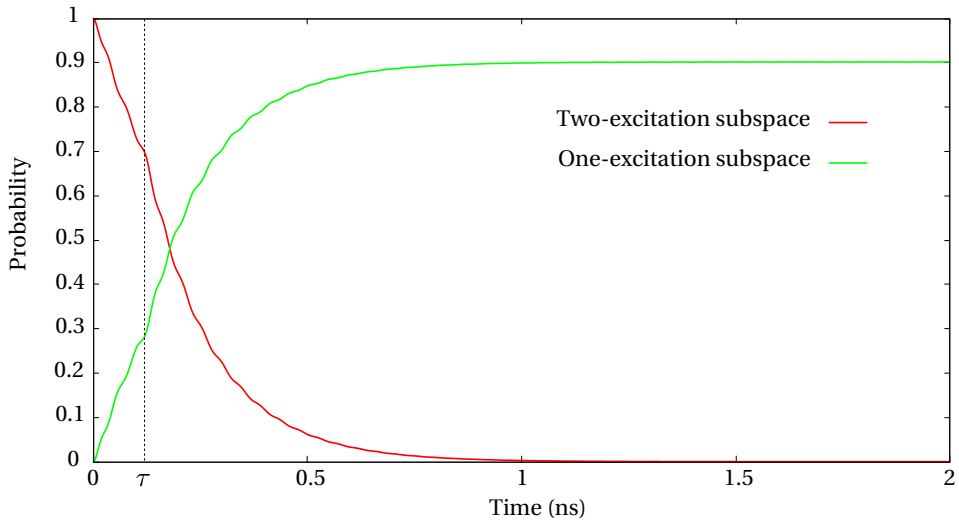

Fig. 5.6.: Jaynes-Cummings system subject to time-delayed feedback (delay time τ is marked by the dashed line and set via $L = 10\,000.00\,\text{fs} \cdot 2\pi \cdot c_0$). Plotted are the probabilities to be in the 2- and 1-excitation subspace. The results show that the probability to be in the 1-excitation subspace is stabilized, comparable to the stabilization of the 1-photon Fock state in case of the Kerr medium (see discussion above). In contrast, the probability to be in the 2-excitation subspace is reduced to zero.

Rabi oscillations would be stabilized. In our case, strong oscillatory behavior is visible. In the long term, the system starts to oscillate with the vacuum Rabi frequency as well. However, the oscillations have a very small amplitude around a finite value. If the two curves are added, which is a measure for the number of excitations in the system, the oscillations cancel out – this shows that the *excitation number* is stabilized. This situation is comparable to the stabilization of a Fock state by a Kerr medium: In both cases, the probability of having 2 excitations in the system strongly decreases, while the probability of having 1 excitation equilibrates at a finite level. This behavior is demonstrated in Fig. 5.6. There, "1-excitation subspace" describes the states $|$*excited, 0 photons*$\rangle$ and $|$*ground, 1 photon*$\rangle$, while "2-excitation subspace" describes the states $|$*excited, 1 photon*$\rangle$ and $|$*ground, 2 photons*$\rangle$. As a side note the "wiggles" visible in Fig. 5.6 are not numerical errors due to a bad resolution, but actual features: In the presented model, the system only experiences losses by losing a photon in the feedback reservoir, which makes the decay rate of the plotted quantities dependent on the photon number. Since the photon number oscillates, this decay rate oscillates as well.

As a second step, the feedback time was changed, in analogy to the Kerr case above, such that the phase $\exp(i\omega_0\tau)$ of the feedback at ω_0 is reversed, but the delay time τ is almost kept constant. This is achieved for $L = 10\,000.25\,\text{fs} \cdot 2\pi \cdot c_0$. This small change in the feedback drastically modifies the dynamics, as seen in Figs. 5.7 and 5.8. Now the results show that the 2-excitation subspace dominates the dynamics: In Fig. 5.7, prolonged oscillations of the photon number as well as of the excitation probability are visible. The frequency of this oscillation is $\sqrt{2}$ times faster than in the previous case, which shows that

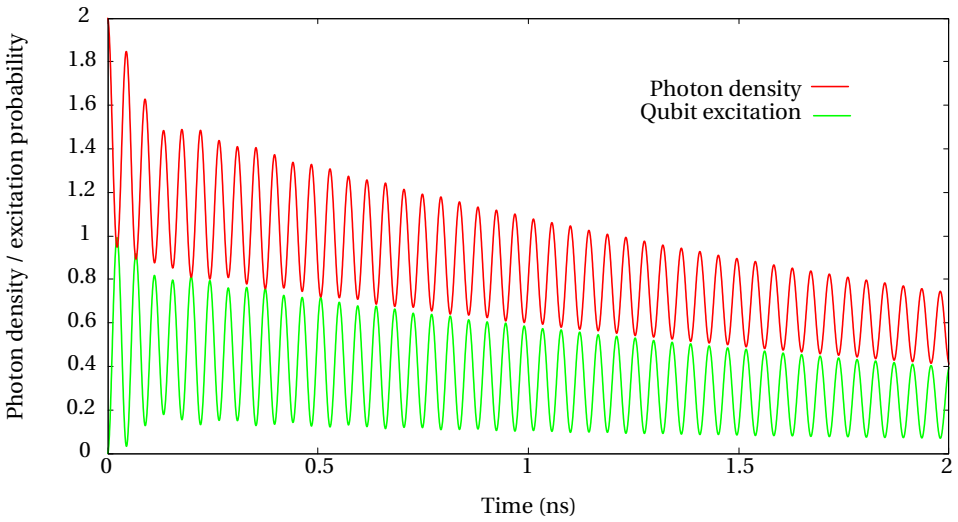

Fig. 5.7.: Jaynes-Cummings system subject to time-delayed feedback with opposite phase compared to Figs. 5.5 and 5.6. Prolonged oscillations in the dynamics of the photon density $\langle c^\dagger c \rangle$ as well as in the dynamics of the excitation probability of the two level system are present. The frequency of the oscillation matches the Rabi frequency of the two-excitation subspace of the JCM.

the oscillations are Rabi oscillations within the 2-excitation subspace. This demonstrates that the "second step of the Jaynes-Cummings ladder" is observed here.

The dominance of the 2-excitation manifold is again best seen when the probability of being in that manifold is plotted directly. In Fig. 5.8, the probability to have 1 respectively 2 excitations in the JCM system id plotted. A finite, but slow decrease of the 2-excitation probability is visible after the delayed feedback sets in – the onset of feedback is visible through the abrupt change of the decay rates. The 1-excitation probability decreases with a similar rate, but at a much lower level. This demonstrates that the power of Pyragas-type feedback is indeed to selectively stabilize processes with a certain oscillation frequency. Changing the delay time only a minuscule amount modifies the dynamics such that it allows to switch form one subspace to another by selecting different Rabi frequencies.

5.3 Conclusion

What was found in the last two examples is that time-delayed feedback is suitable for the control of non-classical states in quantum optics. The method can work as soon as different states have different oscillatory behavior: The delayed signal then interferes differently with the radiation emitted from these states, thereby creating different decay dynamics. This was used to selectively stabilize non-classical states, since it is possible to reduce the decay rate substantially for one specific state – be it a Fock state or an n-excitation state. Due to numerical constraints, only states up to 2 excitations were studied. It is certainly highly interesting to expand the model to higher excitation numbers. Similar

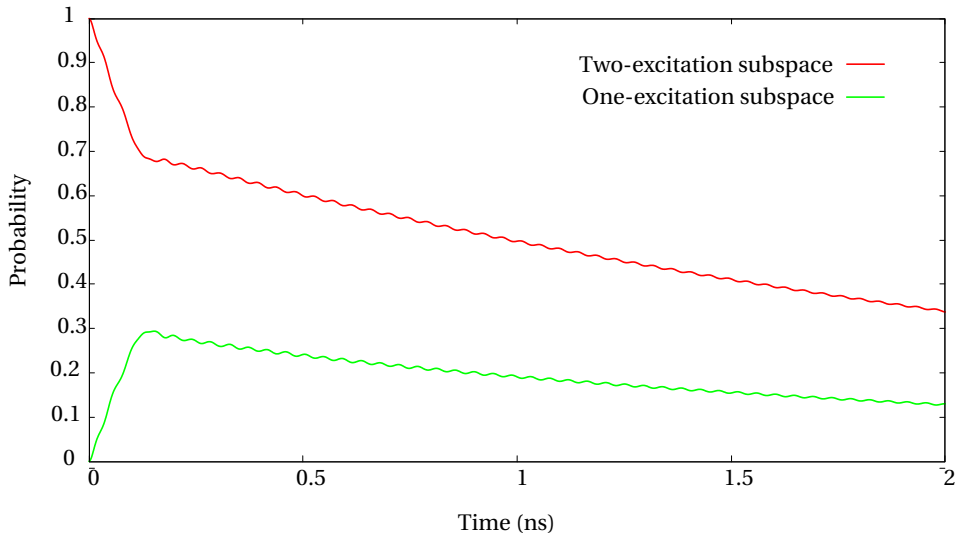

Fig. 5.8.: Jaynes-Cummings system subject to time-delayed feedback, parameters as in Fig. 5.7. Plotted are the probabilities to find 1 resp. 2 excitations in the JCM system. After the delayed feedback sets in, one finds that both probabilities decay slowly, with the 2-excitation probability being substantially higher.

behavior can be expected – however it might be that higher-order states are not as easily stabilized, since it can already be seen that 2-excitation states might not be perfectly stabilized, in contrast to 1-excitation states. However, more initial excitations might also help in the stabilization process, since they generally increase the number of excitations in the system. The fundamental problem is, that as soon as a higher excited state decays, and the excitation is lost, it might be lost "forever" – i.e., there is only one time, τ, after which it might interact again with the system, which is only done with a small probability. Once the system arrived in such a low-excitation state, feedback will not bring it back to a high-excitation state, unless there are other photons "in the delay line" that can do this.

6 Feedback control of photons emitted in a biexciton cascade

Parts of the results discussed in this chapter have been published in Physical Review Letters [117] as well as in two conference proceedings [118, 119].

The controlled creation of polarization-entangled photons is crucial for many protocols of quantum information science [120]. The polarization degree of freedom is a natural candidate for qubits – e.g., take a horizontally polarized photon as $|0\rangle$ and a vertically polarized photon as $|1\rangle$ – and, additionally, photons are easy to manipulate with well-established technology (mirrors, lenses, etc.). For applications in quantum information such as quantum cryptography [12, 121, 122] or quantum computing [15] it is necessary to prepare the photons in non-classically correlated, entangled, states.

The most prominent creation mechanism of polarization-entangled photons is currently parametric down-conversion of a laser beam [123]. This produces very bright beams of entangled photons, however statistically distributed in time due to the Poissonian photon distribution of laser light.

This problem can be circumvented by using the decay of biexcitons [124–127] in a quantum dot (QD) as a source of polarization-entangled photons. Quantum dots can act as efficient single- or few-photon emitters [112, 128] that can be triggered by pulsed laser excitation, which will then produce photons on demand. This approach can also be used for *integrated* photon pair emitters due to the small size of QDs.

Biexcitons consist of two bound electron-hole pairs, which decay in the so-called "biexciton cascade" by the emission of two photons (cf. Fig. 6.1). Without any fine-structure splitting present in the cascade, the two photons must have opposite circular polarization in order to conserve angular momentum. However, it is not specified which photon is emitted by the biexciton→exciton decay and which by the exciton→ground state decay, so there exist two indistinguishable decay paths. This leads to a polarization-entangled two-photon state of the type $\big(|\text{right}\rangle|\text{left}\rangle + |\text{left}\rangle|\text{right}\rangle\big)/\sqrt{2}$ [124].

Unfortunately, usually the intermediate (exciton) levels are of slightly different energy due to exciton fine structure splitting (FSS) [129, 130] (cf. Fig. 6.1). Due to this symmetry breaking, the two photons are either both horizontally or both vertically polarized. Moreover, they become distinguishable by their frequency - at least partly, since the spectral

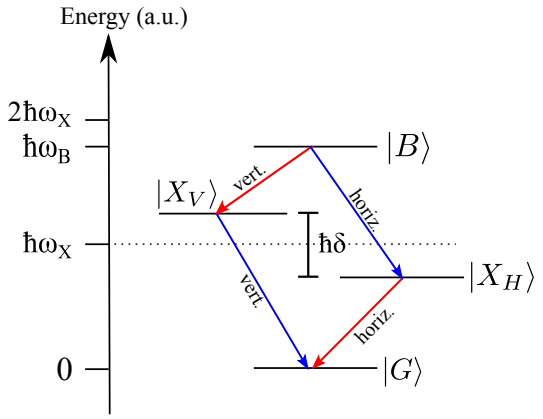

Fig. 6.1.: Energy levels involved in a biexciton cascade. The upper state $|B\rangle$ is the biexciton state with the energy $\hbar\omega_B$, which is usually different to twice of the single exciton energy $\hbar\omega_X$. The biexciton can decay to the ground state $|G\rangle$ via two different paths, either emitting two horizontally or two vertically polarized photons. The intermediate states, after the emission of one photon, are the single exciton states, $|X_H\rangle$ and $|X_V\rangle$. Due to the fine-structure splitting (FSS) of $\hbar\delta$ (greatly exaggerated in the scheme), they usually are of different energy which leads to a blue- respectively red-shift of the emitted photons.

lines still overlap. This makes them polarization- and energy-entangled, which drastically reduces the pure polarization entanglement. In a hand-waving way, one can say that the decay path can be determined by the order in which the red- and blue-shifted photon emission occurs. In the cascade depicted by Fig. 6.1, this means that if a blue-shifted photon is detected first, it was emitted in the decay path that leads to horizontally polarized photons. Due to the finite lifetime of all the involved states, the respective lines are broadened, which leads to a finite spectral overlap. Therefore the entanglement is not destroyed completely, but still it will be strongly reduced.

Over the last couple of years, several approaches have been developed to deal with this problem. Quantum dots with small FSS can be grown by a sophisticated growth process [127, 131, 132]. Also strain [133] and external fields [127, 134] can strongly diminish the FSS, however might be hard to implement in an integrated setup. Entanglement can also be enhanced by post-processing such as temporal [135] or spectral [136] filtering or by reversing the time order of the emitted photons [137–139], all of which erases the which-path information at the expense of losing a lot of photons. A promising approach is to implement the biexciton in a high-q cavity and use the Purcell effect to increase the linewidths of the involved transitions [140–147]. This raises the probability that both decay paths lead to photons of the same frequency, which eliminates the distinguishability by frequency and therefore leads to entanglement. However, one problem is that high-q cavities have only small losses by definition, which means that the photons are "trapped" within the cavity and are not released directly after creation. This decreases the "on-demand" property of the photons.

What is proposed and studied in this chapter is an approach similar to the Purcell-based mechanism, which however keeps the system open – time-delayed quantum-coherent feedback. The possibility to strongly modify the photon emission probability *depending on the photon frequency* provides a tool to shape the spectrum in a way to enhance the emission of photons with equal frequency.

6.1 Model

In accordance to Fig. 6.1, the biexciton cascade is modeled using biexciton annihilation (creation) operators $\hat{b}^{(\dagger)}$, two types of intermediate exciton annihilation (creation) operators $\hat{x}^{(\dagger)}_{H/V}$, and a ground state annihilation (creation) operator $\hat{g}^{(\dagger)}$. The horizontally polarized photons with wave vector k are annihilated (created) using $\hat{c}^{(\dagger)}_{H,k}$. Equivalently, $\hat{c}^{(\dagger)}_{V,k}$ is introduced for vertically polarized photons. In the following all four transitions (cf. Fig. 6.1) couple equally to the photon continuum with a wave-vector dependent coupling constant $\gamma(k)$. As before, this wave-vector dependence will be used to model Pyragas-type time-delayed feedback. The Hamiltonian then reads in the interaction picture

$$\begin{aligned}\hat{H} = \hbar \int_{-\infty}^{\infty} \mathrm{d}k\, \gamma(k) \Big(& e^{i(\omega_B-\omega_X-\omega_k+\delta/2)t} \hat{b}^\dagger \hat{x}_H \hat{c}_{H,k} + e^{i(\omega_B-\omega_X-\omega_k-\delta/2)t} \hat{b}^\dagger \hat{x}_V \hat{c}_{V,k} \\ & + e^{i(\omega_X-\omega_k-\delta/2)t} \hat{x}_H^\dagger \hat{g} \hat{c}_{H,k} + e^{i(\omega_X-\omega_k+\delta/2)t} \hat{x}_V^\dagger \hat{g} \hat{c}_{V,k} \Big) + \text{h.c.}\,. \end{aligned} \tag{6.1}$$

Here, the biexciton energy $\hbar\omega_B$, the average exciton energy $\hbar\omega_X$, and the fine-structure splitting δ were introduced. Photons with wave vector k in our model have the angular frequency $\omega_k = c_0 k$ with the speed of light c_0. The biexciton and the exciton angular frequencies are related by the biexciton binding energy $\hbar\beta$ via $\omega_B = 2\omega_X - \beta$. Pyragas control will be included by setting

$$\gamma(k) = \gamma_0 \sin(kL) \tag{6.2}$$

with L being, in a very broad sense, the "distance of the mirror that induces the feedback". Therefore, the light emitted by the biexciton cascade will interact with the quantum dot again after the feedback delay time $\tau = 2L/c_0$.

This idea of a "mirror at distance L" should however not predefine that one needs to use a setup consisting of a lens and a mirror, as described in the theoretical work of Dorner and Zoller [67] and implemented experimentally by the group of Rainer Blatt [68–70]. If the QD is put inside a hemispherical mirror [70], the lens might not be necessary. A setup that uses a waveguide [148, 149] to store the light for the period τ might also be an experimental implementation. Another challenge might be to extract the photons of the host medium of the quantum dot, which usually is a semiconductor with very high

refractive index. Apart from all these issues, the aim of these simulations is to find out whether Pyragas-type feedback terms have an influence on the photon entanglement—and it will be shown that they do. At this point, the aim is not to describe a certain experimental realization.

An important quantity is the phase φ with which the electric field arrives back at the QD. It can be calculated from the mirror distance via $\varphi = (\pi + 2\omega_k L/c_0) \mod 2\pi$. Later on, the dependence of the entanglement on the feedback phase at the bare exciton angular frequency without FSS, ω_X, which will be described by φ_X, will be discussed.

The Hamiltonian of Eq. 6.1 is used to solve the Schrödinger equation. This has the benefit that a large number of external modes can be included numerically, however it makes it impossible to include decoherence effects, except by using a stochastic Schrödinger equation approach [79], which will not be used. The effects of, e.g., pure dephasing, will later on be estimated. Inhomogeneous broadening will later be included by averaging over a whole range of simulations at different exciton energies. Further Markovian decay channels can be included by adding a second reservoir [67] or modifying the coupling constant $\gamma(k)$. For the solution of the Schrödinger equation the following state is used:

$$\begin{aligned}|\Psi\rangle = &b|B\rangle + \sum_k \Big(x_{H,k}|X_H\rangle|k_H\rangle + x_{V,k}|X_V\rangle|k_V\rangle \Big) \\ &+ \sum_{k,k'} \Big(g_{H,k,k'}|G\rangle|k_H, k'_H\rangle + g_{V,k,k'}|G\rangle|k_V, k'_V\rangle \Big). \end{aligned} \tag{6.3}$$

In analogy to the Hamiltonian, the states $|B\rangle$,$|X_{H/V}\rangle$, and $|G\rangle$ describe the QD in a biexciton, in one of the two exciton, or in the ground state, respectively. The kets $|k_V\rangle$ ($|k_H\rangle$) describe single photon states with wave vector k and vertical (horizontal) polarization. The respective two-photon states with wave vectors k and k' are given by $|k_V, k'_V\rangle$ ($|k_H, k'_H\rangle$). The interesting quantity is the entanglement of the photons in the external field. For this, a term will be analyzed which can be interpreted as the "normalized two-photon wavefunction overlap ζ":

$$\zeta(t) = \frac{|\iint g^*_{H,k,k'} g_{V,k,k'} \,\mathrm{d}k\mathrm{d}k'|}{\frac{1}{2}\iint |g_{H,k,k'}|^2 + |g_{V,k,k'}|^2 \,\mathrm{d}k\mathrm{d}k'}. \tag{6.4}$$

In the limit of long times, $t \to \infty$, this quantity will be a measure for the photon entanglement and is usually called the *concurrence* C:

$$C = \zeta(t \to \infty). \tag{6.5}$$

The explanation why this is the case was first given by Akopian *et al.* [136]: In the long term, the quantum dot will have fully decayed into the ground state $|G\rangle$, and the photons will be in the external field, described by the wave packets given through $g_{V,k,k'}$ and $g_{H,k,k'}$. The two photons are purely polarization-entangled if the two wave packets

are not distinguishable. On the other hand, if the two wave packets are orthogonal to each other, they are perfectly distinguishable and the polarization entanglement is lost. The overlap $\iint g^*_{H,k,k'} g_{V,k,k'} \mathrm{d}k\mathrm{d}k'$ between the two wave packets is therefore directly related to the entanglement. In case that not all photons are emitted in the external field described by $g_{H,k,k'}$ and $g_{V,k,k'}$, the normalization by the absolute squares of the probability amplitudes becomes important. In our case it is kept for consistency with literature [136]. The factor $\frac{1}{2}$ ensures that perfect entanglement leads to a value of $C = 1$. Measuring the entanglement as a "long-term limit" means that the whole photon wave packet is taken into account. This is equivalent to a *time-integrated* measurement of the entanglement. One must not confuse the value $\zeta(t)$ with a *time-dependent* entanglement measure, it is simply a time-dependent measure of the wave packet distinguishability. It only becomes a measure for the entanglement once the quantum dot is in a unique state, i.e., the ground state.

6.2 Numerical results

In order to assess the influence of time-delayed feedback on the photon entanglement, the Schrödinger equation is solved numerically. First, the biexciton binding energy is set to 0, which makes $\omega_B = 2\omega_X$. It was shown experimentally [150] that positive as well as negative values for the biexciton binding energy can be realized. In particular, it is also possible to grow quantum dots with diminishing biexciton binding energy. This assumption is useful to understand later on how the concurrence is influenced by the feedback. Including a biexciton binding energy would introduce a further time-scale (given by the inverse of the binding energy) that would be needed in the discussion of the results. Later on, it will be examined how non-zero binding energies influence the results. Let us set $\omega_X = 2\,\mathrm{fs}^{-1}$, which is equivalent to an exciton energy of about 1.3 eV and a photon wavelength of $\lambda_0 = 942\,\mathrm{nm}$. The chosen fine structure splitting is $\delta = 10\,\mathrm{ns}^{-1} \approx 6.58\hbar^{-1}\,\mu\mathrm{eV}$, unless mentioned otherwise. Let us set the coupling to the external mode continuum γ_0 such that it leads to an initial (i.e. before any feedback effects set in) biexciton decay time of about 300 ps. In the presented simulations there is one external mode continuum, which is modeled using 8000 modes with angular frequencies distributed equally around ω_X over a range of $0.4\,\mathrm{ps}^{-1}$. For the simulations *without* feedback, $\gamma(k) = \gamma_0/\sqrt{2}$ is used instead of Eq. 6.2 to achieve the same initial behavior up to $t = \tau$. This means that effects of further decay channels are not included, which in an experiment would unavoidably be present. However, this allows to analyze the maximal amount of entanglement that this scheme could provide.

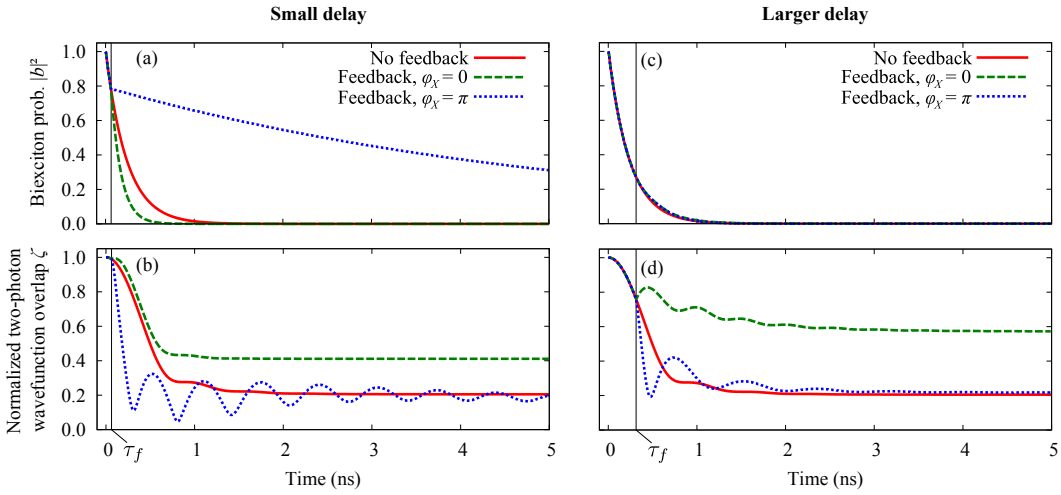

Fig. 6.2.: Time dependence of the probability to be in the biexciton state, $|b|^2$ ((a) and (c)), as well as two-photon wavefunction overlap $\zeta(t)$ ((b) and (d)) for various parameters. Red: no feedback, green: feedback with $\varphi_X = 0$, blue: feedback with $\varphi_X = \pi$. (a),(b): Short feedback delay time τ_f of approx. 63 ps. (c),(d): Longer delay time with τ_f five times larger than in the short delay case.
(This figure is already published in Ref.[117], Copyright 2014 American Physical Society, used with permission)

6.2.1 Small delay

First, the effects of feedback with a small delay time $\tau \approx 63\,\text{ps}$ are discussed. Later on, this value will be increased. This delay time can be achieved by setting L between $10000\lambda_0$ and $10000\lambda_0 + \lambda_0/4$. In this range, the feedback *phase* φ_X takes on all possible values. In particular, it is $\varphi_X = 0$ for $L = 10000.00\lambda_0$ and $\varphi_X = \pi$ for $L = 10000.25\lambda_0$. This corresponds to mirror distances in the micrometer range, which might be hard to realize using current macroscopic optical instruments (lenses, mirrors), but should be well in the reach of integrated devices. First the dynamics of the biexciton probability $|b(t)|^2$ (cf. Fig. 6.2(a)) are examined. Without feedback (red curve), there is, as expected, an exponential decay. With feedback, the two extreme cases of $\varphi_X = 0$ (in green) and $\varphi_X = \pi$ (in blue) are shown. The vertical line marks the onset of feedback. The decay dynamics strongly change after the delay time: For $\varphi_X = 0$, the decay is enhanced, while for $\varphi_X = \pi$, the decay is inhibited. This can be explained as a Purcell effect due to the mirror: There is either a larger or smaller density of states available for the emitted photons. Since the QD can only experience these Purcell effects after τ, the delay is directly visible. Already in case of QDs coupled to a high-Q cavity, the Purcell effect has strong influence on the photon entanglement. Looking at the wavefunction overlap $\zeta(t)$ (Fig. 6.2(b)), one finds that without feedback it decreases to a value of about 0.2 which clearly demonstrates the deteriorating effect of the fine structure splitting. With feedback, however, the dynamics change: For $\varphi_X = \pi$, it decreases even more and then shows a long trail of oscillations around 0.2. For very long times (not shown in the plot), the simulations show that it equilibrates at about 0.1. The oscillation period is approximately the time given through the FSS, which indicates that the oscillation is

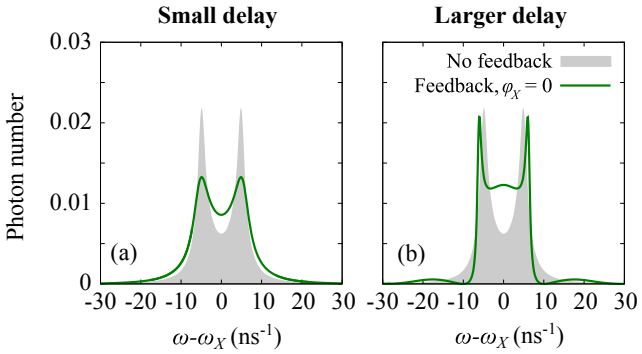

Fig. 6.3.: Frequency-dependent photon number spectrum for (a) short and (b) long feedback delay times. In grey the results without feedback are shown, in green the results with feedback for a feedback phase $\varphi_X = 0$. The curves are calculated for $t \to \infty$. Subfigure (a) clearly demonstrates the peak widening due to the increased decay rate, while (b) shows a strong feedback-induced frequency dependence of the intensity.

an interference effect between the two decay paths. The more interesting results are acquired for $\varphi = 0$: After the feedback, the decay of $\zeta(t)$ is reduced and equilibrates at a concurrence of about $C = 0.4$. This demonstrates that time-delayed feedback is capable of increasing the achievable concurrence. To understand this behavior better, let us look at the frequency-dependent photon number in the external continuum, presented in Fig. 6.3(a). These spectra are calculated via $n(\omega) = \left\langle \hat{c}^\dagger_{H,k} \hat{c}_{H,k} \right\rangle + \left\langle \hat{c}^\dagger_{V,k} \hat{c}_{V,k} \right\rangle$ for $t \to \infty$. In gray, the results without feedback are plotted. A double-peak structure due to the FSS is clearly visible. With feedback (green curve) in the small delay case, the peaks are broadened, as it would be expected in case of an increased decay rate. In analogy to other Purcell-enhanced entanglement, the broader peaks overlap more, which leads to a higher indistinguishability of the decay paths since it is "harder" to distinguish the decay path by the photon frequency. In particular, there is a substantial increase at the center angular frequency $\omega = \omega_X$.

The similarity to other Purcell-based entanglement enhancement schemes is striking. While these schemes usually work with even higher enhancements, they suffer by the fact that the photons are trapped within the cavity. This strongly reduces the possibility to produce them on demand. In contrast, with our scheme that reflects photons emitted into one half-space back into the QD, while they can leave the system to the other side, the whole system is open and the photons can be retrieved opposite of the mirror. One issue might be where to place the substrate then. This might be resolved by manufacturing the feedback as a integrated waveguide-based system on the substrate.

In Fig. 6.4 the dependence of the achievable concurrence is plotted for several values of the FSS δ. Over a wide range, the feedback mechanism can increase the concurrence. In terms of relative values, the effect is even stronger for larger FSS.

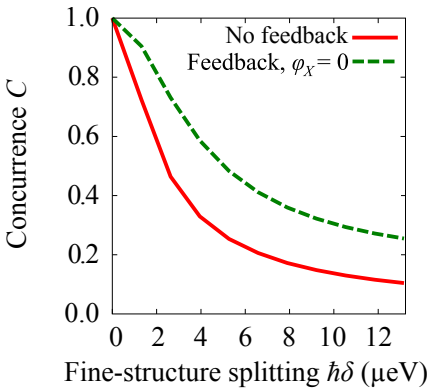

Fig. 6.4.: Achievable concurrence in the short delay limit for different values of the FSS δ. The simulations show that even for large δ one can get quite a substantial increase. In terms of percentages, the increase is even higher for large δ.
(This figure is already published in Ref.[117], Copyright 2014 American Physical Society, used with permission)

6.2.2 Larger delay

In the small delay limit, the results were explainable by simple Purcell effects. One would expect different behavior as soon as one leaves this realm and increases the delay such that the phase of the feedback varies substantially over the whole width of the double peak. Longer delay times allow to modify the spectrum much more precisely, however make the whole system also more delicate (this will be covered later in section 6.3). In order to examine this regime, a delay time 5 times larger than in the previous section is simulated. This brings the delay time in the same order of magnitude as the time defined by the FSS. All other values are left identical.

First, the biexciton probability, given in Fig. 6.2(c), is studied. The plots show that the curves with and without feedback do not differ strongly. There seems to be a minor decrease of the decay rate for the case with feedback (for both phases), however it is barely visible compared to the results of the previous section. This demonstrates that simple Purcell effects will not be enough to describe the behavior. In case of the *exciton* probability (cf. Fig. 6.5), the numerical simulations still show a strong dependence on the existence of delay and its phase.

The value of ζ is also strongly modified by the feedback: While for $\varphi_X = \pi$, it equilibrates at a value comparable to the one without feedback, it reaches a much higher value for $\varphi_X = 0$. This achievable concurrence is even larger than in the short delay time case. This can be explained again by looking at the spectrum given in Fig. 6.3(b): Instead of just broadening, one now finds a strongly modulated spectrum with steep flanks and a third maximum at $\omega = \omega_X$. The reason for this is the interference between the current and the reflected parts of the photon wave function: At the flanks, these two waves interfere destructively, strongly decreasing the available phase space for the photons (in the ideal case, this even reduces the phase space to 0 at one frequency). This effectively hinders

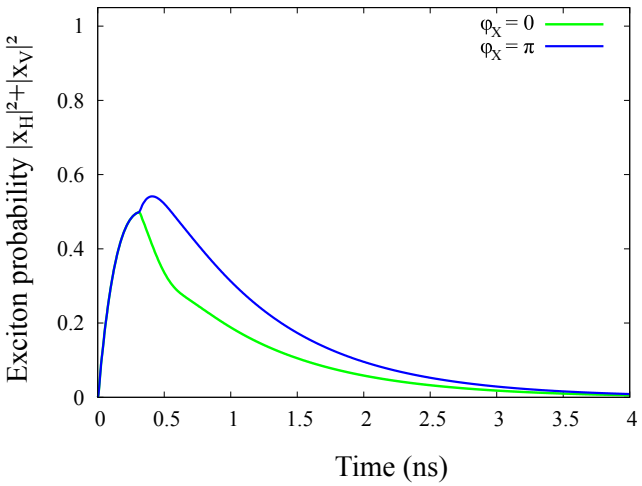

Fig. 6.5.: The probability to be in one of the exciton states in case of long feedback with $\varphi_X = 0$ (green) and $\varphi_X = \pi$ (blue). Although the long feedback did not have a substantial effect on the *biexciton* probability (cf. Fig. 6.2 (c)), the exciton states are modified. There is an increased (decreased) decay after τ_f for $\varphi_X = 0$ ($\varphi_X = \pi$). One can also see the effects of multiple reflections at the mirror for the $\varphi_X = 0$ case, which reduce the decay rate after $2\tau_f$.

the QD to emit photons at these frequencies. However, at $\omega = \omega_X$, the two waves interfere constructively, enhancing the probability that the QD emits photons of this frequency. This effectively "pushes" the emission to the center of the double-peaked spectrum. This again makes the two decay paths less distinguishable by the photon frequencies and therefore leads to a higher entanglement.

Since a larger time delay has a positive effect on the achievable entanglement, as a next step it will be checked at what time delay one can reach the maximum entanglement. As for the phase, maximum entanglement is reached when $\varphi_X = 0$, since then enhanced emission at the angluar frequency between the two exciton states, $\omega = \omega_X$, is happening. In Fig. 6.6 the achievable concurrence is plotted depending on the delay time. There is a maximum at about $\tau_f = 0.3\,\text{ns}$. At this point, the delay is equivalent to the time given by the inverse fine structure splitting. As it is often found in time-delayed control, the influence of time delay is the strongest when the time scales match. As this result is acquired in an idealized setting, it has to be taken with a grain of salt: Long feedback times make the system much more sensitive to decoherence [151] as well as to shifts of the frequencies, e.g. due to charges in the vicinity of the (bi)exciton. All these effects will move the peak to shorter delay times.

6.3 Deteriorating effects

The calculations above were ideal in a way that the effect of time-delayed feedback was maximal: Neither other decay channels were considered, nor dephasing. Also, a

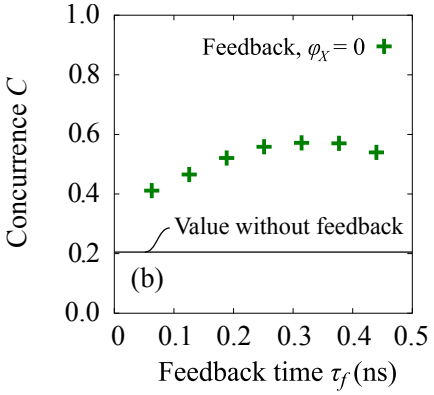

Fig. 6.6.: Maximally achievable entanglement for $\varphi_X = 0$ at different delay times τ_f. There is a maximum at about 0.3 ns, which coincides with the time given by the inverse of the FSS. This is not surprising, since delay effects usually are the strongest when the timescale of the delay matches the timescale of the phenomenon that should be controlled.

vanishing biexciton binding energy was chosen and inhomogeneous broadening was not accounted for. All of these effects may diminish the achievable entanglement, and are therefore worth looking at.

6.3.1 Dephasing

The literature [151] reports experimentally measured coherence times (T_2 times) in the range of 100 ps. This is longer than the delay time that was used used for "short delay" feedback, however shorter than what was used for "longer delay". A loss of coherence minimizes interference effects, which the time-delayed feedback mechanism is based upon. It is necessary to work at very low temperatures to minimize the influence of phonons [144, 152, 153] to keep coherence as long as possible. Unfortunately, direct numerical simulations of dephasing processes are not possible within the Schrödinger equation approach without using stochastic wavefunctions in a monte carlo approach. This, or other approaches based on expectation values rather than wavefunctions, are however much more numerically demanding. Therefore it was not possible to perform a numerical study on the effects of dephasing.

6.3.2 Biexciton binding energy

Having a non-vanishing biexciton binding energy β complicates the scheme since it introduces a further timescale given by $1/\beta$. A situation with $\beta = 100\,\mathrm{ns}^{-1}$ was simulated, which makes it 10 times as large as the FSS. The results for short and longer feedback delay are shown in Fig. 6.7. All other parameters, including the delay times, are kept as before. One finds that in case of short feedback delay, one can still reach an entanglement of about 0.4, comparable to the results with $\beta = 0$. However, in case of long delay times,

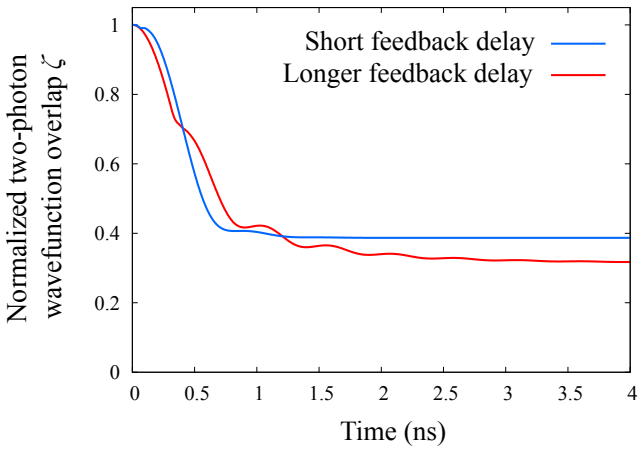

Fig. 6.7.: Normalized two-photon wavefunction overlap $\zeta(t)$ for a biexciton binding energy $\hbar\beta = \hbar \cdot 100\,\mathrm{ns}^{-1}$. In case of short feedback, there is not a strong difference to the situation without binding energy. For longer feedback, however, the achievable concurrence equilibrates *below* the value for short feedback, in contrast to the results without biexciton binding energy.

the achievable concurrence falls below 0.4 and is therefore worse than in the short delay limit. For the given values, in the longer delay case, the feedback phase at ω_X as well as at $\omega_X - \beta$ is 0, therefore one would expect similar behavior to the case with no binding energy. However this seems to be not the case. Since the two double-peaked features are aligned around two different center frequencies, feedback has a slightly different implication on the spectral shapes. This difference becomes more important the longer the delay time is, since for long delay times the modulation in the density of states becomes stronger. This seems to deteriorate the positive effects of long feedback delay that appear for $\beta = 0$.

6.3.3 Inhomogeneous broadening

In a typical sample, several quantum dots with slightly different properties are present. If they are excited electrically, one cannot predefine which quantum dot will emit light. The incoherent overlap of these different lines creates an inhomogeneous broadening of all features. One can counteract this by exciting one quantum dot coherently [113]. But even in case of a single QD, additional charges may appear that shift the QD energy levels in time. This effect is called *spectral diffusion* and also leads to inhomogeneous broadening. In the short delay limit, no strong detrimental effects of inhomogeneous broadening should be expected, since the feedback phase is almost constant over the range of frequencies covered by the inhomogeneous broadening. This situation is simulated using 40 numerical simulations with varying ω_X, that are weighted with a Gaussian. The full width at half maximum (FWHM) of this Gaussian is given by the inhomogeneous broadening. The simulations are run with $\beta = 0$. The results show (cf. Fig.6.8) that the achievable concurrence is only decreased slightly due to inhomogeneous broadening, and therefore the method should also work in this case. However, for longer delay times,

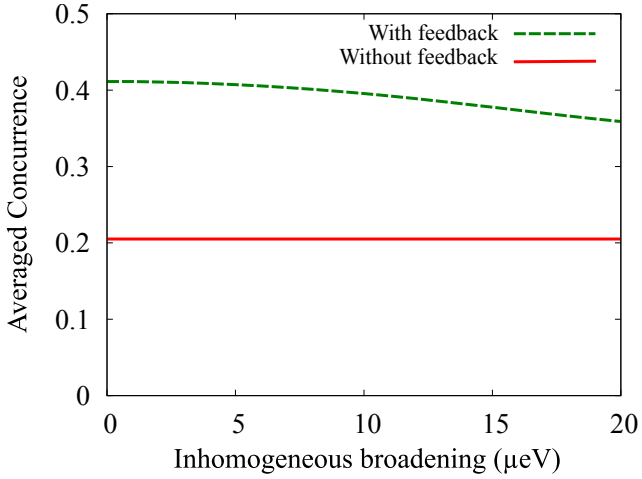

Fig. 6.8.: Dependence of the achievable concurrence in the short delay limit on inhomogeneous broadening. To get the figure, the concurrence was averaged over 40 simulations with varying ω_X, weighted with a Gaussian with a FWHM given by the inhomogeneous broadening. The results demonstrate that substantial concurrence can be achieved even with inhomogeneous broadening.
(This figure is already published in Ref.[119], Copyright 2015 Society of Photo-Optical Instrumentation Engineers, used with permission)

the feedback phase φ_X can vary between 0 and π if the exciton frequency is varied in the same way. This eliminates all feedback effects. Therefore, in this case, one needs to minimize inhomogeneous broadening. As discussed, this is possible through optical excitation. Also, spectral diffusion usually happens on slower timescales that the biexciton decay [113]. This may give the possibility to adapt the feedback delay time to the current state of the QD.

6.4 Conclusion

The effects of time-delayed quantum coherent feedback on the photon emission of a biexciton cascade with finite fine-structure splitting were presented. It was found that due to the Purcell effect, enhanced entanglement between the photons could be created. For longer delay times, the frequency-dependent decay dynamics of the biexciton can lead to even higher entanglement, however this effect is much more sensitive to frequency variations as well as to decoherence. These effects can reduce the achievable entanglement. Without these detrimental effects, a maximum entanglement was found as soon as the timescale given by the FSS matches the time of the feedback delay.

7

Controlling quantum statistics through cavity-based photonic reservoirs

In this chapter, results acquired during a research visit in the group of Hakan Türeci, Department of Electrical Engineering, Princeton University, will be presented.

One of the biggest problems in quantum computation is to maintain quantum correlations despite the presence of noise sources. No system can be perfectly separated from its environment, even when working at very low temperatures. System–environment interactions can either make the system decay from a highly entangled state into a state of lower intensity (e.g., a disentangled ground state), or reduce only the correlations between entangled states (pure dephasing). Instead of minimizing the effect of the environment, it is also very promising to actually *utilize* the environment to bring the system into the desired state. Losses are counteracted by continuously pumping the system with a laser. This will lead to a non-equilibrium steady state, in which losses are balanced by pumping. Structured environments can be used to modify the non-equilibrium steady-state such that it contains the desired entangled states with a high probability.

Time-delayed feedback is, of course, not the only way to structure an environment coupled to a quantum-optical system – in fact, it is one of the more complex ways of doing so, with its own benefits and drawbacks. The easiest way to produce a "structured environment" is a photonic cavity, which in the previous chapters was usually part of the "system". However, this distinction is somewhat arbitrary – a cavity mode can also be seen as a reservoir with a strongly peaked density of states. As it was shown in the chapter on pseudomodes, this description is equivalent.

The main subject of this chapter is the creation and control of entanglement between qubits coupled to one or several cavities. At the beginning, the case of two qubits coupled to one cavity mode will be analyzed, and it will be investigated if entanglement and bistability are as closely related as semiclassical analysis makes one believe [154, 155]. In the proceeding sections a system described in Ref. [46] will be examined, consisting of two coupled driven Jaynes-Cummings systems. It will be analyzed how a finite delay in the coupling influences the system. Furthermore, a method to enhance the entanglement between the two two-level systems by including a second driving field will be presented.

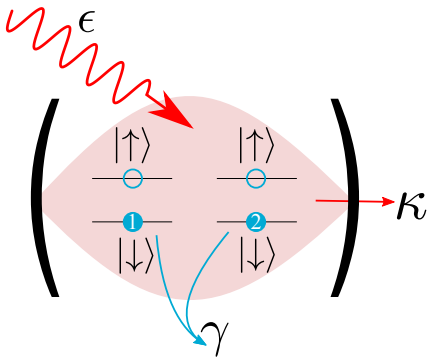

Fig. 7.1.: Setup of two qubits in a single-mode cavity, driven by coherent laser light of the strength ϵ. Losses of the cavity are described by the phenomenological decay rate κ. The qubits also decay coherently into other modes which is included by a coherent decay rate γ. The drive can initiate an excitation of the qubits, which leads to an entangled qubit state for certain drive strengths.

7.1 Two qubits coupled to a driven cavity mode: Entanglement and bistability

In the following, the setup presented by Mitra and Vyas [154] will be discussed, however taking the full quantization of the photonic field into account. The setup consists of a photonic cavity mode with angular frequency ω_c and two qubits with identical level splitting $\hbar\omega_\mathrm{q}$. The cavity is driven by an external laser with angular frequency ω_d and strength ϵ (cf. Fig. 7.1). The qubits couple to the cavity mode with coupling strength g and also directly with each other via Förster coupling of strength F. The Hamiltonian therefore reads

$$H = \hbar\omega_\mathrm{c} c^\dagger c + \hbar\omega_\mathrm{q} \frac{\sigma_1^z + \sigma_2^z}{2} + ig \sum_{j=1}^{2} \left(c^\dagger \sigma_j^- - c\sigma_j^+ \right) + F\left(\sigma_1^+\sigma_2^- + \sigma_2^+\sigma_1^-\right) + i\epsilon\left(c^\dagger \mathrm{e}^{-i\omega_\mathrm{d} t} + c\mathrm{e}^{i\omega_\mathrm{d} t}\right). \tag{7.1}$$

$\sigma_{1,2}^z$ describes the standard Pauli matrix acting on the first resp. second two-level system. The ladder operators are defined as $\sigma_j^\pm = \sigma_j^x \pm i\sigma_j^y$, also using standard Pauli matrices. Cavity decay and the decay of the qubits is included using a Lindblad operator $\mathscr{L}\rho = 2\kappa D[c]\rho + \gamma D[\sigma_1^- + \sigma_2^-]\rho$, with the dissipators defined as $D[x]\rho = (x\rho x^\dagger - x^\dagger x\rho + \mathrm{H.c.})$. This kind of qubit decay only acts on the symmetric state of the qubit, $|T_0\rangle = (|\uparrow\downarrow\rangle + |\downarrow\uparrow\rangle)/\sqrt{2}$, while the antisymmetric "singlet" state $|S\rangle = (|\uparrow\downarrow\rangle - |\downarrow\uparrow\rangle)/\sqrt{2}$ remains unaffected. This, together with the other symmetries of the Hamiltonian, fully separates the singlet state $|S\rangle$ from all of the dynamics. It can therefore be excluded from the calculations. The other states the two-qubit system may be in are the ground state $|T_-\rangle = |\downarrow\downarrow\rangle$ and the biexciton state, $|T_+\rangle = |\uparrow\uparrow\rangle$, which form the "triplet states" together with $|T_0\rangle$ (hence the naming).

Mitra and Vyas [154] give an extensive analysis of this system, using semiclassical equations which do treat the photon field classically. They find that the system exhibits

bistability in the variable of the cavity photon number for a certain range of parameters. They continue to calculate the concurrence of the two-qubit system, using the formula of Wootters (Eq. 2.21). They calculate numerically the dependence of the concurrence on the pump rate and find that with stronger pump, the two qubits become more and more entangled (starting from the qubit ground state and zero photons in the cavity). This is understandable since pumping populates the entangled $|T_0\rangle$ state, but not the $|S\rangle$ state. If the parameters are chosen such that bistability in the photon intensity occurs, the maximal entanglement appears in the semiclassical case [154] at the onset of bistability on the low-pump end. As soon as the bistability region ends on the high-pump end, the concurrence sharply drops to zero. The authors attribute that to the sudden increase of intensity of the cavity mode, which also distributes the probability evenly between $|T_-\rangle$, $|T_0\rangle$, and $|T_+\rangle$ – which is a disentangled state. All this points towards a strong interconnection between entanglement and bistability. The authors suggest to use the photon properties to measure the entanglement between the qubits.

In the few-excitation limit of the cavity mode, the semiclassical analysis of Ref. [154] is no longer applicable, and the quantization of the electromagnetic field has to be taken into account. The occurrence of "quantum noise" makes the usual approach for bistability impossible. In fact, due to the linearity of quantum mechanics, actual bistabilities will not be part of the equations. As it was shown by Savage and Carmichael [156], a similar bistability in a system with *one* qubit coupled to a cavity mode appears in the quantum limit as a double peak in the photon number distribution. One can therefore expect to see such a double peak in the photon distribution as well for the simulations of the two-qubit system. The system dynamics was simulated starting with an empty cavity and the qubits in the ground state. The used values are $\omega_c = \omega_q = \omega_d = 1\,\mathrm{fs}^{-1}$, $g = 3.0\,\mathrm{ps}^{-1}$, $\gamma = 1.35\,\mathrm{ps}^{-1}$, and $\kappa = 0.5\,\mathrm{ps}^{-1}$. The Förster coupling is tuned to bring the system in and out of the bistability region. The breakdown of bistability due to Förster interaction occurs in the semiclassical case [154] and is therefore also used here as the parameter to control the strength of the bistability. Different Förster coupling strengths were chosen: $F = 0.0$, $F = 3.0\,\mathrm{ps}^{-1}$, and $F = 6.0\,\mathrm{ps}^{-1}$. The photonic Hilbert space was truncated at 200 cavity photons. First, the photon number distribution dependent on the drive strength as well as on the Förster coupling was analyzed. Three results are plotted in Fig. 7.2. For small F values, the photon distribution is sharply peaked at low (even zero) photons. However, at a finite driving strength, a second "branch" emerges with a much broader photon distribution at higher photon numbers. For a certain range of driving strengths, both branches coexist and thereby show the typical behavior of quantum-optical bistability: a double-peaked photon number distribution. Due to the finite widths of the branches, it is not possible – in contrast to semiclassical models – to precisely locate the onset of bistability. This is exactly the same as in the case of one qubit in a cavity [156]. For larger F, this double-peak structure disappears and the photon number distribution shifts smoothly to higher photon numbers for increasing pump strength. At this point, the Förster interaction has eliminated the bistability. This behavior is in

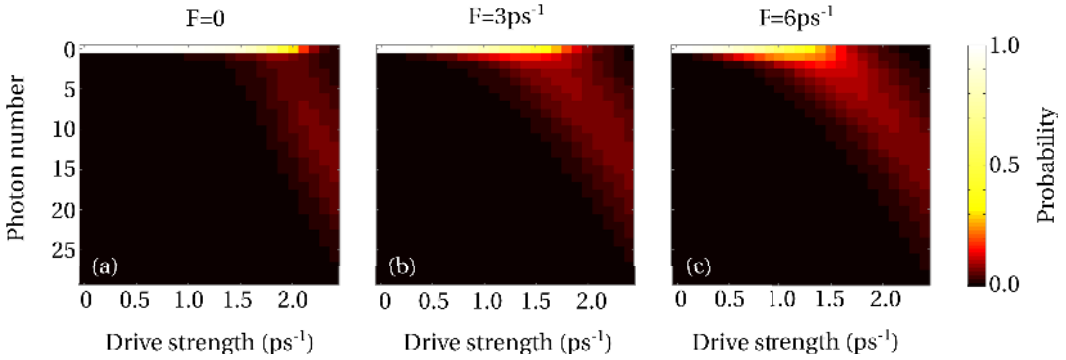

Fig. 7.2.: Photon number distribution, depending on drive strength ϵ and Förster coupling F. (a) $F = 0.0$, (b) $F = 3.0\,\mathrm{ps}^{-1}$, (c) $F = 6.0\,\mathrm{ps}^{-1}$. For low Förster coupling, a large probability at very low (down to 0) photon numbers is found, with a second "branch" of higher probabilities at higher photon numbers emerging at finite drive strength. In (a) as well as in (b) the bistability is clearly visible through a double-peaked photon number distribution (in the right half of the panel). For $F = 6.0\,\mathrm{ps}^{-1}$, the bistability is not visible any more. Instead, the probability peak smoothly moves to higher photon numbers for higher pump strengths.

exact analogy to the semiclassical case of Ref. [154], plotted there in Fig. 1 (b). Let us continue by analyzing the concurrence between the quantum dots for the same set of parameters. The results are depicted in Fig. 7.3. An asymmetric drive dependence of the concurrence is found, which becomes more symmetric for larger F. The maximal concurrence increases with increasing F, at least for the depicted range of values. As in the semiclassical calculations, the concurrence becomes exactly zero at one finite pump strength. However, the connection to bistability is not as straightforward as the semiclassical analysis suggests. For vanishing F, the disappearance of entanglement happens at about the same drive strength as the *appearance* of bistability, while in the semiclassical case bistability was connected to a *maximal* concurrence. This analysis can of course be extended to study dependencies on other parameters, such as decay or coupling rates. However, the semiclassical analysis predicts that no entanglement above 0.43 can be reached [154]. The coupling of both qubits to the same cavity also limits its use for quantum-information applications, since usually entanglement between *distant* qubits is the goal. It seems that the most interesting aspect of the system studied by Mitra and Vyas [154] is the unintuitive connection between entanglement and bistability, which unfortunately does not "survive" the transition to the highly quantum-mechanical low-intensity limit.

A more promising approach will be studied next, describing two coupled cavities, containing a qubit each.

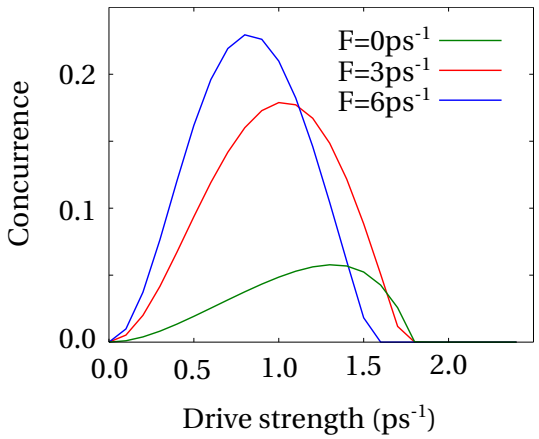

Fig. 7.3.: Entanglement between the two qubits, measured by the concurrence, dependent on the drive strength ϵ and Förster interaction F. For small F, a steady increase of the concurrence is visible when increasing the drive strength, followed by a rapid drop. For higher F, the situation becomes more symmetric, and also leads to overall higher entanglement. Side note: The small kinks on the right hand side end of the curve are artifacts due to the finite ϵ resolution on the abscissa.

7.2 Two qubits coupled to two cavities: Entanglement through resonant Raman processes

Aron *et al.* recently proposed a protocol to entangle two qubits in two separate, but coupled cavities [46]. In this section, this system will be re-examined. In contrast to the publication by Aron *et al.*, transition rates will be derived via a time-dependent perturbation theory approach, which offers further insights into the proposal.

The system consists of two qubits, modeled as two-level systems. Each is located within a photonic cavity, and both cavities are coupled with each other (cf. Fig. 7.4). Experimentally, such a coupling can be achieved either through a short waveguide or through evanescent fields. The two-level energy splitting, cavity angular frequency, qubit-cavity coupling and cavity-cavity coupling are $\hbar\omega_\mathrm{q}$, ω_c, g, and J, respectively. Both cavities are also driven in-phase with a laser[1] of strength ϵ_d and angular frequency ω_d. The Hamiltonian therefore reads, using $\hbar = 1$ [46]:

$$\begin{aligned} H(t) = & \sum_{i=1}^{2} \omega_\mathrm{c} a_i^\dagger a_i - J\left(a_1^\dagger a_2 + a_2^\dagger a_1\right) \\ & + \sum_{i=1}^{2} \omega_\mathrm{q} \frac{\sigma_i^z}{2} + g \sum_{i=1}^{2} \left(a_i^\dagger \sigma_i^- + a_i \sigma_i^+\right) \\ & + 2\sqrt{2}\epsilon_\mathrm{d} \cos(\omega_\mathrm{d} t) \sum_{i=1}^{2} \left(a_i + a_i^\dagger\right) \end{aligned} \tag{7.2}$$

[1] The term "laser" will be used exchangably with "drive" or "driving" in this chapter, and it describes a coherent photonic driving. It does not need to be an actual optical laser though; it could as well be a coherent microwave source.

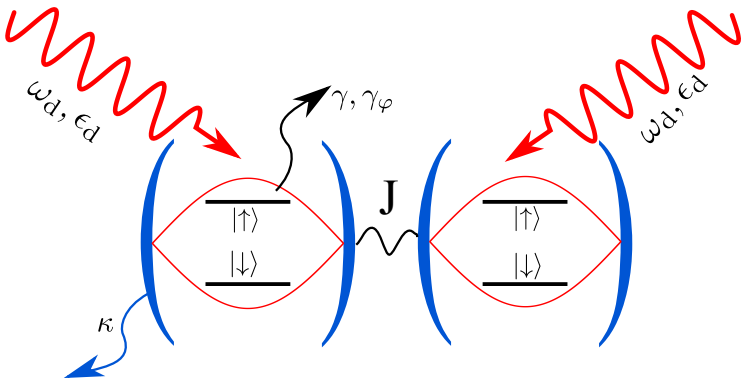

Fig. 7.4.: The setup of Ref. [46], which shall be analyzed and extended in the following sections: Two single mode cavities (frequency ω_c) are coupled (coupling constant J) and also contain a two-level system each (energy difference ω_q, coupling constant g). They are pumped by a laser with strength ϵ_d and frequency ω_d. The cavities experience losses by a rate κ. Additionally, the qubits experience losses by a rate γ and pure dephasing by a rate γ_φ.

To stay in the language of Ref. [46], $a_{1,2}^{(\dagger)}$ are the annihilation (creation) operators for photons in the first and second cavity. $\sigma_{1,2}^{x,y,z}$ operators denote the standard Pauli spin operators for the first and second two-level system. The corresponding raising and lowering operators are $\sigma_i^{\pm} \equiv (\sigma_i^x \pm i\sigma_i^y)/2$. The system is in the large detuning regime, with

$$\Delta \equiv \omega_q - \omega_c \gg g, \tag{7.3}$$

which will later on allow a Schrieffer-Wolff transformation to acquire analytical results. The coupling of the two cavities leads to the formation of two collective modes. There exists a symmetric mode with angular frequency $\omega_c^- := \omega_c - J$, described by the operators $A^{(\dagger)} = \left(a_1^{(\dagger)} + a_2^{(\dagger)}\right)/\sqrt{2}$, as well as an antisymmetric mode with angular frequency $\omega_c^+ := \omega_c + J$, described by the operators $a^{(\dagger)} = \left(a_1^{(\dagger)} - a_2^{(\dagger)}\right)/\sqrt{2}$.

The eigenstates of the fermionic system are the three triplet states, $|T_-\rangle = |\downarrow\downarrow\rangle$, $|T_0\rangle = \left(|\uparrow\downarrow\rangle + |\downarrow\uparrow\rangle\right)/\sqrt{2}$, and $|T_+\rangle = |\uparrow\uparrow\rangle$ as well as the singlet state $|S\rangle = \left(|\uparrow\downarrow\rangle - |\downarrow\uparrow\rangle\right)/\sqrt{2}$. The states $|T_0\rangle$ and $|S\rangle$ are maximally entangled Bell states, and they are the states the two-qubit system shall be brought into. Without any interaction between the qubits, these two Bell states would be degenerate in energy. However, as it will be shown below, the degeneracy is lifted by a photon-mediated interaction. Initially, the system is prepared in the ground state $|T_-\rangle$.

The system also experience losses, which are introduced via a master equation on the system density matrix, which reads as

$$\partial_t \rho = -i[H(t), \rho] + \sum_i \kappa \mathscr{D}[a_i]\rho + \gamma \mathscr{D}[\sigma_i^-]\rho + \frac{\gamma_\varphi}{2} \mathscr{D}[\sigma_i^z]\rho. \tag{7.4}$$

Here, Lindblad-type dissipators are introduced: $\mathscr{D}[X]\rho \equiv \left(X\rho X^\dagger - X^\dagger X\rho + \text{H.c.}\right)/2$. κ denotes the loss of the single cavities, γ a decay of the two-level system (without emission of a photon into a cavity mode), and γ_φ models pure dephasing between the qubits.

The general idea brought forward by Aron *et al.* is the following: In order to pump the system to one of the Bell states, the system is driven by a coherent AC drive (a laser or a microwave tone) at such a frequency that in addition to exciting the system a photon will be deposited in one of the photon modes. The effectiveness of this two-photon process will be highly pump-frequency-dependent: If the cavity resonance is hit perfectly, the high photonic density of states at this frequency will strongly enhance the process. For other frequencies, though, there is no "space" for the photon to go to. This selectiveness will make it possible to selectively drive the system into the desired state. The overall process is slightly more complex, since there are other competing processes, and also symmetry constraints. As it will turn out, symmetries actually make the selectiveness higher.

To get a better insight into the system, the authors use a Schrieffer-Wolff transform $H \mapsto \widetilde{H} \equiv \mathrm{e}^X H \mathrm{e}^{X^\dagger}$ to eliminate terms linear in g/Δ in the undriven Hamiltonian. This is achieved by

$$X \equiv \frac{g}{\sqrt{2}}\left[\frac{A(\sigma_1^+ + \sigma_2^+)}{\omega_\mathrm{q} - \omega_\mathrm{c}^-} + \frac{a(\sigma_1^+ - \sigma_2^+)}{\omega_\mathrm{q} - \omega_\mathrm{c}^+} - \text{H.c.}\right]. \tag{7.5}$$

If all terms of order $(g/\Delta)^3$ or higher are neglected, one arrives at a Hamiltonian which can be partitioned as follows,

$$\widetilde{H} = \widetilde{H}_a + \widetilde{H}_\sigma + \widetilde{H}_{\sigma a} + \widetilde{H}_d(t). \tag{7.6}$$

The different parts of the Hamiltonian are defined as

$$\widetilde{H}_a = \omega_\mathrm{c}^- A^\dagger A + \omega_\mathrm{c}^+ a^\dagger a \tag{7.7}$$

$$\widetilde{H}_\sigma = \sum_{i=1}^{2} \omega_\mathrm{q} \frac{\sigma_i^z}{2} - \frac{1}{2} J \left(\frac{g}{\Delta}\right)^2 \left(\sigma_1^x \sigma_2^x + \sigma_1^y \sigma_2^y\right) \tag{7.8}$$

$$\widetilde{H}_{\sigma a} = \frac{g^2}{2\Delta}\left[\left(1 + A^\dagger A + a^\dagger a\right)\left(\sigma_1^z + \sigma_2^z\right) + \left(A^\dagger a + a^\dagger A\right)\left(\sigma_1^z - \sigma_2^z\right)\right] \tag{7.9}$$

$$\begin{aligned}\widetilde{H}_d(t) =& 2\sqrt{2}\epsilon_\mathrm{d}\cos(\omega_\mathrm{d} t)\left(A + A^\dagger\right) + 2\frac{g}{\Delta}\epsilon_\mathrm{d}\cos(\omega_\mathrm{d} t)\left(\sigma_1^x + \sigma_2^x\right) \\ &+ \frac{1}{\sqrt{2}}\left(\frac{g}{\Delta}\right)^2 \epsilon_\mathrm{d}\cos(\omega_\mathrm{d} t)\left[A\left(\sigma_1^z + \sigma_2^z\right) + a\left(\sigma_1^z - \sigma_2^z\right) + \text{H.c.}\right].\end{aligned} \tag{7.10}$$

The terms can be interpreted as follows: $\widetilde{H}_a$ describes the cavity system, $\widetilde{H}_\sigma$ the spin system, $\widetilde{H}_{\sigma a}$ the interaction between spins and photons independently of the drive, and finally $\widetilde{H}_d(t)$ the time-dependent terms for the coherent drive. The term $J\left(\frac{g}{\Delta}\right)^2\left(\sigma_1^x\sigma_2^x + \sigma_1^y\sigma_2^y\right)$ in $\widetilde{H}_\sigma$ describes a photon-mediated transverse coupling between the two qubits, which

leads to a breakup of the degeneracy within the Bell-state subspace. Let us split the cavity photon operators up into a coherent part and a noise term:

$$A \equiv \overline{A}\mathrm{e}^{-i\omega_\mathrm{d} t} + D, \text{ using } \overline{A} = \frac{-\sqrt{2}\epsilon}{\omega_\mathrm{c}^- - i\kappa/2} \tag{7.11}$$

$$a \equiv \overline{a}\mathrm{e}^{-i\omega_\mathrm{d} t} + d, \text{ using } \overline{a} = 0 \tag{7.12}$$

Let us also define $N = |\overline{A}|^2$. The reason for $a = d$ is that the antisymmetric mode is not not pumped, and therefore this mode is only populated by incoherent "noise" photons. From Eq. 7.6, it is possible to derive the energies of the eigenstates of the *undriven* Hamiltonian: $E(T_\pm) = \pm\omega_\mathrm{q} + O\left(\left(\frac{g}{\Delta}\right)^2\right)$, $E(T_0) = -J(g/\Delta)^2$, and $E(S) = J(g/\Delta)^2$. Note that the energy values of $|T_\pm\rangle$ are given only up to $O\left(\left(\frac{g}{\Delta}\right)^2\right)$, since they depend on ϵ_d at higher orders, and for the full system then need to be evaluated with finite ϵ_d. More accurate values are given in Ref. [46]. At this point it is sensible to perform a rotating wave approximation and eliminate terms not rotating along with the undriven resonance. This is equivalent to removing all terms which would be oscillating with $2\omega_\mathrm{d}$ after a transformation in the frame rotating with ω_d. Note that up to this point the only difference in the analysis between Ref. [46] and this section is that here the analysis stays in the lab frame. This will make the subsequent derivation of transition rates via second order time-dependent perturbation theory clearer. Note that Ref. [46] does not provide such a derivation, and instead derives new eigenstates of the transformed Hamiltonian. In Ref. [46], these eigenstates are then used to calculate transition rates within the framework of Fermi's Golden Rule, which in the way it is used is based on first-order perturbation theory. Since the presented mechanism is however a two-photon process, the two photons are not treated on equal footing in such an approach, and therefore a second-order time-dependent perturbation theory approach is more elegant and insightful. It will also make it straightforward to discuss the inclusion of further driving fields, as presented in section 7.4. The terms which will contribute to the transitions discussed in Ref. [46] are

$$\widetilde{H}_{\sigma,d} = \frac{1}{2}\left(\frac{g}{\Delta}\right)^2\left(\bar{A}\Delta + \frac{\epsilon_\mathrm{d}}{\sqrt{2}}\right)\left[D^\dagger(\sigma_1^z + \sigma_2^z) + d^\dagger(\sigma_1^z - \sigma_2^z)\right]e^{-i\omega_\mathrm{d} t} + \mathrm{H.c.}, \tag{7.13}$$

as well as

$$\widetilde{H}_{\sigma^x} = \frac{g}{\Delta}\epsilon_\mathrm{d}(\sigma_1^+ + \sigma_2^+)e^{-i\omega_\mathrm{d} t} + \mathrm{H.c.}. \tag{7.14}$$

Note that Eq. 7.14 is derived from $\widetilde{H}_d(t)$ by using $\sigma^x = \sigma^+ + \sigma^-$ and then applying the rotating wave approximation.

The transitions discussed in the paper are two photon transitions, therefore *second order* perturbation theory is necessary. The equation of the transition rate from $|i\rangle$ to $|f\rangle$, using the perturbation $V \equiv \widetilde{H}_{\sigma,d} + \widetilde{H}_{\sigma^x}$ that oscillates with ω_d is

$$\Gamma_{i\to f} = 2\pi\left|\sum_m \frac{\langle f|V|m\rangle\langle m|V|i\rangle}{\omega_m - \omega_i - \omega_\mathrm{d}}\right|^2 \delta(\omega_f - \omega_i - 2\omega_\mathrm{d}) \tag{7.15}$$

Here, $\{|m\rangle\}$ are intermediate states that do not need to fulfill energy conservation. The delta function in the end makes sure energy is conserved in the whole process, and will be replaced by a density of states in realistic situations, which will be discussed in a moment. The denominator shows that a state $|m\rangle$ is weighted the highest, when it is reached from $|i\rangle$ by the energy of one driving photon, i.e., when it lies halfway between $|i\rangle$ and $|f\rangle$. For the analysis of "our" two-photon process, it is important to know what the intermediate state(s) is/are. In order to do this, let us have a closer look at the action of the Hamiltonians $\widetilde{H}_{\sigma,d}$ and $\widetilde{H}_{\sigma^x}$ on the qubit subspace. The terms acting on the qubits are actually of three types:

- $(\sigma_1^z + \sigma_2^z)$: Terms like these are proportional to the total (pseudo)"spin" in "z" direction of the two-spin system. While $\langle T_\pm|(\sigma_1^z + \sigma_2^z)|T_\pm\rangle = \pm 2$, the Bell states $|T_0\rangle$ and $|S\rangle$ have an expectation value of 0. Since the spin eigenstates of the unperturbed Hamiltonian are also eigenstates of terms like these, no transition between spin states is initiated. Consequently, all parts of the Hamiltonian with such spin dependence only act upon the photonic subspace.
- $(\sigma_1^z - \sigma_2^z)$: Terms like these evaluate to zero if acted upon by a state with two equal spins, i.e., $|T_\pm\rangle$. On the other hand, it transforms $|T_0\rangle$ into $|S\rangle$ and vice versa: $\langle S|(\sigma_1^z - \sigma_2^z)|T_0\rangle = 2$. It can therefore initiate transitions between the Bell states, however it cannot change the number of excitations in the two-qubit system.
- $(\sigma_1^\pm + \sigma_2^\pm)$: Terms like these are responsible for transitions within the triplet state subspace, as they initiate transitions between $|T_-\rangle$ and $|T_0\rangle$ as well as between $|T_0\rangle$ and $|T_+\rangle$. Acting with it upon the $|S\rangle$ state results in 0, it therefore does not initiate any transitions to or from the $|S\rangle$ state.

Let us now discuss the δ-function in Eq. 7.15. As it will be shown below, any pumping mechanism in the spin subspace will also deposit a (noise) photon in one of the modes described by D or d. In a first approximation, these modes can be treated as a zero temperature bath. In order for this approximation to work, a very low value of $\langle D^\dagger D\rangle$ as well as $\langle d^\dagger d\rangle$ is needed, which is achieved through the finite photon loss rate κ. This approximation also allows to neglect terms in the Hamiltonian of the form $...XD^\dagger D$ and $...Xd^\dagger d$, which lead to finite frequency shifts [46]. Although cavities are certainly a non-Markovian reservoir, for the calculation of steady state transition rates one can just use the photonic density of states of the cavity at the respective frequency in Eq. 7.15 instead of the delta function. This density of states is given as

$$\rho_\pm(\omega) = -\frac{1}{\pi}\mathrm{Im}\frac{1}{\omega - \omega_c^\pm + i\kappa/2}. \tag{7.16}$$

The sharp peak of this density of states is what gives the selectivity of the protocol: Rates in which the resonance is not matched will be strongly suppressed. Now all the ingredients to calculate transition rates are present. Let us describe the states by their fermionic degree of freedom, as well as by the number of noise photons in the symmetric and

antisymmetric modes: $|\psi\rangle \equiv |\{Spins\}, n(D), n(d)\rangle$. Since the photon modes are described as zero-temperature baths, the initial state will always have zero photons in both modes. It will therefore be $|i\rangle = |T_-, 0, 0\rangle$.

It is remarkable that the pumping to $|T_0\rangle$ actually takes a very different route than pumping to $|S\rangle$. The only way to arrive at $|S\rangle$ using $H_{\sigma^x} + H_{\sigma,d}$ is via the following transition:

$$|T_-, 0, 0\rangle \overset{\widetilde{H}_{\sigma^x}}{\rightarrow} |T_0, 0, 0\rangle \overset{\widetilde{H}_{\sigma,d}}{\rightarrow} |S, 0, 1\rangle \tag{7.17}$$

This can be used to calculate

$$\langle T_0, 0, 0|\widetilde{H}_{\sigma^x}|T_-, 0, 0\rangle = \Omega_R/\sqrt{2} \tag{7.18}$$

$$\langle S, 0, 1|\widetilde{H}_{\sigma,d}|T_0, 0, 0\rangle = \lambda. \tag{7.19}$$

Here, $\Omega_R \equiv 2\epsilon_\mathrm{d} g/\Delta$ as well as $\lambda = (g/\Delta)^2(\overline{A}\Delta + \epsilon_\mathrm{d}/\sqrt{2})$ was introduced just as in Ref. [46]. The transition path of Eq. 7.17 nicely demonstrates that the transition to $|S\rangle$ coincides with a deposition of a photon in the *antisymmetric* mode (d). There exists no term in $\widetilde{H}$ which can initiate a transition from $|T_-\rangle$ to $|S\rangle$ which at the same time deposits a photon in the *symmetric* mode. Therefore one has to evaluate the photonic density of states $\rho_+(\omega)$ to arrive at the right transition rate.

The denominator in Eq. 7.15 will give (on resonance) $(\omega_\mathrm{q} - \omega_\mathrm{c}^+)/2 + O\big((g/\Delta)^2\big)$, which is equal to the quantity "Δ_q" in Ref. [46] up to terms $O\big((g/\Delta)^2\big)$. Checking terms $O\big((g/\Delta)^2\big)$ gave almost equal results to Ref. [46], however slight differences in the denominator appear coming from terms proportional to $J(g/\Delta)^2$. These can be contributed to approximations during the transformations from $|T_{\pm,0}\rangle$ to $|\tilde{T}_{\pm,0}\rangle$ in Ref. [46]. In conclusion, the rates calculated in Ref. [46] can be reproduced by a time-dependent perturbation theory approach.

The transition to arrive at $|T_0\rangle$ is actually very different. The transition path is:

$$|T_-, 0, 0\rangle \overset{\widetilde{H}_{\sigma,d}}{\rightarrow} |T_-, 1, 0\rangle \overset{\widetilde{H}_{\sigma^x}}{\rightarrow} |T_0, 1, 0\rangle \tag{7.20}$$

First of all, the order in which the two parts of the Hamiltonian are applied, is switched. Also this time, $H_{\sigma,d}$ is used to only deposit a photon in the symmetric mode while keeping the spins in the ground state $|T_-\rangle$. Afterwards, the spin state is changed to $|T_0\rangle$ using H_{σ^x}. Interestingly, this different path leads to the same transition rates:

$$\langle T_-, 1, 0|\widetilde{H}_{\sigma,d}|T_-, 0, 0\rangle = \lambda \tag{7.21}$$

$$\langle T_0, 0, 1|\widetilde{H}_{\sigma^x}|T_-, 1, 0\rangle = \Omega_R/\sqrt{2} \tag{7.22}$$

The energy denominator will now give $(\omega_q - \omega_c^-)/2 + O\big((g/\Delta)^2\big)$, which will finally also lead to the same transition rate as in Ref. [46] up to $O\big((g/\Delta)^2\big)$. Note that this time a photon is scattered into the symmetric mode, so one needs to evaluate ρ_-.

Let us briefly summarize the results of Ref. [46] which are confirmed by the second-order time-dependent perturbation theory presented above:

For two qubits coupled to two cavities, there exists a pumping mechanism to bring the qubits into an entangled Bell state. It works as follows: One pumps the symmetric cavity mode. To bring the system into the symmetric Bell state $|T_0\rangle$, starting from the ground state $|T_-\rangle$, the pump frequency is chosen such that the energy of two pump photons ($2\omega_d$) matches the energy of the symmetric cavity mode (ω_c^-) plus the energy needed to bring the qubit system from $|T_-\rangle$ to $|T_0\rangle$. On the other hand, to bring the system into the symmetric Bell state $|S\rangle$, starting from the ground state $|T_-\rangle$, the pump frequency is chosen such that the energy of two pump photons ($2\omega_d$) matches the energy of the *antisymmetric* cavity mode (ω_c^+) plus the energy needed to bring the qubit system from $|T_-\rangle$ to $|S\rangle$. The crucial point for this transition is that the two modes have a frequency difference of $2J$, which is orders of magnitude larger than the frequency difference between $|S\rangle$ and $|T_0\rangle$ (which is $2J(g/\Delta)^2$). It is this high selectivity that allows one to precisely populate one of the two states. However, as it is also mentioned in Ref. [46], one problem persists: The same process that pumps from the ground state to the desired Bell state also pumps from the Bell state to the biexciton state $|T_+\rangle$. Although this process is not at resonance of the cavity, its energy difference is still only of the order $2J(g/\Delta)^2$. Such processes not only lead to a nonzero population of $|T_+\rangle$, which reduces entanglement, but also to an effective dephasing, since $|T_+\rangle$ decays with decay rate γ into both Bell state equally. It therefore couples the Bell states via $|T_0\rangle \leftrightarrow |T_+\rangle \leftrightarrow |S\rangle$. Suppressing these processes demands for very low cavity losses, at least $\kappa < 2J(g/\Delta)^2$. However, if the cavity losses are too weak, the zero temperature bath approximation is no longer valid. There will be non-negligible intensity within the cavity mode. If the cavities have a non-negligible photon density, however, this can be used to drive *backwards processes* that utilize a cavity photon to drive the system away from the Bell state back to the ground state in a process similar to stimulated emission. Therefore the cavity must not be too "perfect". After all, if one only considers, e.g., the subsystem made from $|T_-\rangle$ and $|T_0\rangle$, driving to $|T_0\rangle$ creates a strong inversion within this subsystem. However it is well-known that in a pure two-level system inversion is not possible. Including the photon degrees of freedom, it is apparent that the system actually rather looks like a three-level system, consisting of $|T_-,0,0\rangle$, $|T_0,1,0\rangle$, and $|T_0,0,0\rangle$. There is no inversion between the states $|T_-,0,0\rangle$ and $|T_0,1,0\rangle$, which are coupled via the drive. The finite photon decay κ however translates $|T_0,1,0\rangle$ to $|T_0,0,0\rangle$, while there is no process at zero temperature in the other direction. This creates the high occupation of the $|T_0,0,0\rangle$ state. For very small κ, this process should manifest itself through Rabi oscillations between $|T_-\rangle$ and $|T_0\rangle$. A similar argument holds for the transition from $|T_-\rangle$ to $|S\rangle$.

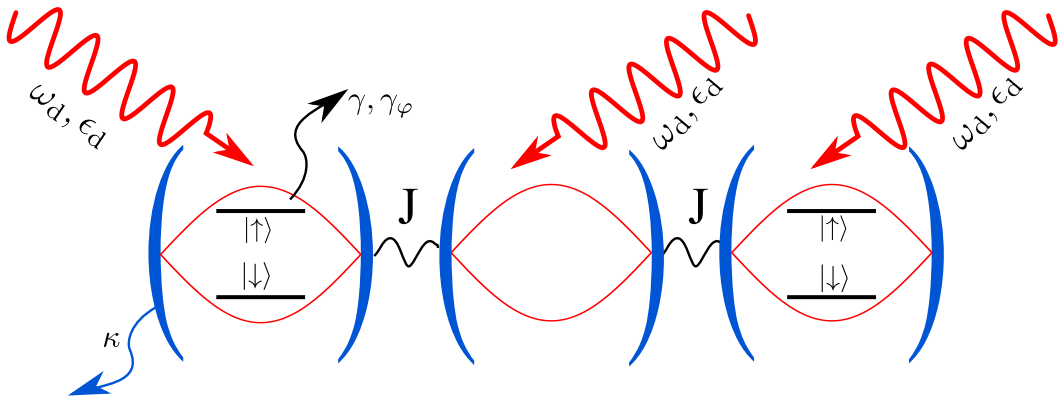

Fig. 7.5.: A way to model cavities which are not directly coupled, but by a waveguide or similar, is to describe the coupling as a cavity as well. On resonance, the cavity-cavity interaction is maximal, which is why the coupling between right and left cavity is modeled as a resonant single mode cavity in the middle. For a waveguide, this may be an approximation which takes only one resonant waveguide mode into account.

7.3 Two qubits coupled to three cavities

One of the benefits of entangling two qubits in two separate cavities, as discussed above, is that the two qubits are spatially distant. This makes the two qubits easily addressable. Coupling between the cavities can either be achieved by tunnel coupling or through a short waveguide. The waveguide option diminishes the coupling between the cavities however, which makes the entanglement scheme work less well. What is to be studied in this section is what happens if the cavities are coupled via a third resonant cavity. This shall be a model for distantly coupled cavities, e.g. through longer waveguides. Such a system can be described by the Hamiltonian [46]:

$$\begin{aligned} H_3(t) = & \sum_{i=1}^{3} \omega_c a_i^\dagger a_i - J\left(a_1^\dagger a_2 + a_2^\dagger a_1 + a_2^\dagger a_3 + a_3^\dagger a_2\right) \\ & + \sum_{i=\{1,3\}} \omega_q \frac{\sigma_i^z}{2} + g \sum_{i=\{1,3\}} \left(a_i^\dagger \sigma_i^- + a_i \sigma_i^+\right) \\ & + 2\sqrt{2}\epsilon_d \cos(\omega_d t) \sum_{i=1}^{3} \left(a_i + a_i^\dagger\right) \end{aligned} \tag{7.23}$$

This setup is equivalent to the one discussed before, however now containing three coupled cavities (without periodic boundary conditions). Only the first and third cavity contain a qubit, which is why they are now described with $\sigma_{1,3}$-operators. Again, all

cavities are pumped equally and in phase. In order to diagonalize the photonic subspace, let us introduce the three new modes

$$
\begin{aligned}
a_s^{(\dagger)} &= \frac{1}{2}\left(a_1^{(\dagger)} + \sqrt{2}\,a_2^{(\dagger)} + a_3^{(\dagger)}\right) \text{ (referred to as "+ + +")} \\
a_0^{(\dagger)} &= \frac{1}{\sqrt{2}}\left(a_1^{(\dagger)} - a_3^{(\dagger)}\right) \text{ (referred to as "+0−")} \\
a_a^{(\dagger)} &= \frac{1}{2}\left(a_1^{(\dagger)} - \sqrt{2}\,a_2^{(\dagger)} + a_3^{(\dagger)}\right) \text{ (referred to as "+ − +")}
\end{aligned}
\tag{7.24}
$$

The eigenfrequencies of these modes are $\omega_c^s = \omega_c - \sqrt{2}J$, $\omega_c^0 = \omega_c$, and $\omega_c^a = \omega_c + \sqrt{2}J$. Compared to the two-cavity case, the mode frequency splitting is reduced from $2J$ to $\sqrt{2}J$. This however should not be a big problem: To differentiate between pumping to $|S\rangle$ and pumping to $|T_0\rangle$, the splitting is still large enough, since it can still be much larger than κ. For the values used in Ref. [46], the difference is three orders of magnitude.

A big problem is however the photon-mediated spin-spin coupling. Due to the third cavity, this coupling is reduced from being in the order of $J(g/\Delta)^2)$ to J^2g^2/Δ^3. For the values used in Ref. [46], this puts the Bell state energy splitting on the same order of magnitude as the cavity decay rate κ. Therefore, the decrease about a factor J/Δ will strongly enhance the transition rate away from the Bell states up to the $|T_+\rangle$ biexciton state, since the selectivity of the cavity mode is not sufficient. It will therefore be very hard to create substantial entanglement between the qubits. In summary, it can be said that distantly coupled qubits are harder to entangle using the discussed method – delay does not help in this case. The system will have a substantial excitation probability in the two-excitation subspace (which only exists of $|T_+\rangle$ in our case). This system must be differentiated from a system consisting of three coupled cavities containing a qubit each, which is discussed by Aron *et al.* in another paper [47]. In such a system, the qubit eigenstates within the one-excitation subspace actually differ in energy by $J(g/\Delta)^2)$, just as in the case of two cavities. In particular, one of the qubit eigenstates is $\left(|\uparrow\downarrow\downarrow\rangle - |\downarrow\downarrow\uparrow\rangle\right)/\sqrt{2}$. The density matrix of this state, traced over the central qubit, is equal to $|S\rangle\langle S|$. Would such a setup be more favorable to create distant entanglement? In other words: Would it help to put a qubit in the transmission channel to gain higher energy splitting? The problem with only an empty cavity as a connection was that the two-excitation subspace was also populated. In the case of three coupled qubit-cavity systems, there actually exists a state in the two-excitation subspace with twice the energy of $\left(|\uparrow\downarrow\downarrow\rangle - |\downarrow\downarrow\uparrow\rangle\right)/\sqrt{2}$, namely the state $\left(|\uparrow\uparrow\downarrow\rangle - |\downarrow\uparrow\uparrow\rangle\right)/\sqrt{2}$. The problem might exist that pumping from the ground state to $\left(|\uparrow\downarrow\downarrow\rangle - |\downarrow\downarrow\uparrow\rangle\right)/\sqrt{2}$ simultaneously pumps from $\left(|\uparrow\downarrow\downarrow\rangle - |\downarrow\downarrow\uparrow\rangle\right)/\sqrt{2}$ to $\left(|\uparrow\uparrow\downarrow\rangle - |\downarrow\uparrow\uparrow\rangle\right)/\sqrt{2}$. However a close look at the equations in Ref. [47] reveal that for this transition a different photonic mode must be used. This was also confirmed through personal communication with C. Aron, the lead author of Ref. [47]. One might therefore actually get a substantial fidelity of the state $\left(|\uparrow\downarrow\downarrow\rangle - |\downarrow\downarrow\uparrow\rangle\right)/\sqrt{2}$ and therefore substantial entanglement between the first and the last qubit. So, the answer is yes: Adding a qubit in the coupling cavity will help to increase the selectivity.

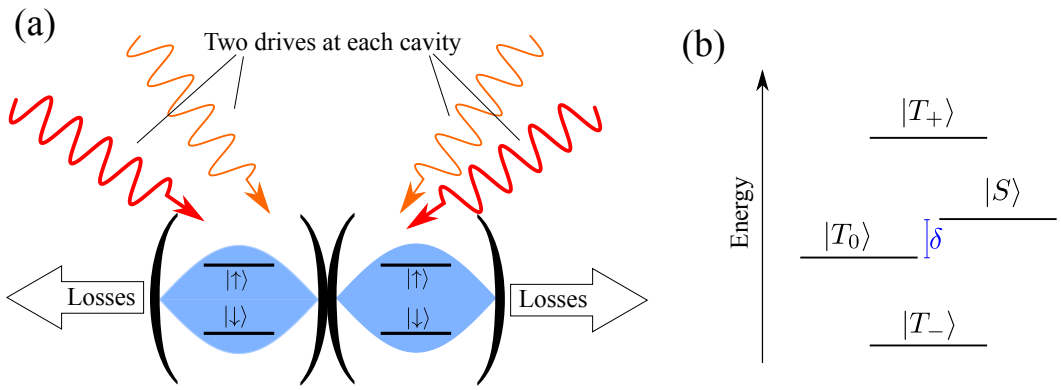

Fig. 7.6.: (a) Setup that was calculated to demonstrate the anti-dephasing protocol: Two qubits in a cavity each, in the same setup as in Ref. [46]. Cavity-cavity coupling is J. The cavities experience losses with rate κ, and the qubits experience decay with rate γ as well as pure dephasing with rate γ_φ. The cavities are pumped by two lasers with angular frequencies ω_d and ω'_d and strengths ϵ_d respectively ϵ'_d. The cavities are pumped in phase. (b) Energy level scheme of the qubit subspace. Note that due to photon-mediated qubit-qubit interactions, the states $|T_0\rangle$ and $|S\rangle$ have an energy difference δ.

7.4 Fighting dephasing through a second resonant Raman process

A manuscript covering parts of this section is in preparation for submission

Although it is possible to achieve quite high fidelities of Bell states with the protocol discussed in Ref. [46], which is also confirmed by experiment [157], there is still much room for improvement. Reported fidelities are in the area of 70% [157]. One obstacle to reach higher values is dephasing: It is not possible to suppress the interaction of the qubits with their environment, which creates entanglement also between the environment and the system. For the system itself, this can lead to a smaller overall entanglement [158], since information is lost to the environment. If the system also experiences a loss of energy, this leads to decay; if the loss only affects *phase* information, this leads to dephasing.

The analysis of Ref. [46] was performed for values typical of superconductor-based artificial atoms in microwave cavities [159–161]. In such a setup, noise in the applied magnetic flux can make the artificial atoms decay, while noise in the voltage across the Josephson junction creates pure dephasing [161, 162].

To reach really high entanglement, a protocol to fight dephasing must be developed. This is the topic of the following analysis. The idea of Ref. [46] can be extended by adding another drive to the cavities, which in a similar process reduces dephasing. The idea in itself is simple: To fight dephasing, one needs to drive from $|T_0\rangle$ to $|S\rangle$ or vice versa, on demand – however for best results only in one direction. This is achieved by again

utilizing the strongly structured photonic environment provided by the cavity modes. The two cavities provide us with two modes of opposite parity. The idea behind the proposed anti-dephasing scheme is to pump one mode almost at the frequency of the other. The small mismatch to the mode frequency is chosen such that it is the same as the energy difference between $|T_0\rangle$ and $|S\rangle$. In a resonant Raman process, one pump photon can now be used to drive the system from $|T_0\rangle$ to $|S\rangle$ (or vice versa, depending on the sign of the detuning) and at the same time excite the cavity mode. Since the cavity modes are sharp, this is a highly frequency-selective process and only the desired transition will be strong.

The main ingredients for this scheme are two coupled qubits and two bosonic modes of opposite parity – two things that are already present in the scheme discussed by Aron *et al.* [46]. It can therefore be easily applied to this system. The setup is pictured in Fig. 7.6. However, there may be a lot of other systems that can profit from the proposed mechanism - e.g., in a setup of quantum dots (which provide the qubits) coupled to a microcavity. The bosonic modes might in practice also be plasmonic modes (however here the width of the mode might be a problem) or mechanical modes of an optomechanical setup.

The Hamiltonian of Ref. [46] with an additional anti-dephasing drive is

$$\begin{aligned} H(t) = & \sum_{i=1}^{2} \omega_\mathrm{c} a_i^\dagger a_i - J\left(a_1^\dagger a_2 + a_2^\dagger a_1\right) \\ & + \sum_{i=1}^{2} \omega_\mathrm{q} \frac{\sigma_i^z}{2} + g \sum_{i=1}^{2} \left(a_i^\dagger \sigma_i^- + a_i \sigma_i^+\right) \\ & + 2\epsilon_\mathrm{d} \cos(\omega_\mathrm{d} t) \sum_{i=1}^{2} \left(a_i + a_i^\dagger\right) \\ & + 2\epsilon_\mathrm{d}' \cos(\omega_\mathrm{d}' t) \sum_{i=1}^{2} \left(a_i + a_i^\dagger\right). \end{aligned} \tag{7.25}$$

Again there are two qubits (angular frequency ω_q, operators $\sigma_{1,2}^z, \sigma_{1,2}^\pm$) coupled to two cavities (frequency ω_c, operators $a_{1,2}^{(\dagger)}$) with coupling strength g. The two cavities are coupled with strength J. This leads, again, to the buildup of the two modes $A^{(\dagger)} \equiv \left(a_1^{(\dagger)} + a_2^{(\dagger)}\right)/\sqrt{2}$ and $a^{(\dagger)} \equiv \left(a_1^{(\dagger)} - a_2^{(\dagger)}\right)/\sqrt{2}$. Due to the coupling, A oscillates with $\omega_\mathrm{c}^- = \omega_\mathrm{c} - J$ and a oscillates with $\omega_\mathrm{c}^+ = \omega_\mathrm{c} + J$.

The system is driven by two lasers, both coupling to the symmetric mode. The laser angular frequencies are ω_d and ω_d', and their respective strengths are ϵ_d and ϵ_d'. Let us

transform the Hamiltonian into a rotating frame with ω_d through the unitary transformation $H \mapsto U_\mathrm{rot}\,(H - i\partial_t)\,U_\mathrm{rot}^\dagger$ with

$$U_\mathrm{rot} = \exp\left[i\omega_\mathrm{d} t\left(\frac{\sigma_1^z + \sigma_2^z}{2} + A^\dagger A + a^\dagger a\right)\right]. \tag{7.26}$$

After the transformation, all the terms rotating with $2\omega_\mathrm{d}$ as well as with $\omega_\mathrm{d} + \omega_\mathrm{d}'$ will be neglected. This is a kind of rotating wave approximation. However, terms rotating with $\omega_\mathrm{d} - \omega_\mathrm{d}'$ are kept. For the scheme to work, ω_d and ω_d' are of the same order of magnitude. They will differ by about $\Delta/2$, with $\Delta \equiv \omega_\mathrm{q} - \omega_\mathrm{c}$. Therefore $\Delta \ll \omega_\mathrm{d}$ holds.

In contrast to Ref. [46], the combination of a transformation to the rotating frame and a rotating wave approximation does not eliminate the full time-dependence of the Hamiltonian (Eq. 7.25). This makes it much harder to distinguish (and even define) a steady state. Without a time dependence, steady states can be found by solving the equation $\partial_t \rho = 0$, using the master equation for the density matrix ρ. This equation can be found by a simple matrix inversion. As it will be demonstrated later on, it is in many cases possible to create an approximate time-independent Hamiltonian even in the two-laser setup.

Again, losses are included through a Lindblad approach, cf. Eq. 7.4 with the decay rates κ for the cavity, γ for the qubit decay, and γ_φ for the qubit pure dephasing. Note that due to the Purcell effect, qubits placed in cavities experience lower losses than in free space. This will be already considered by choosing a γ which is appropriate for qubits in cavities. Additionally, the finite energy difference between $|T_0\rangle$ and $|S\rangle$ already substantially reduces pure dephasing between the qubits, since the environment is probed at the finite frequency Δ. This will also be directly included in the choice of γ_φ.

The Hamiltonian in the rotating frame, after the rotating wave approximation, reads

$$\begin{aligned} H(t) = \; & \sum_{i=1}^{2} \left(\omega_\mathrm{c} - \omega_\mathrm{d}\right) a_i^\dagger a_i - J\left(a_1^\dagger a_2 + a_2^\dagger a_1\right) \\ & + \sum_{i=1}^{2} \left(\omega_\mathrm{q} - \omega_\mathrm{d}\right) \frac{\sigma_i^z}{2} + g \sum_{i=1}^{2} \left(a_i^\dagger \sigma_i^- + a_i \sigma_i^+\right) \\ & + \sqrt{2}\epsilon_\mathrm{d} \sum_{i=1}^{2} \left(a_i + a_i^\dagger\right) \\ & + \sqrt{2}\epsilon_\mathrm{d}' \sum_{i=1}^{2} \left(\mathrm{e}^{\mathrm{i}(\omega_\mathrm{d}' - \omega_\mathrm{d})t} a_i + \mathrm{e}^{-\mathrm{i}(\omega_\mathrm{d}' - \omega_\mathrm{d})t} a_i^\dagger\right). \end{aligned} \tag{7.27}$$

7.4.1 Analytical derivation of transition rates

Before direct numerical simulations of the Hamiltonian of Eq. 7.27 are discussed, it will be analyzed analytically. Therefore the Schrieffer-Wolff transform $H \mapsto \widetilde{H} \equiv \mathrm{e}^X H \mathrm{e}^{X^\dagger}$

is applied, with X as discussed above (cf. Eq. 7.5). Discarding all terms of order higher than $(g/\Delta)^2$ leads to the approximate Hamiltonian

$$\widetilde{H}(t) = \widetilde{H}_a + \widetilde{H}_\sigma + \widetilde{H}_{\sigma a} + \widetilde{H}_\mathrm{d} + \widetilde{H}'_\mathrm{d}(t), \tag{7.28}$$

using

$$\widetilde{H}_a = \left(\omega_\mathrm{c}^- - \omega_\mathrm{d}\right) A^\dagger A + \left(\omega_\mathrm{c}^+ - \omega_\mathrm{d}\right) a^\dagger a \tag{7.29}$$

$$\widetilde{H}_\sigma = \sum_{i=1}^{2} \left(\omega_\mathrm{q} - \omega_\mathrm{d}\right) \frac{\sigma_i^z}{2} - \frac{1}{2} J \left(\frac{g}{\Delta}\right)^2 \left(\sigma_1^x \sigma_2^x + \sigma_1^y \sigma_2^y\right) \tag{7.30}$$

$$\widetilde{H}_{\sigma a} = \frac{g^2}{2\Delta} \left[\left(1 + A^\dagger A + a^\dagger a\right) \left(\sigma_1^z + \sigma_2^z\right) + \left(A^\dagger a + a^\dagger A\right) \left(\sigma_1^z - \sigma_2^z\right) \right] \tag{7.31}$$

$$\widetilde{H}_\mathrm{d} = \sqrt{2}\epsilon_\mathrm{d} \left(A + A^\dagger\right) + \frac{g}{\Delta} \epsilon_\mathrm{d} \left(\sigma_1^x + \sigma_2^x\right) + \frac{1}{2\sqrt{2}} \left(\frac{g}{\Delta}\right)^2 \epsilon_\mathrm{d} \left[A \left(\sigma_1^z + \sigma_2^z\right) + a \left(\sigma_1^z - \sigma_2^z\right) + \mathrm{H.c.} \right] \tag{7.32}$$

$$\begin{aligned} \widetilde{H}'_\mathrm{d}(t) = {} & \sqrt{2}\epsilon'_\mathrm{d} \left[A \mathrm{e}^{\mathrm{i}(\omega'_\mathrm{d} - \omega_\mathrm{d})t} + A^\dagger \mathrm{e}^{-\mathrm{i}(\omega'_\mathrm{d} - \omega_\mathrm{d})t} \right] \\ & + \frac{g}{\Delta} \epsilon'_\mathrm{d} \left[\cos((\omega'_\mathrm{d} - \omega_\mathrm{d})t) \left(\sigma_1^x + \sigma_2^x\right) + \sin((\omega'_\mathrm{d} - \omega_\mathrm{d})t) \left(\sigma_1^y + \sigma_2^y\right) \right] \\ & + \frac{1}{2\sqrt{2}} \left(\frac{g}{\Delta}\right)^2 \epsilon'_\mathrm{d} \left[A \mathrm{e}^{\mathrm{i}(\omega'_\mathrm{d} - \omega_\mathrm{d})t} \left(\sigma_1^z + \sigma_2^z\right) + a \mathrm{e}^{\mathrm{i}(\omega'_\mathrm{d} - \omega_\mathrm{d})t} \left(\sigma_1^z - \sigma_2^z\right) + \mathrm{H.c.} \right]. \end{aligned} \tag{7.33}$$

Here the Hamiltonian is divided in the same way as above in the one-drive scheme. However due to the second drive, $\widetilde{H}'_\mathrm{d}(t)$ appears additionally. Since the description is not in the rotating frame of ω'_d, this Hamiltonian looks very complex.

Again, a qubit-qubit interaction is present through the term $-\frac{1}{2} J \left(\frac{g}{\Delta}\right)^2 \left(\sigma_1^x \sigma_2^x + \sigma_1^y \sigma_2^y\right)$, which leads to an energy splitting between $|T_0\rangle$ and $|S\rangle$ of $2Jg^2/\Delta^2 \equiv \delta$.

Let us again separate the photonic parts into "coherent" and "noise" parts. The modes only have "coherent" parts if they are actually driven by the laser. Since the antisymmetric mode ($a^{(\dagger)}$) is not pumped, it will only be populated by noise:

$$a \equiv d. \tag{7.34}$$

This is different for the symmetric mode. The symmetric mode is driven with two different frequencies, leading to

$$A \equiv \overline{A}_\mathrm{d} + e^{-\mathrm{i}(\omega'_\mathrm{d} - \omega_\mathrm{d})t} \overline{A}'_\mathrm{d} + D, \tag{7.35}$$

where

$$\overline{A}_\mathrm{d} \approx \frac{\sqrt{2}\epsilon_\mathrm{d}}{\omega_\mathrm{d} - \omega_\mathrm{c}^- + \mathrm{i}\kappa/2}, \; \overline{A}'_\mathrm{d} \approx \frac{\sqrt{2}\epsilon'_\mathrm{d}}{\omega'_\mathrm{d} - \omega_\mathrm{c}^- + \mathrm{i}\kappa/2}. \tag{7.36}$$

The approximation lies in the fact that no interaction between the coherent parts is included; their intensities are calculated as if the respective laser were the only laser driving the system. For simplicity, let us also abbreviate $\overline{N}_\mathrm{d} \equiv |\overline{A}_\mathrm{d}|^2$ as well as $\overline{N}'_\mathrm{d} \equiv |\overline{A}'_\mathrm{d}|^2$.

At this point, the eigenenergies of the system must be discussed. This is difficult, since parts of the Hamiltonian introduce transitions between the eigenenergies, so they are not in fact the energies of the eigenstates of the full Hamiltonian. A good way to distinguish between "system Hamiltonian", "bath Hamiltonian", and "system-bath coupling" is to include in the system Hamiltonian all parts of the Hamiltonian, which do not contain the operators $D^{(\dagger)}$ or $d^{(\dagger)}$. This is also consistent with Ref. [46].

There is one time-dependent term in $\widetilde{H}'_\mathrm{d}(t)$ which also fulfills this criterion – it is $+\frac{g}{\Delta}\epsilon'_\mathrm{d}\Big[\cos((\omega'_\mathrm{d}-\omega_\mathrm{d})t)\left(\sigma_1^x+\sigma_2^x\right)+\sin((\omega'_\mathrm{d}-\omega_\mathrm{d})t)\left(\sigma_1^y+\sigma_2^y\right)\Big]$. This term can be neglected, since it creates oscillations of the order of ϵ'_d on top of terms scaling with ϵ_d. In all applications of the scheme, $\epsilon'_\mathrm{d} \ll \epsilon_\mathrm{d}$. Those terms might therefore only play a role if they can resonantly excite some transitions. As it will be discussed below, this will not be the case. With this, the eigenenergies and eigenstates of the system are (cf. Fig. 7.6(b))

$$E(\widetilde{T}_+) = \Delta_\mathrm{q} + \frac{\Omega_R^2}{2\Delta_\mathrm{q}} \text{ for } |\widetilde{T}_+\rangle = |T_+\rangle + \frac{\Omega_R}{\sqrt{2}\Delta_\mathrm{q}}|T_0\rangle \tag{7.37}$$

$$E(\widetilde{S}) = J(g/\Delta)^2 \text{ for } |\widetilde{S}\rangle = |S\rangle \tag{7.38}$$

$$E(\widetilde{T}_0) = -J(g/\Delta)^2 \text{ for } |\widetilde{T}_0\rangle = |T_0\rangle + \frac{\Omega_R}{\sqrt{2}\Delta_\mathrm{q}}\big(|T_-\rangle - |T_+\rangle\big) \tag{7.39}$$

$$E(\widetilde{T}_-) = -\Delta_\mathrm{q} - \frac{\Omega_R^2}{2\Delta_\mathrm{q}} \text{ for } |\widetilde{T}_+\rangle = |T_-\rangle - \frac{\Omega_R}{\sqrt{2}\Delta_\mathrm{q}}|T_0\rangle \tag{7.40}$$

using the abbreviations $\Omega_R \equiv 2\epsilon_\mathrm{d}(g/\Delta)$ and

$$\Delta_\mathrm{q} \equiv \omega_\mathrm{q} - \omega_\mathrm{d} + (g/\Delta)^2\left[(\overline{N}_\mathrm{d}+\overline{N}'_\mathrm{d}+1)\Delta + \sqrt{2}\mathrm{Re}(\epsilon_\mathrm{d}\overline{A}_\mathrm{d}+\epsilon'_\mathrm{d}\overline{A}'_\mathrm{d})\right]. \tag{7.41}$$

Note that the states exactly look like in Ref. [46], however the value Δ_q now also has components depending on ϵ'_d. The corrections on the eigenstates are actually very small, they are however crucial for the derivation of the transition rates from $|T_-\rangle$ to the one-excitation subspace as discussed in Ref. [46]. For the anti-dephasing scheme discussed here, they are however of no importance. With Ref. [46], there exists a method to get into the one-excitation subspace.

Let us now concentrate on the action of the second drive. As mentioned, terms in the Hamiltonian of the form $\frac{g}{\Delta}\epsilon'_\mathrm{d}\Big[\cos((\omega'_\mathrm{d}-\omega_\mathrm{d})t)\left(\sigma_1^x+\sigma_2^x\right)+\sin((\omega'_\mathrm{d}-\omega_\mathrm{d})t)\left(\sigma_1^y+\sigma_2^y\right)\Big]$ are neglected. In a first order time-dependent perturbation theory approach, these terms drive transitions between states with different quantum number $m = \langle\sigma_1^z+\sigma_2^z\rangle$, however

the frequency of our second drive will be tuned far off these resonances (by an amount on the order of Δ).

The term in $\epsilon'_{\mathrm{d}} D \mathrm{e}^{\mathrm{i}(\omega'_{\mathrm{d}}-\omega_{\mathrm{d}})t}\left(\sigma_1^z+\sigma_2^z\right)+\mathrm{H.c.}$ is also neglected since it only couples to $|T_{\pm}\rangle$ and does not change the qubit state. The important parts of the Hamiltonian are

$$\frac{1}{2\sqrt{2}}\left(\frac{g}{\Delta}\right)^2 \epsilon'_{\mathrm{d}} \mathrm{e}^{\mathrm{i}(\omega'_{\mathrm{d}}-\omega_{\mathrm{d}})t}\left(\sigma_1^z-\sigma_2^z\right) d+\mathrm{H.c.}, \tag{7.42}$$

coming from $\widetilde{H}'_{\mathrm{d}}(t)$, as well as

$$\frac{g^2}{2\Delta}\overline{A}'_{\mathrm{d}} \mathrm{e}^{\mathrm{i}(\omega'_{\mathrm{d}}-\omega_{\mathrm{d}})t}\left(\sigma_1^z-\sigma_2^z\right) d+\mathrm{H.c.}, \tag{7.43}$$

coming from the right hand side of $\widetilde{H}_{\sigma a}$ and getting a time-dependence through the substitution of Eq. 7.35. These terms contain the $d^{(\dagger)}$ operator, so they couple to the antisymmetric mode. One can use Fermi's Golden Rule to calculate transition rates between $|T_0\rangle$ and $|S\rangle$ with the simultaneous deposition of one noise photon in the antisymmetric mode to be

$$\Gamma'_{T_0\to S} = 2\pi\left|\Lambda\right|^2 \rho_+(E_{T_0}-E_S+\omega'_{\mathrm{d}}), \tag{7.44}$$

$$\Gamma'_{S\to T_0} = 2\pi\left|\Lambda\right|^2 \rho_+(E_S-E_{T_0}+\omega'_{\mathrm{d}}), \tag{7.45}$$

with

$$\Lambda \equiv \left(g/\Delta\right)^2 (\overline{A}'_{\mathrm{d}}\Delta+\epsilon'_{\mathrm{d}}/\sqrt{2}). \tag{7.46}$$

These are the rates for the anti-dephasing protocol. For an effective anti-dephasing, ω'_{d} must be chosen such that ρ_+ is evaluated at its maximum. When optimized for a stabilization of $|T_0\rangle$, one can estimate the transition rate of the anti-dephasing scheme as

$$\Gamma'_{S\to T_0} \simeq 2\frac{g^4 {\epsilon'_{\mathrm{d}}}^2}{\Delta^2 J^2 \kappa}. \tag{7.47}$$

A stabilization of $|S\rangle$ leads to the same rate.

However, all of these rates are calculated by treating the photon modes as zero-temperature baths, i.e., in the approximation that $\langle D^\dagger D\rangle = \langle d^\dagger d\rangle = 0$. This is however a very crude approximation. First, "zero temperature" is not possible in experiment, so there will always be some thermal excitation of the modes. Furthermore, scattering into the modes populates the modes. This is only counteracted by the decay rate κ, which may be in the same order of magnitude as the pumping rates calculated above. This leads to a buildup of a nonzero equilibrium photon number in the cavity modes.

The problem with nonzero excitation in the cavity modes is that they allow a backwards process: A cavity photon may be used to drive the system *away* from the desired state.

When the forward process is in resonance, the backwards process is so as well – therefore a significant decrease of the effectiveness might be induced by nonzero cavity excitation. Numerical studies (see below) show that the photon cavity number might be around 0.1.

This nonzero excitation may be included in the rate description. As a good approximation, it is safe to say that there is at most one photon in the mode. Let us work with the antisymmetric mode $d^{(\dagger)}$. The probability to be in the one-photon subspace is therefore $\langle d^\dagger d\rangle$, while the probability to be in the zero-photon subspace is $1-\langle d^\dagger d\rangle$. With one excitation in the mode, the forward process is also increased by a factor of two. This leads to a ratio between forward and backwards process of

$$\frac{\Gamma_{\text{backw.}}}{\Gamma_{\text{forw.}}} \simeq \frac{\langle d^\dagger d\rangle}{(1-\langle d^\dagger d\rangle)+2\langle d^\dagger d\rangle} = \frac{\langle d^\dagger d\rangle}{1+\langle d^\dagger d\rangle}. \tag{7.48}$$

The best way to reduce this is to minimize the number of photons in the mode. This means that a larger κ might actually also be beneficial – one therefore needs to choose κ such that the optimal compromise between selectivity and backwards process suppression is reached. It is also advisable to make the two processes, i.e., the driving to the one-excitation subspace and the anti-dephasing scheme by the second drive, use different modes. For driving to the $|T_0\rangle$ state, this is naturally the case, since the transition from $|T_-\rangle$ to $|T_0\rangle$ is achieved by scattering in the symmetric mode, while the driving from $|S\rangle$ to $|T_0\rangle$ is achieved by scattering in the antisymmetric mode. The similar process for $|S\rangle$ however would use the antisymmetric mode for both processes. This can be counteracted in several ways by choosing different phases for the drives of cavity 1 and cavity 2. If, e.g., the second drive drives both cavities with a phase difference of π, the symmetric mode can be used for the anti-dephasing scheme. It is therefore always possible to use different modes for the different processes.

7.4.2 Approximate Hamiltonian for steady-state analysis

Although the rates based on Fermi's Golden Rule already give a good tool to estimate the steady state values, a method that does not use the quite crude first-order perturbation theory would be very useful. For a system with only one drive, as in Ref. [46], this is quite easy to achieve: Due to the transformation into the rotating frame, the Hamiltonian becomes time-independent. This also makes the right-hand side of the master equation (cf. Eq. 7.4) time-independent. For steady state analysis, this reduces the numerical complexity to a matrix inversion by simply solving $\partial_t \rho = 0$ (with ρ being the density matrix).

For two drives, there is no rotating frame that renders the whole Hamiltonian time-independent. Remarkably, it is still possible to define an *approximate* time-independent Hamiltonian. Let us start from the Hamiltonian after the Schrieffer-Wolff transform,

Eq. 7.28 (hence it's an approximate Hamiltonian). Again let us also split the photon modes into a coherent and a noise part, using Eqs. 7.34 and 7.35. Note that as long as *the two processes, driven by the two drives, scatter into different modes*, there exists a "dominant" process for $D^{(\dagger)}$ and another "dominant" process for $d^{(\dagger)}$. Let us assume that $D^{(\dagger)}$ is used to bring the system into the one-excitation subspace (the process connected to the first drive), while $d^{(\dagger)}$ is used for the anti-dephasing mechanism (the process connected to the second drive). The idea is to rotate all the terms connected with $d^{(\dagger)}$ with the angular frequency ω_{d}', while all the other terms are kept rotating with ω_{d}. Let us now rotate all the terms connected with $d^{(\dagger)}$ into a rotating frame rotating with ω_{d}' by applying $\widetilde{H} \mapsto U[\widetilde{H} - i\partial_t]U^\dagger$ with $U = \exp(i(\omega_{\mathrm{d}}' - \omega_{\mathrm{d}})\, t\, d^\dagger d)$.

Note that now all terms used for the derivation of the anti-dephasing transition rates become time-independent. As it was discussed in the last subsection, all other terms oscillating with $(\omega_{\mathrm{d}}' - \omega_{\mathrm{d}})$ in Eq. 7.28. are highly off-resonant of any transition and may safely be neglected. The additional rotating frame transformation created some further time-dependent terms, though. It however did not affect any of the terms used for the calculation of the transition rates induced by the first drive. *Therefore all time-dependent terms are discarded.* The approximate Hamiltonian can be written as the sum of a "system" part governing the qubits, a "reservoir" part describing the cavity modes, and a "system-reservoir coupling" term. This leads to

$$\widetilde{H}^{\text{t.indp.}} = \widetilde{H}^{\text{t.indp.}}_{\text{sys}} + \widetilde{H}^{\text{t.indp.}}_{\text{res}} + \widetilde{H}^{\text{t.indp.}}_{\text{sys-res}}, \tag{7.49}$$

with

$$\widetilde{H}^{\text{t.indp.}}_{\text{sys}} = \sum_{i=1}^{2} \vec{h}^{\text{t.indp.}} \frac{\vec{\sigma}_i}{2} - \frac{1}{2} J \left(\frac{g}{\Delta}\right)^2 \left(\sigma_1^x \sigma_2^x + \sigma_1^y \sigma_2^y\right) \tag{7.50}$$

$$\widetilde{H}^{\text{t.indp.}}_{\text{res}} = \left(\omega_{\mathrm{c}}^- - \omega_{\mathrm{d}}\right) D^\dagger D + \left(\omega_{\mathrm{c}}^+ - \omega_{\mathrm{d}}'\right) d^\dagger d \tag{7.51}$$

$$\begin{aligned} \widetilde{H}^{\text{t.indp.}}_{\text{sys-res}} = {} & \frac{1}{2}\frac{g^2}{\Delta}\left(D^\dagger D + d^\dagger d\right)\left(\sigma_1^z + \sigma_2^z\right) \\ & + \frac{1}{2}\left(\frac{g}{\Delta}\right)^2 \left[\left(\overline{A}_{\mathrm{d}}\Delta + \frac{\epsilon_{\mathrm{d}}}{\sqrt{2}}\right) D\left(\sigma_1^z + \sigma_2^z\right) + \text{H.c.}\right] \\ & + \frac{1}{2}\left(\frac{g}{\Delta}\right)^2 \left[\left(\overline{A}_{\mathrm{d}}'\Delta + \frac{\epsilon_{\mathrm{d}}'}{\sqrt{2}}\right) d\left(\sigma_1^z - \sigma_2^z\right) + \text{H.c.}\right], \end{aligned} \tag{7.52}$$

using $\vec{h}^{\text{t.indp.}} \equiv (h^{\text{t.indp.},x}, 0, h^{\text{t.indp.},z})$ defined as

$$\begin{aligned} h^{\text{t.indp.},x} &= \frac{2g}{\Delta}\epsilon_{\mathrm{d}} \\ h^{\text{t.indp.},z} &= \omega_{\mathrm{q}} - \omega_{\mathrm{d}} + \left(\frac{g}{\Delta}\right)^2 \Big(\Delta\left(1 + \overline{N}_{\mathrm{d}} + \overline{N}_{\mathrm{d}}'\right) \\ &\qquad + \sqrt{2}\,\mathrm{Re}(\epsilon_{\mathrm{d}}\overline{A}_{\mathrm{d}} + \epsilon_{\mathrm{d}}'\overline{A}_{\mathrm{d}}')\Big). \end{aligned} \tag{7.53}$$

The spin parts are written using a vector multiplication. This means that the interaction of the qubits with the cavity modes are actually analogous to a spin in a magnetic

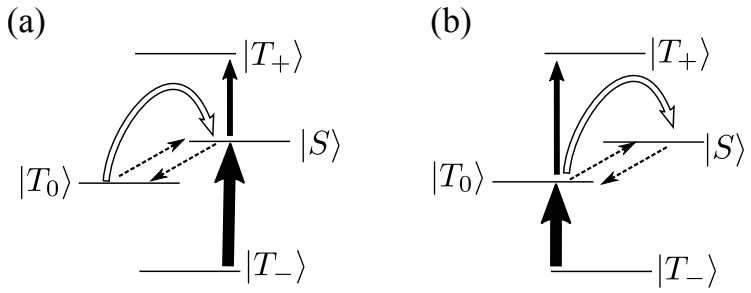

Fig. 7.7.: Two different ways to drive to $|S\rangle$ using two drives. (a) "Regular" scheme: One drives with the first laser (big solid arrow) to $|S\rangle$. Unfortunately, one also drives from $|S\rangle$ to $|T_+\rangle$ off-resonantly, which lowers the fidelity of $|S\rangle$ (smaller solid arrow). The second drive (open arrows) increases the fidelity by counteracting dephasing (dashed arrows). (b) "Switching" scheme: One drives with the first laser to $|T_0\rangle$ and use the second laser to reach $|S\rangle$. Although the transition $|T_0\rangle \rightarrow |T_+\rangle$ is also off-resonantly driven by the first laser, the state $|T_+\rangle$ will still be only slightly populated due to the lack of population of $|T_0\rangle$. a transition from $|S\rangle$ to $|T_0\rangle$ is however not driven by any laser. This allows for higher laser strengths without the problem of populating $|T_+\rangle$.

field. In contrast to the derivation of transition rates above, this time terms of the form $D^\dagger D\sigma^z$ and $d^\dagger d\sigma^z$ are included. This allows the more accurate treatment of finite cavity excitations.

Solving this Hamiltonian for the steady state provides much more accurate results than simple decay rate calculations: It allows to include finite reservoir excitations, since it can be used to calculate the full density matrix, containing the qubit- and the photonic subspace. It is still orders of magnitude faster than full numerical solutions of the time dynamics, though. A comparison to full numerics will be provided below, when numerical results are discussed. It will be shown that the fidelities are reproduced very well by the approximate Hamiltonian, however the exact optimal drive frequencies are shifted.

7.4.3 Switching between Bell states

The second drive can not only be used to purify the state already reached via the first drive – it can also be used to switch between the two Bell states. This leads to two different ways to reach a desired Bell state. Take, for example, the $|S\rangle$ state: One way to arrive there is to use the first drive to get to the $|S\rangle$ state (by scattering into the antisymmetric mode), and then to use the second drive to further purify the $|S\rangle$ state (either by also scattering into the antisymmetric mode, or by driving the antisymmetric mode and scattering into the symmetric one). This is the standard procedure discussed above. Another way to drive to $|S\rangle$ however would be to drive to $|T_0\rangle$ using the first drive, and then drive from there to $|S\rangle$ using the second drive (cf. Fig. 7.7). This will be called the "switching" protocol.

Let us briefly discuss the benefits and drawbacks of this second option: One problem of the usual driving scheme discussed above is that when driving from $|T_-\rangle$ to $|S\rangle$, the

transition from $|S\rangle$ to $|T_+\rangle$ is also driven off-resonantly. When the drive is chosen strong enough to depopulate $|T_-\rangle$, this creates a non-negligible population at $|T_+\rangle$. This not only reduces the fidelity of $|S\rangle$, but also increases dephasing since $|T_+\rangle$ decays to $|T_0\rangle$ via γ.

On the other hand, if $|S\rangle$ is populated via the switching protocol, the first laser is tuned such that it drives from $|T_-\rangle$ to $|T_0\rangle$. This also drives off-resonantly the transition from $|T_0\rangle$ to $|T_+\rangle$ – however, the state $|T_0\rangle$ is almost not populated, since the excitation is transferred away to $|S\rangle$ via the second drive. There is however *no* drive in the system that drives from $|S\rangle$ to $|T_+\rangle$ in this protocol. As a result, $|T_+\rangle$ is almost not populated even for higher pump strengths. This allows to effectively deplete $|T_-\rangle$.

Despite this, the switching protocol is not always favorable: The higher drive strengths also lead to higher populations in the reservoir. One needs higher drive strengths, since it is much harder to transfer the excitation from $|T_0\rangle$, which is constantly pumped, to $|S\rangle$, than to just fight the comparatively low dephasing in the system. As discussed above, higher reservoir populations lead to a "backwards" process in which a cavity photon is destroyed rather than excited, and which reduce fidelity. At this point, a larger cavity loss rate κ is actually favorable: It decreases the number of cavity excitations. This leads to a balance: A high frequency selectivity is needed, which is provided by low κ, but also a low mode excitation, which is helped by higher κ.

Depending on the setup, and especially on the cavity decay rate, either the normal or the switching protocol lead to higher fidelities. For more lossy cavities, the switching protocol may be better, since more lossy cavities lead to higher off-resonant transition rates (which are suppressed by the switching protocol), while they also help reduce the detrimental "backwards" process which is more dominant in the switching protocol. For the values given in Ref. [46], the "usual" protocol leads to higher fidelities (when simulated using the time-independent Hamiltonian discussed above), while for (more realistic) cavity decay rates a factor of 5 higher than in Ref. [46], "switching" is highly preferable. Our simulations predict fidelities above 90% in that case.

This is demonstrated in Fig. 7.8. The time-independent Hamiltonian was used to simulate the steady state for driving to $|S\rangle$, using two different decay rates, $\kappa = 1.0 \times 10^{-4}$ and $\kappa = 5.0 \times 10^{-4}$. All other system properties were identical to Ref. [46]. The first drive had the strength $\epsilon_\mathrm{d} = 0.25$, the second drive $\epsilon'_\mathrm{d} = 0.005$ and frequency $\omega'_\mathrm{d} = 6.102$ (all values in units of 2π GHz). The photonic subspace was truncated at three photons in each mode. The results show that with the lower decay rate, we reach fidelities above 80%, while the higher decay rate even leads to 93% fidelity.

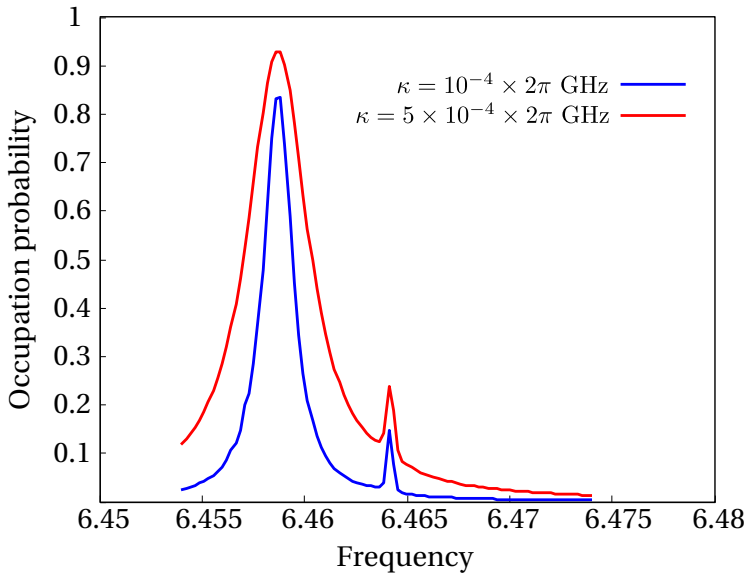

Fig. 7.8.: Fidelities of $|S\rangle$ reachable by the "switching" protocol, depending on ω_d. Two simulations are performed with different cavity decay rates, showing that more lossy ("worse") cavities lead to higher occupaton probabilities of $|S\rangle$.

7.4.4 Numerical simulations

To test all these approximations, numerical simulations were performed, using the Hamiltonian of Eq. 7.25. The Master equation is integrated,

$$\partial_t \rho = -i[H(t), \rho] + \sum_i \kappa \mathscr{D}[a_i]\rho + \gamma \mathscr{D}[\sigma_i^-]\rho + \frac{\gamma_\varphi}{2} \mathscr{D}[\sigma_i^z]\rho, \tag{7.54}$$

with the dissipators defined in the same way as for Eq. 7.4. The simulations are performed in a rotating frame of frequency ω_d. All terms oscillating with $2\omega_d$ and $\omega_d + \omega_d'$ are neglected. Throughout the following discussion, unless specified otherwise, $\omega_c = 6$, $\omega_q = 7$, $g = J = 10^{-1}$, $\kappa = 10^{-4}$, and $\gamma = 10^{-5}$ is used (in units of 2π GHz). These values are in the range of current experiments using superconducting artificial atoms [157], and coincide with the values used by Ref. [46]. The photonic subspace is truncated at 5 photons in each mode. The aim is to pump the system to $|T_0\rangle$. With only one laser, the maximal fidelity for $|T_0\rangle$ is found for $\omega_d = 6.45484 \times 2\pi$ GHz.

First, the full time dynamics are simulated for the system with (in units of 2π GHz) $\omega_d = 6.4548$, $\omega_d' = 6.098$, $\epsilon_d = 0.1$, and $\epsilon_d' = 0.01$. Pure dephasing is set to $\gamma_\varphi = 8.0 \times 10^{-6}$. For comparison, the exact same setup is also simulated with only ϵ_d present. The results are shown in fig. 7.9. Just as predicted by the analytical results, the steady state value for the fidelity of $|T_0\rangle$ is increased by the introduction of the second pump. It is apparent that this increased fidelity comes from $|S\rangle$, whose occupation probability is strongly reduced. This is especially good for high entanglement, since entanglement also needs a high *difference* in the occupation probabilities of $|T_0\rangle$ and $|S\rangle$ (for example, a 50 : 50 mixture of

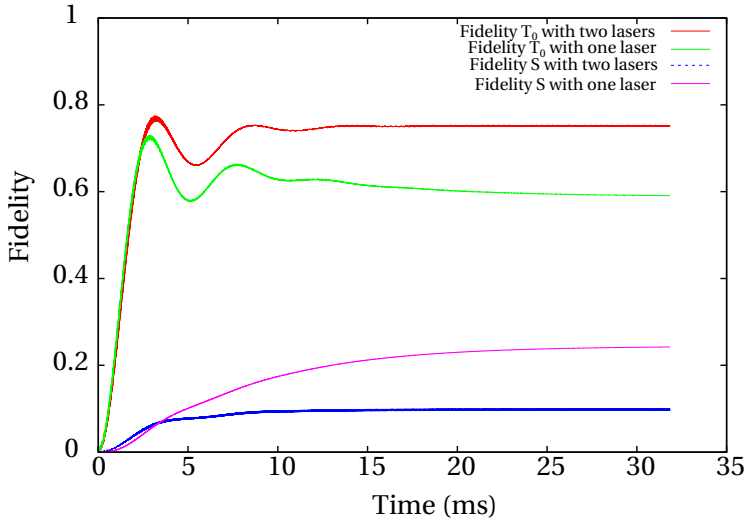

Fig. 7.9.: Time dynamics of the fidelities of $|T_0\rangle$ and $|S\rangle$ with and without the anti-dephasing laser. The results show that using the second laser the fidelity of $|T_0\rangle$ is increased, while the fidelity of $|S\rangle$ is reduced – just as expected by the analytical results.

the two would not be entangled at all). Although there are two drive frequencies present in the setup, the equilibrium is nevertheless reached - only very minuscule oscillations can be seen on top of the main behavior. This demonstrates that the time-independent formulas derived analytically are sensible, since for sustaining large oscillations, a "steady state" (and a transition rate to that state) cannot be defined. The situation is different for the photon probabilities, depicted in Fig. 7.10. In both cases, there are strong intensity fluctuations in the symmetric mode – the one which is pumped. They however die out in case of only one laser. This can be explained as follows: The initial oscillations with only one laser are due to the detuning between cavity and pump frequency, but they die out as soon as the drive has forced its frequency upon the system. With two lasers, there are always two frequencies present driving the mode, so there are strong oscillations in the steady state. These oscillations mainly stem from the coherent part of the mode excitation ($\overline{A}$). The antisymmetric mode is almost not occupied in case of only one laser, since there is no resonant process scattering into this mode. With two lasers, however, the antisymmetric mode is used for the dephasing scheme. This populates the mode by "noise" photons.

In Fig. 7.11, the fidelity (also called the occupation probability) of $|T_0\rangle$, $|S\rangle$, and $|T_+\rangle$ depending on ω_d is displayed. In contrast to above, the pure dephasing rate was reduced slightly to $5.0 \times 10^{-6} \times 2\pi$ GHz. As expected, a large peak is present in the fidelity of $|T_0\rangle$. However, there are also side peaks on the right hand side of the main peak. They are not visible in case of only one drive. For very low ϵ'_d, the peaks move together at $\tilde{\omega} \equiv (\omega_\mathrm{c}^- + E(S) - E(T_-))/2$ (frequencies and energies given in the lab frame). This points to a process that drives to $|S\rangle$ using the deposition of two photons in the symmetric mode (which has frequency ω_c^-). Such a process is not possible in case of only one laser for

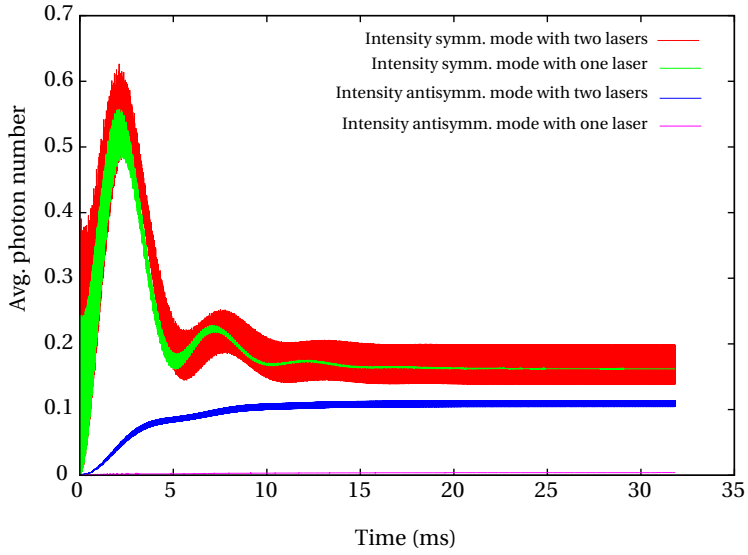

Fig. 7.10.: Time dynamics of the intensity of the photon modes in the setup with and without the second laser. There are strong oscillations and higher occupations with the second laser, which is not surprising since the two lasers interfere, creating an oscillatory intensity in the cavity modes. The antisymmetric cavity mode is not used if only one laser is on, therefore it is only slightly opulated by strongly off-resonant processes.

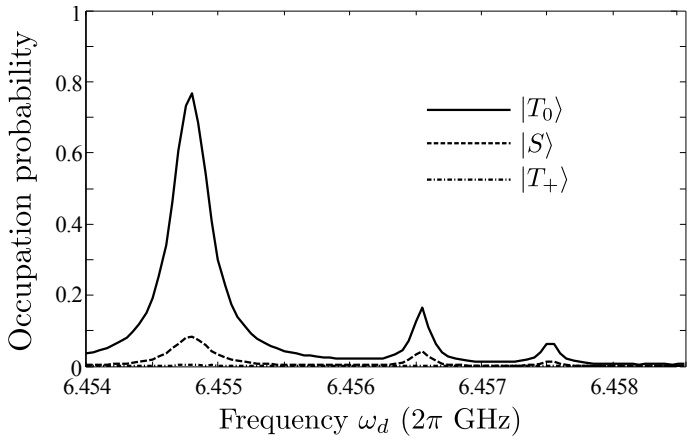

Fig. 7.11.: Steady state fidelity of $|T_0\rangle$, $|S\rangle$, and $|T_+\rangle$ with two lasers, depending on the frequency ω_d of the first laser (in units of 2π GHz). A large peak is present in the fidelity of $|T_0\rangle$, but also two extra peaks at the right hand side of it. $|T_+\rangle$ is almost not populated.

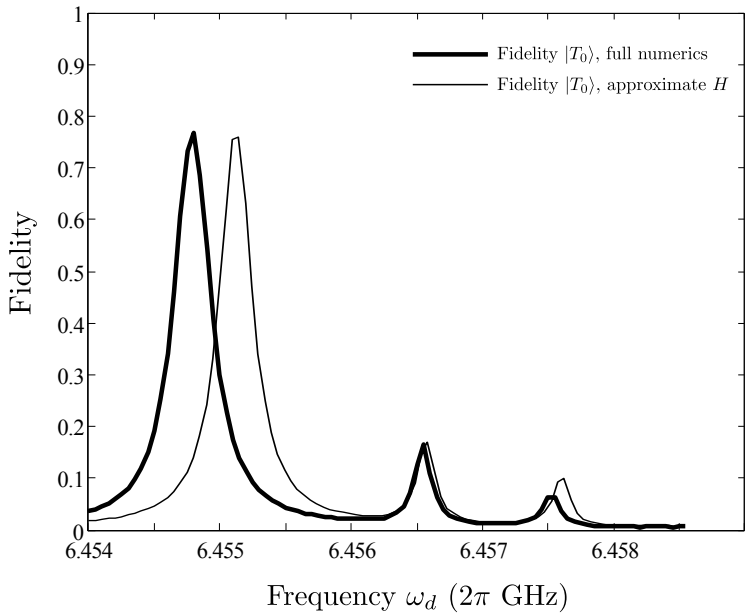

Fig. 7.12.: Comparison of full numerics (thick line) with steady-state results using the time-independent Hamiltonian from above. here is a very good agreement in terms of maximal fidelity, however the exact peak frequency is slightly off.

symmetry reasons. The second laser, however, breaks this symmetry slightly by mixing $|S\rangle$ and $|T_0\rangle$. Such a process is therefore in principle allowed. The second laser also then takes the occupation probability away from $|S\rangle$ and drives to $|T_0\rangle$. This in the end leads to the buildup of a peak in the fidelity of $|T_0\rangle$ around $\tilde{\omega}$. This peak is now split into different peaks by even higher order photon processes, which can be demonstrated by truncating the cavity photon number at 1 photon, which makes the two peaks merge into one. The exact process that splits the peak might be a topic of future research.

At this point it is also possible to compare the numerical results with the ones acquired by the time-independent approximate Hamiltonian. A comparison of the results of Fig. 7.11 with simulations of the exact same parameters using the time-independent Hamiltonian can be found in Fig. 7.12. The results show that although the exact frequencies are shifted, the time-independent Hamiltonian can reproduce the fidelities remarkably well. It also reproduces the side peaks.

To actually check the power of the anti-dephasing protocol, the dynamics are simulated for different values of γ_φ. The value $\epsilon_\mathrm{d} = 0.1$ is kept and ϵ'_d is set to $\epsilon'_\mathrm{d} = 0.005$ (again in units of 2π GHz). The results with and without a second laser are depicted in Fig. 7.13. The frequency without the second laser is now chosen to be such that the fidelity is maximized. This is achieved by setting $\omega_\mathrm{d} = 6.45484 \times 2\pi$ GHz in that case. For the two-drive case, ω_d is set to $\omega_\mathrm{d} = 6.45480 \times 2\pi$ GHz. The strength of the second laser is $\epsilon'_\mathrm{d} = 0.005 \times 2\pi$ GHz.

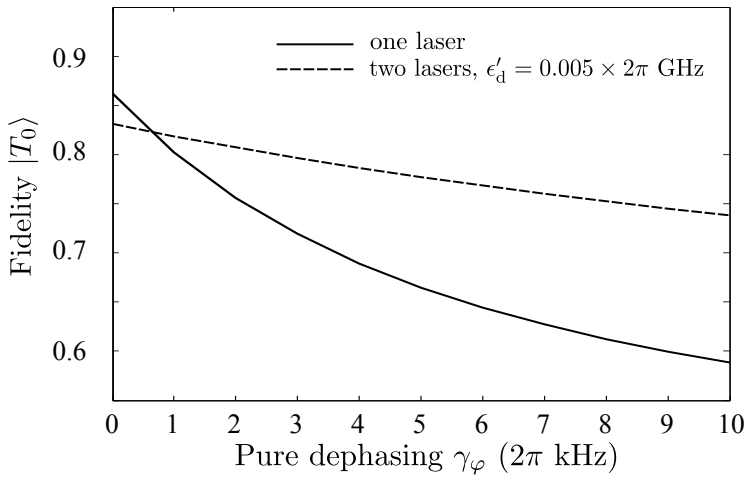

Fig. 7.13.: Fidelity of $|T_0\rangle$ depending on different pure dephasing rates, with and without the second laser. While pure dephasing strongly affects the fidelity, the second laser reduces its effect considerably. This demonstrates that especially for large dephasing the second laser is useful. For very low dephasing, the second laser is actually counterproductive.

The simulations show that pure dehasing strongly reduces the fidelity. The second laser however helps to create and maintain higher fidelity, especially in case of larger dephasing. This demonstates that adding a second laser is actually a very powerful way to reduce dephasing. Interestingly, for very low dephasing, the second laser deteriorates fidelity. The reason is the "backwards" process discussed above that is present at finite mode populations. If this backwards process is larger than the intrinsic dephasing, the second laser acts as a source of dephasing. This is also the reason why a very low power for the second laser was chosen. Higher powers extend the region of γ_φ in which the second laser makes the fidelity worse.

7.4.5 Extension to multiple qubits

It is possible to extend the proposal by Aron *et al.*[46] to more than two qubits [47]. In such a setup, there are n cavities coupled in a network, each containing a two-level system acting as the qubit. In the following it will be discussed to what extent the proposed anti-dephasing scheme can be applied to such extended qubit networks.

The eigenmodes of coupled qubits in a quantum network can become very complex [100]. In a first step, let us restrict ourselves to the setup of n qubits coupled in a circle (i.e., a chain with periodic boundary conditions). In such a system, one eigenstate is a (generalized) W state [163], which can be written as

$$|W(n)\rangle = \frac{1}{\sqrt{n}} \sum_{i=1}^{n} |0...1_i...0\rangle. \tag{7.55}$$

Here, $|0...1_i...0\rangle$ denotes a n-qubit state in which all qubits are 0 exept the one at position i, which is 1. W states are a "natural" extension of Bell states to n qubits with the remarkable property that also a subset of the bits of a Bell state is also entangled (which, e.g., is not the case for another extension of Bell states, the GHZ state [163, 164]).

Let us first discuss the situation of three cavities: the cavity modes as well as the eigenstates of the coupled qubits can be described by the quasi-momentum k, which can take the three values $0, \pm 2\pi/3$. The qubit eigenstates are

$$|k\rangle = \left(|\uparrow\downarrow\downarrow\rangle + e^{ik}|\downarrow\uparrow\downarrow\rangle + e^{2ik}|\downarrow\downarrow\uparrow\rangle\right)/\sqrt{3}. \tag{7.56}$$

The state $|k=0\rangle$ is a W state.For symmetry reasons, the states $|k=\pm 2\pi/3\rangle$ are degenerate, while the $|k=0\rangle$ state is energetically offset. This offset shall be called δ in analogy to above. In the same way as the qubits, the photonic subspace also has three modes, of which two are degenerate. One may now use the first laser to drive to the $|k=0\rangle$ state [46]. Dephasing will however also populate the other states in the one-excitation manifold (the two-excitation manifold will not be considered here). One can now use a second laser tuned at $\omega_{\mathrm{d}}' = \omega_{\mathrm{d}}^{2\pi/3} - \delta$ to increase the fidelity of the $|k=0\rangle$ state by scattering into the $k = \pm 2\pi/3$ modes. Due to the degeneracy, only one additional drive is necessary, since it targets both states. This degeneracy also is a problem when one wants to stabilize any other state $|\pm 2\pi/3\rangle$ of the one-excitation manifold. One cannot use a second laser to drive between the two degenerate states. This demonstrates that for more than 2 qubits, some states actually cannot be stabilized by the procedure.

It might also be necessary to use more than two lasers. For more than three qubits, the states which are not W states are not all degenerate, so one needs an extra frequency to drive from each of the existing energy levels of the 1-excitation manifold to the $k=0$ state. For example, for 5 qubits, two lasers are needed to fight dephasing.

7.5 Conclusion

Cavities are the most prominent way to shape photonic environments due to their sharp and pronounced frequency modulation of the photonic density of states. It was demonstrated that this fact can be utilized to generate and sustain entanglement between two-level systems. In case of two two-level systems in one cavity, only mediocre values for the entanglement were found, and unfortunately the strong connection between bistability and entanglement, as suggested by semiclassical calculations [154], could not be confirmed.

Another setup is more promising, consisting of two coupled cavities with a qubit located in each one. The results of Aron *et al.* were derived using a time-dependent perturbation theory approach, which gave deeper insights into the present processes.

Starting from this, it was possible generalize the system to cavities coupled through a third cavity in between – however, this setup was shown to be less performant since the qubit-qubit coupling is strongly reduced. In the third, and main part of the presented analysis, it was studied whether pumping with two lasers could further enhance entanglement by using a resonant Raman transition to fight dephasing. This approach produced very high entanglement in the numerical simulations, and a good stability against decoherence. Also, approximate analytic formulas and a time-independent Hamiltonian were presented to calculate steady-state entanglement quickly. Their results are consistent with the full numerical simulations.

There are already experiments [157] implementing the design of Ref. [46]. It is apparent that they can benefit strongly from implementing the second drive as discussed in the last chapter. The system was also shown to be extendable to a chain or even network of qubit-cavity units, which can be used for the creation of highly interesting W states.

8 Conclusion and outlook

Since the pioneering work of Purcell [165], it is known that the environment strongly influences the behavior of quantum systems. The power of non-Markovian environments is that this influence is highly frequency-dependent, which thereby influences different states of the system in totally different ways. This strong frequency dependence is however also what makes such systems hard to compute, since standard approximations often break down as soon as the dynamics become “interesting”.

In this thesis, special kinds of non-Markovian environments were studied, in particular such that lead to time-delayed feedback of the Pyragas type. Time-delayed feedback is a challenge for numerical simulations, since the delay time introduces a time scale which might be much larger than any time scale of the system, demanding a high resolution in frequency space. This demands for new approaches to solve time-delayed dynamics in quantum optics.

One promising approach, based upon pseudomode theory was developed and presented. It uses the dissipative aspects of Pyragas control by modeling time-delayed feedback as a complex network of lossy harmonic oscillators. It was shown that results acquired with this technique agree extraordinarily well with full numerical simulations, and at the same time reduce the numerical complexity from a system with several hundreds of photonic modes to about 20.

Furthermore, the influence of time-delayed feedback on quantum-optical systems was studied. First, it was demonstrated that a network of qubits can be stabilized at complex entangled states if time-delayed feedback is introduced. The mechanism behind this approach is to create large decay rates for all un-wanted states, while reducing the decay rate for the target state. This can create entangled final states from totally separable inital states.

To cover more complex dynamics, time-delayed feedback as added to nonlinear systems. It was found that in a cavity containing a Kerr medium time-delayed feedback could lead to a stabilization of 1-photon Fock states. Also the decay rate of the 2-photon Fock state could be selectively reduced. In case of a Jaynes-Cummings system subject to feedback, very similar dynamics could be found, however not stabilizing Fock states, but dressed states in the 1- or 2-excitation subspace.

A biexciton cascade subject to time-delayed feedback was also studied. The numerical simulations showed that feedback can increase the photon entanglement by increasing the biexciton decay rate, which reduced the detrimental influence of exciton fine-structure splitting. It was also shown that increasing the delay time can even further enhance the entanglement by steering the emission into a narrower frequency region.

Finally, systems without time-delayed feedback were discussed. The structured environment was instead given by one or several high-Q cavities. The results demonstrated the power of structured environments to create stable non-equilibrium entangled states. Especially in case of two coupled cavities containing a qubit each, a technique was developed to counteract dephasing between the qubits, using resonant raman scattering. Fidelities of entangled Bell states above 90% are predicted using numerical simulations. This technique is easily extended to more qubits, e.g. for the stabilization of entangled W states.

What topics of future research are there in these fields? First, it is still a challenge to calculate Pyragas-type dynamics for complex systems or long times. If the issue on how to include the noise terms in time-delayed operator equations was solved, it would make it possible to study much more complex systems subject to time-delayed feedback, and maybe even study the transition from the quantum regime to classical nonlinear dynamics. Interesting systems for such dynamics could be multilevel systems, lasers [45], or even just the discussed systems with a higher number of excitations.

Concerning the qubits located in cavities, an interesting way to extend this is to use many lasers on a setup of a complex qubit network, and see which higher-excited states can be reached.

Acknowledgements

This thesis would not have been possible without the support of many others. First and foremost, I want to thank my advisor, Prof. Dr. Andreas Knorr for providing me the opportunity to work on the highly interesting subject of time-delayed feedback control in his group, and for offering his advice uncountable times. I also want to thank Prof. Dr. Harald Giessen for offering to be my second advisor, and also for drawing my interest to the fascinating physics of nanophotonics in the first place many years ago.

This thesis was produced using funding of the DFG SFB 910 "Control of Self-Organizing Nonlinear Systems" as part of project B1.

I am very grateful that I had the opportunity to work at Princeton University for two months. Many thanks to everyone who made this possible – in particular Prof. Hakan E. Türeci and Camille Aron, and also the rest of the "Mesoscopic Quantum Optics" group, and of course the SFB 787 "School of Nanophotonics" for providing funding.

The time at TU Berlin was particularly pleasant due to my awesome colleagues at the institute. Many thanks to my long-term office mate and very good friend Franz Schulze, for providing support way beyond quantum mechanics. Sorry again for the towel incident. Many thanks also to my current office mate, Manuel Kraft – hopefully "the paper" will be finished soon!

Many thanks to Alex Carmele for the support in writing our common publications. Last but not least many thanks to the "11 am" and "1 pm" lunch groups (Sandra, Anke, Judith, Franz, Nicolas, Manuel, Michael, Markus, Florian, Gunnar, Torben, Malte, Leon, etc...) for making the Mensa enjoyable, even if the food is sub-optimal...

This thesis is dedicated to my parents, Rose and Hauke. Without their constant backing, this whole "Berlin and beyond" adventure would have been impossible. *You're the best.*

A Appendix: Derivation of the Lindblad equation

In this appendix, the standard derivation of Lindblad-type dissipation is presented. It is mainly based upon Ref. [60].

Let us describe the system with density matrix ρ_S and the bath with density matrix ρ_B. The complete system-bath density operator shall be ρ. The derivation will be in the interaction picture, such that the whole dynamics of the density matrix can be expressed as

$$\partial_t \rho = -\frac{i}{\hbar}[H_{SB}(t), \rho]. \tag{A.1}$$

Due to the description in the interaction picture, the system-bath interaction Hamiltonian is time-dependent:

$$H_{SB}(t) = U^\dagger(t) H_{SB} U(t), \tag{A.2}$$

using $U = \exp\left(-\frac{i}{\hbar}(H_S + H_B)\, t\right)$. Here, H_S is the system operator, H_B the bath operator, and H_{SB} the system-bath interaction. Integrating Eq. A.1 formally gives the time-dependence of ρ, depending on ρ at earlier times:

$$\rho(t) = \rho(0) - \frac{i}{\hbar}\int_0^t \mathrm{d}t' [H_{SB}(t), \rho(t')]. \tag{A.3}$$

One can use this solution to again derive a differential equation for ρ to arrive at

$$\partial_t \rho = -\frac{i}{\hbar}[H_{SB}(t), \rho(0)] - \frac{1}{\hbar^2}\int_0^t \mathrm{d}t' [H_{SB}(t), [H_{SB}(t'), \rho(t')]]. \tag{A.4}$$

This is just a very "complicated" way to write Eq. A.1, and no approximations were made until now. However, an ansatz like this is the first step in a development of $\partial_t \rho$ in powers of H_{SB}. Let us now assume that initially system and reservoir are non-correlated: $\rho(0) = \rho_S(0)\rho_B(0)$. Let us also assume that initially the bath operators coupling to the system have zero mean: $\mathrm{tr}_B\big(H_{SB}(t)\rho_B(0)\big) = 0$. With these assumptions, one can create a differential equation for ρ_S alone by tracing over the bath degrees of freedom:

$$\partial_t \rho_B = -\frac{1}{\hbar^2}\int_0^t \mathrm{d}t' \mathrm{tr}_B\big([H_{SB}(t), [H_{SB}(t'), \rho(t')]]\big). \tag{A.5}$$

Let us now apply the *Born approximation* by only including terms up to second order in H_{SB}. For this, let us write $\rho(t) = \rho_S(t)\rho_B(0) + O(H_{SB})$, which says that the coupling to the bath is very weak, and $\rho(t)$ only deviates in order H_{SB} from an uncorrelated state. Weak

coupling also leaves the reservoir virtually unchanged, which is why one may use $\rho_B(0)$ in the first term. This brings us to

$$\partial_t \rho_B = -\frac{1}{\hbar^2}\int_0^t \mathrm{d}t' \mathrm{tr}_B\big([H_{SB}(t),[H_{SB}(t'),\rho_S(t')\rho_B(0)]]\big). \tag{A.6}$$

The *Markov approximation* further simplifies this equation by replacing $\rho_S(t')$ by $\rho_S(t)$. For a system in equilibrium, this is trivially true; in all other cases, it is an approximation. It can be motivated physically by stating that the reservoir does not store any memory of earlier states of ρ_S if the reservoir correlation time is shorter than the time scales of the system. We end up with

$$\partial_t \rho_B = -\frac{1}{\hbar^2}\int_0^t \mathrm{d}t' \mathrm{tr}_B\big([H_{SB}(t),[H_{SB}(t'),\rho_S(t)\rho_B(0)]]\big). \tag{A.7}$$

If a bilinear system–reservoir coupling is present, $H_{SB} = \hbar\sum_i S_i(t)\Gamma_i(t)$, with S_i a system operator and Γ_i a bath operator, after a lengthy calculation [115], one arrives at the Lindblad equation without further approximations. For a harmonic oscillator mode of angular frequency ω_0, the coupling looks like

$$H_{SB} = \hbar c^\dagger \sum_j g_j b_j e^{-i(\omega_j-\omega_0)t} + \text{H.c.}, \tag{A.8}$$

with bath operator $b_j^{(\dagger)}$, bath mode angular frequency ω_j, system operator $c^{(\dagger)}$, and system-bath coupling g_j. During the derivation [115] it becomes clear that the Markov approximation is only valid if g_j is slowly varying in frequency and can be pulled out of the sum.

B

Appendix: Equations of motion of a cavity with Kerr-nonlinearity subject to time-delayed feedback in the pseudomode approach

Here the equations of motion for a Kerr medium in a cavity subject to time-delayed feedback are presented, as discussed in section 5.1. To model the feedback with a $\sin^2(kL)$ density function, the pseudomode approach is applied (cf. section 3.3). Also, the nonlinear modeling of the feedback reservoir (in the case here, the pseudomodes) is used, as discussed in section 3.1. The nonlinear approximation method employed is exact up to 2 excitations. Since the initial state contains 2 excitations in the system, and no pumping is present, the method does not introduce any further approximations.

Note that this section differentiates between the strength of the coupling to the feedback reservoir, γ, as introduced in Eq. 2.38, which is a parameter of the experimental setup, and the strength of the coupling to the k-th pseudomode $d_k^{(\dagger)}$, D_k, which is a parameter of the pseudomode approximation. γ also appears in the full Hamiltonian as the prefactor of the sine-modulation, while D_k is chosen such that the pseudomodes model a $\sin^2$ function the best. In particular, it can become negative to take care of negative Lorentz peaks.

The other parameters to describe the different pseudomodes are their decay rate, κ_k, and frequency, ω_k. The symmetries of the sine function allow us to choose the same κ for all pseudomodes: $\kappa_k = \kappa$. Additionally, the decay rate for the initial markovian decay before τ is needed, which will be called κ_0. The switch form ζ_k to d_k to name the pseudomodes (compared to section 3.3) is just done for better legibility. For the calculation of the pseudomode parameters, see section 3.3.

The results are presented in the rotating frame, using the transition $H \to U[H - i\partial_t]U^\dagger$ with the unitary transformation

$$U = \exp\left[i\left(\hbar\omega_0 c^\dagger c + \hbar \sum_k \omega_k d_k^\dagger d_k\right) t \right]. \tag{B.1}$$

The coupling to the external reservoir therefore becomes time-dependent,

$$G_k = \gamma e^{i(\omega_0-\omega_k)t}. \tag{B.2}$$

For the nonlinear reservoir modeling, let us introduce the following nonlinear functions:

$$\Omega \equiv \sum_k G_k D_k \frac{\langle c^\dagger d_k^\dagger cc\rangle^*}{\langle c^\dagger c^\dagger cc\rangle} \tag{B.3}$$

$$\Theta_k \equiv \sum_{k'} G_{k'}^* D_{k'} \frac{\langle d_k^\dagger d_{k'}^\dagger cc\rangle}{\langle c^\dagger c^\dagger cc\rangle} \tag{B.4}$$

Then the following equations of motion can be derived:

$$\partial_t\langle c^\dagger c\rangle = -2\kappa_0\langle c^\dagger c\rangle + \sum_k D_k\left(-iG_k^*\langle d_k^\dagger c\rangle + iG_k\langle d_k^\dagger c\rangle^*\right) \tag{B.5}$$

$$\partial_t\langle c^\dagger c^\dagger cc\rangle = -4\kappa_0\langle c^\dagger c^\dagger cc\rangle + \sum_k D_k\left(-2iG_k^*\langle c^\dagger d_k^\dagger cc\rangle + 2iG_k\langle c^\dagger d_k^\dagger cc\rangle^*\right) \tag{B.6}$$

$$\partial_t\langle d_k^\dagger c\rangle = -(\kappa_0+\kappa)\langle d_k^\dagger c\rangle - iG_k\langle c^\dagger c\rangle - 2i\chi\langle c^\dagger d_k^\dagger cc\rangle + \sum_{k'} iD_{k'}G_{k'}\langle d_k^\dagger d_{k'}\rangle \tag{B.7}$$

$$\begin{aligned}\partial_t\langle c^\dagger d_k^\dagger cc\rangle = &-(3\kappa_0+\kappa)\langle c^\dagger d_k^\dagger cc\rangle - iG_k\langle c^\dagger c^\dagger cc\rangle - 2i\chi\langle c^\dagger d_k^\dagger cc\rangle \\ &-\sum_{k'} D_{k'}\left(iG_{k'}^*\langle d_k^\dagger d_{k'}^\dagger cc\rangle + 2iG_{k'}\langle c^\dagger d_k^\dagger cd_{k'}\rangle\right)\end{aligned} \tag{B.8}$$

$$\partial_t\langle d_k^\dagger d_{k'}\rangle = -2\kappa\langle d_k^\dagger d_{k'}\rangle - iG_k\langle d_{k'}^\dagger c\rangle^* + iG_{k'}^*\langle d_k^\dagger c\rangle \tag{B.9}$$

$$\begin{aligned}\partial_t\langle c^\dagger d_k^\dagger cd_{k'}\rangle = &-(2\kappa_0+2\kappa)\langle c^\dagger d_k^\dagger cd_{k'}\rangle - iG_k\langle c^\dagger d_{k'}^\dagger cc\rangle^* + iG_{k'}^*\langle c^\dagger d_k^\dagger cc\rangle \\ &-i\Theta_k\langle c^\dagger d_{k'}^\dagger cc\rangle^* + i\Theta_{k'}^*\langle c^\dagger d_k^\dagger cc\rangle\end{aligned} \tag{B.10}$$

$$\begin{aligned}\partial_t\langle d_k^\dagger d_{k'}^\dagger cc\rangle = &-(2\kappa_0+2\kappa)\langle d_k^\dagger d_{k'}^\dagger cc\rangle - iG_k\langle c^\dagger d_{k'}^\dagger cc\rangle - iG_{k'}\langle c^\dagger d_k^\dagger cc\rangle \\ &-2i\chi\langle d_k^\dagger d_{k'}^\dagger cc\rangle + 2i\Omega\langle d_k^\dagger d_{k'}^\dagger cc\rangle\end{aligned} \tag{B.11}$$

This can also serve as a hands-on example on how to interpret the nonlinear method (section 3.1). One finds that Ω serves as an effective oscillation frequency, which only affects terms that have two annihilation (or two creation) operators of the d type. Θ_k, in contrast, looks like an additional coupling to the external modes. The numerical advantage of this approach is straightforward: Only terms with k and k' appear, so the number of terms scales quadratically with the number of external (pseudo-)modes. Without the nonlinear approach, it would scale with an exponent of 4. The approach however becomes numerically unstable as soon as $\langle c^\dagger c^\dagger cc\rangle$ becomes very small.

Bibliography

1. Weisstein, E. W. *Kelvin, Lord William Thomson* Eric Weisstein's World of Biography `http://scienceworld.wolfram.com/biography/Kelvin.html`. Retrieved 30.09.2014.
2. Hermann, A. *Frühgeschichte der Quantentheorie: 1899-1913.* (Physik-Verlag, Mosbach in Baden, Germany, 1969).
3. Planck, M. Ueber das Gesetz der Energieverteilung im Normalspectrum. *Annalen der Physik* **309,** 553–563 (1901).
4. Einstein, A. Über einen die Erzeugung und Verwandlung des Lichtes betreffenden heuristischen Gesichtspunkt. *Annalen der Physik* **322,** 132–148 (1905).
5. Schrödinger, E. Die gegenwärtige Situation in der Quantenmechanik. German. *Naturwissenschaften* **23,** 807–812 (1935).
6. Horodecki, R., Horodecki, P., Horodecki, M. & Horodecki, K. Quantum entanglement. *Rev. Mod. Phys.* **81,** 865–942 (2 June 2009).
7. Einstein, A., Podolsky, B. & Rosen, N. Can Quantum-Mechanical Description of Physical Reality Be Considered Complete? *Phys. Rev.* **47,** 777–780 (10 1935).
8. Bell, J. S. On the Einstein-Podolsky-Rosen paradox. *Physics* **1,** 195–200 (1964).
9. Freedman, S. J. & Clauser, J. F. Experimental Test of Local Hidden-Variable Theories. *Phys. Rev. Lett.* **28,** 938–941 (14 1972).
10. Aspect, A., Grangier, P. & Roger, G. Experimental Tests of Realistic Local Theories via Bell's Theorem. *Phys. Rev. Lett.* **47,** 460–463 (7 1981).
11. Tittel, W., Brendel, J., Gisin, B., *et al.* Experimental demonstration of quantum correlations over more than 10 km. *Phys. Rev. A* **57,** 3229–3232 (5 1998).
12. Jennewein, T., Simon, C., Weihs, G., Weinfurter, H. & Zeilinger, A. Quantum Cryptography with Entangled Photons. *Phys. Rev. Lett.* **84,** 4729–4732 (20 May 2000).
13. Gisin, N., Ribordy, G., Tittel, W. & Zbinden, H. Quantum cryptography. *Rev. Mod. Phys.* **74,** 145–195 (1 Mar. 2002).
14. Nielsen, M. & Chuang, I. *Quantum Computation and Quantum Information* (Cambridge University Press, 2000).
15. Kok, P., Munro, W. J., Nemoto, K., *et al.* Linear optical quantum computing with photonic qubits. *Rev. Mod. Phys.* **79,** 135–174 (1 Jan. 2007).
16. Kimble, H. J. The quantum internet. *Nature* **453,** 1023–1030 (June 2008).

17.Lloyd, S. Coherent quantum feedback. *Phys. Rev. A* **62,** 022108 (2 July 2000).

18.Bechhoefer, J. Feedback for physicists: A tutorial essay on control. *Rev. Mod. Phys.* **77,** 783–836 (3 Aug. 2005).

19.Pyragas, K. Continuous control of chaos by self-controlling feedback. *Physics Letters A* **170,** 421–428 (1992).

20.Pyragas, K. Analytical properties and optimization of time-delayed feedback control. *Phys. Rev. E* **66,** 026207 (2 Aug. 2002).

21.Von Loewenich, C., Benner, H. & Just, W. Experimental Relevance of Global Properties of Time-Delayed Feedback Control. *Phys. Rev. Lett.* **93,** 174101 (17 Oct. 2004).

22.Hövel, P. & Schöll, E. Control of unstable steady states by time-delayed feedback methods. *Phys. Rev. E* **72,** 046203 (4 Oct. 2005).

23.Yanchuk, S., Wolfrum, M., Hövel, P. & Schöll, E. Control of unstable steady states by long delay feedback. *Phys. Rev. E* **74,** 026201 (2 Aug. 2006).

24.Lang, R. & Kobayashi, K. External optical feedback effects on semiconductor injection laser properties. *Quantum Electronics, IEEE Journal of* **16,** 347–355 (1980).

25.*Unlocking Dynamical Diversity: Optical Feedback Effects on Semiconductor Lasers* (eds Kane, D. M. & Shore, K. A.) (Wiley VCH, Weinheim, 2005).

26.Levine, A. M., van Tartwijk, G. H. M., Lenstra, D. & Erneux, T. Diode lasers with optical feedback: Stability of the maximum gain mode. *Phys. Rev. A* **52,** R3436–R3439 (5 Nov. 1995).

27.Heil, T., Fischer, I., Elsäßer, W., *et al.* Delay dynamics of semiconductor lasers with short external cavities: Bifurcation scenarios and mechanisms. *Phys. Rev. E* **67,** 066214 (6 June 2003).

28.Globisch, B., Otto, C., Schöll, E. & Lüdge, K. Influence of carrier lifetimes on the dynamical behavior of quantum-dot lasers subject to optical feedback. *Phys. Rev. E* **86,** 046201 (4 Oct. 2012).

29.Soriano, M. C., García-Ojalvo, J., Mirasso, C. R. & Fischer, I. Complex photonics: Dynamics and applications of delay-coupled semiconductors lasers. *Rev. Mod. Phys.* **85,** 421–470 (1 Mar. 2013).

30.Albert, F., Hopfmann, C., Reitzenstein, S., *et al.* Observing chaos for quantum-dot microlasers with external feedback. *Nature Communications* **2,** 366 (June 2011).

31.Schöll, E., Hövel, P., Flunkert, V. & Dahlem, M. A. in *Complex Time-Delay Systems* (ed Atay, F. M.) 85–150 (Springer Berlin Heidelberg, 2010).

32.Wiseman, H. M. & Milburn, G. J. *Quantum measurement and control* (Cambridge University Press, 2009).

33.Brif, C., Chakrabarti, R. & Rabitz, H. Control of quantum phenomena: past, present and future. *New Journal of Physics* **12,** 075008 (2010).

34.Serafini, A. Feedback Control in Quantum Optics: An Overview of Experimental Breakthroughs and Areas of Application. *ISRN Optics* **2012,** 15 (2012).

35.Ahn, C., Doherty, A. C. & Landahl, A. J. Continuous quantum error correction via quantum feedback control. *Phys. Rev. A* **65,** 042301 (4 Mar. 2002).

36.Schaller, G. Fighting decoherence by feedback-controlled dissipation. *Phys. Rev. A* **85,** 062118 (6 June 2012).

37.Steck, D. A., Jacobs, K., Mabuchi, H., Bhattacharya, T. & Habib, S. Quantum Feedback Control of Atomic Motion in an Optical Cavity. *Phys. Rev. Lett.* **92,** 223004 (22 June 2004).

38.Yanagisawa, M. Quantum Feedback Control for Deterministic Entangled Photon Generation. *Phys. Rev. Lett.* **97,** 190201 (19 Nov. 2006).

39.Mancini, S. & Wiseman, H. M. Optimal control of entanglement via quantum feedback. *Phys. Rev. A* **75,** 012330 (1 Jan. 2007).

40.Vijay, R., Macklin, C., Slichter, D. H., *et al.* Stabilizing Rabi oscillations in a superconducting qubit using quantum feedback. *Nature* **490,** 77–80 (Oct. 2012).

41.Sayrin, C., Dotsenko, I., Zhou, X., *et al.* Real-time quantum feedback prepares and stabilizes photon number states. *Nature* **477,** 73–77 (Sept. 2011).

42.Yan, Z., Jia, X., Xie, C. & Peng, K. Coherent feedback control of multipartite quantum entanglement for optical fields. *Phys. Rev. A* **84,** 062304 (6 Dec. 2011).

43.Mabuchi, H. Coherent-feedback control strategy to suppress spontaneous switching in ultralow power optical bistability. *Applied Physics Letters* **98,** 193109 (2011).

44.Carmele, A., Kabuss, J., Schulze, F., Reitzenstein, S. & Knorr, A. Single Photon Delayed Feedback: A Way to Stabilize Intrinsic Quantum Cavity Electrodynamics. *Phys. Rev. Lett.* **110,** 013601 (1 Jan. 2013).

45.Schulze, F., Lingnau, B., Hein, S. M., *et al.* Feedback-induced steady-state light bunching above the lasing threshold. *Phys. Rev. A* **89,** 041801 (4 Apr. 2014).

46.Aron, C., Kulkarni, M. & Türeci, H. E. Steady-state entanglement of spatially separated qubits via quantum bath engineering. *Phys. Rev. A* **90,** 062305 (6 Dec. 2014).

47.Aron, C., Kulkarni, M. & Türeci, H. E. Photon-mediated interactions: a scalable tool to create and sustain entangled many-body states. eprint: `arxiv:1412.8477` (Dec. 2014).

48.Scully, M. O. & Zubairy, M. S. *Quantum Optics* (Cambridge University Press, Cambridge (England), 1997).

49.Shankar, R. *Principles of Quantum Mechanics, 2nd edition* (Springer-Verlag, Heidelberg, 2011).

50.Weinberg, S. Quantum mechanics without state vectors. *Phys. Rev. A* **90,** 042102 (4 Oct. 2014).

51.Eisert, J. & Plenio, M. B. A comparison of entanglement measures. *Journal of Modern Optics* **46,** 145–154 (1999).

52.Plenio, M. B. & Virmani, S. An introduction to entanglement measures. *Quant. Inf. Comp.* **7,** 001–051 (2007).

53.Bennett, C. H., Bernstein, H. J., Popescu, S. & Schumacher, B. Concentrating partial entanglement by local operations. *Phys. Rev. A* **53,** 2046–2052 (4 Apr. 1996).

54.Wootters, W. K. Entanglement of Formation of an Arbitrary State of Two Qubits. *Phys. Rev. Lett.* **80,** 2245–2248 (10 Mar. 1998).

55.Coffman, V., Kundu, J. & Wootters, W. K. Distributed entanglement. *Phys. Rev. A* **61,** 052306 (5 Apr. 2000).

56.Herreno-Fierro, C. & Luthra, J. R. Generalized concurrence and limits of separability for two qutrits. eprint: arxiv:quant-ph/0507223 (2007).

57.Jami, S. & Sarbishei, M. Degree of entanglement for qubit-qutrit state. eprint: arxiv:quant-ph/0606039 (2007).

58.Yu, T. & Eberly, J. H. Sudden Death of Entanglement. *Science* **323,** 598–601 (2009).

59.Hanbury Brown, R. & Twiss, R. Q. Correlation between photons in two coherent beams of light. *Nature* **177,** 27–29 (1956).

60.Carmichael, H. *An Open Systems Approach to Quantum Optics* (Springer Berlin Heidelberg, 1993).

61.Itano, W. M., Heinzen, D. J., Bollinger, J. J. & Wineland, D. J. Quantum Zeno effect. *Phys. Rev. A* **41,** 2295–2300 (5 Mar. 1990).

62.Maniscalco, S., Francica, F., Zaffino, R. L., Lo Gullo, N. & Plastina, F. Protecting Entanglement via the Quantum Zeno Effect. *Phys. Rev. Lett.* **100,** 090503 (9 Mar. 2008).

63.Mazzola, L., Maniscalco, S., Piilo, J., Suominen, K.-A. & Garraway, B. M. Sudden death and sudden birth of entanglement in common structured reservoirs. *Phys. Rev. A* **79,** 042302 (4 Apr. 2009).

64.Xu, J.-S., Li, C.-F., Gong, M., *et al.* Experimental Demonstration of Photonic Entanglement Collapse and Revival. *Phys. Rev. Lett.* **104,** 100502 (10 Mar. 2010).

65.An, J.-H., Yeo, Y., Zhang, W.-M. & Oh, C. H. Entanglement oscillation and survival induced by non-Markovian decoherence dynamics of the entangled squeezed state. *Journal of Physics A: Mathematical and Theoretical* **42,** 015302 (2009).

66.An, J.-H., Yeo, Y. & Oh, C. Exact decoherence dynamics of a single-mode optical field. *Annals of Physics* **324,** 1737–1746 (2009).

67.Dorner, U. & Zoller, P. Laser-driven atoms in half-cavities. *Phys. Rev. A* **66,** 023816 (2 Aug. 2002).

68.Eschner, J., Raab, C., Schmidt-Kaler, F. & Blatt, R. Light interference from single atoms and their mirror images. *Nature* **413,** 495–498 (Oct. 2001).

69.Hétet, G., Slodička, L., Hennrich, M. & Blatt, R. Single Atom as a Mirror of an Optical Cavity. *Phys. Rev. Lett.* **107,** 133002 (13 Sept. 2011).

70.Hétet, G., Slodička, L., Glätzle, A., Hennrich, M. & Blatt, R. QED with a spherical mirror. *Phys. Rev. A* **82,** 063812 (6 Dec. 2010).

71.Bradford, M. & Shen, J.-T. Spontaneous emission in cavity QED with a terminated waveguide. *Phys. Rev. A* **87,** 063830 (6 June 2013).

72.Fang, Y.-L. L. & Baranger, H. U. Waveguide QED: Power spectra and correlations of two photons scattered off multiple distant qubits and a mirror. *Phys. Rev. A* **91,** 053845 (5 May 2015).

73.Koshino, K. & Nakamura, Y. Control of the radiative level shift and linewidth of a superconducting artificial atom through a variable boundary condition. *New Journal of Physics* **14,** 043005 (2012).

74.Wiseman, H. M. Defining the (atom) laser. *Phys. Rev. A* **56,** 2068–2084 (3 Sept. 1997).

75.Naumann, N. L., Hein, S. M., Knorr, A. & Kabuss, J. Steady-state control in an unstable optomechanical system. *Phys. Rev. A* **90,** 043835 (4 Oct. 2014).

76.Schulze, F. *Quantized Description of Optical Feedback* PhD thesis (Technische Universität Berlin, 2014).

77.Grimsmo, A. L. Time-Delayed Quantum Feedback Control. *Phys. Rev. Lett.* **115,** 060402 (6 Aug. 2015).

78.Cerrillo, J. & Cao, J. Non-Markovian Dynamical Maps: Numerical Processing of Open Quantum Trajectories. *Phys. Rev. Lett.* **112,** 110401 (11 Mar. 2014).

79.Gardiner, C. & Zoller, P. *Quantum noise: a handbook of Markovian and non-Markovian quantum stochastic methods with applications to quantum optics* (Springer, 2004).

80.Piilo, J., Maniscalco, S., Härkönen, K. & Suominen, K.-A. Non-Markovian Quantum Jumps. *Phys. Rev. Lett.* **100,** 180402 (18 May 2008).

81.Piilo, J., Härkönen, K., Maniscalco, S. & Suominen, K.-A. Open system dynamics with non-Markovian quantum jumps. *Phys. Rev. A* **79,** 062112 (6 June 2009).

82.Kabuss, J., Krimer, D. O., Rotter, S., *et al. Analytical Study of Quantum Feedback Enhanced Rabi Oscillations* 2015. eprint: `arXiv:1503.05722`.

83.Gardiner, C. W. & Collett, M. J. Input and output in damped quantum systems: Quantum stochastic differential equations and the master equation. *Phys. Rev. A* **31,** 3761–3774 (6 June 1985).

84.Stenius, P. & Imamoglu, A. Stochastic wavefunction methods beyond the Born - Markov and rotating-wave approximations. *Quantum and Semiclassical Optics: Journal of the European Optical Society Part B* **8,** 283 (1996).

85.Garraway, B. M. Nonperturbative decay of an atomic system in a cavity. *Phys. Rev. A* **55,** 2290–2303 (3 Mar. 1997).

86.Dalton, B. J., Barnett, S. M. & Garraway, B. M. Theory of pseudomodes in quantum optical processes. *Phys. Rev. A* **64,** 053813 (5 Oct. 2001).

87.Dalton, B. & Garraway, B. Non-Markovian decay of a three-level cascade atom in a structured reservoir. *Phys. Rev. A* **68,** 033809 (3 Sept. 2003).

88.Barnett, S. & Radmore, P. Quantum theory of cavity quasimodes. *Optics Communications* **68,** 364–368 (1988).

89.Dalton, B. J., Barnett, S. M. & Knight, P. L. Quasi mode theory of macroscopic canonical quantization in quantum optics and cavity quantum electrodynamics. *Journal of Modern Optics* **46,** 1315–1341 (1999).

90.Mazzola, L., Maniscalco, S., Piilo, J., Suominen, K.-A. & Garraway, B. M. Pseudomodes as an effective description of memory: Non-Markovian dynamics of two-state systems in structured reservoirs. *Phys. Rev. A* **80,** 012104 (1 July 2009).

91.Hein, S. M., Schulze, F., Carmele, A. & Knorr, A. Entanglement control in quantum networks by quantum-coherent time-delayed feedback. *Phys. Rev. A* **91,** 052321 (5 May 2015).

92.Rempe, G. Quantum network with individual atoms and photons. *EPJ Web of Conferences* **57,** 03001 (2013).

93.Cirac, J. I., Zoller, P., Kimble, H. J. & Mabuchi, H. Quantum State Transfer and Entanglement Distribution among Distant Nodes in a Quantum Network. *Phys. Rev. Lett.* **78,** 3221–3224 (16 Apr. 1997).

94.Cho, J., Angelakis, D. G. & Bose, S. Heralded generation of entanglement with coupled cavities. *Phys. Rev. A* **78,** 022323 (2 Aug. 2008).

95.Wang, X. F. & Chen, G. Complex networks: small-world, scale-free and beyond. *Circuits and Systems Magazine, IEEE* **3,** 6–20 (2003).

96.Greentree, A. D., Tahan, C., Cole, J. H. & Hollenberg, L. C. L. Quantum phase transitions of light. *Nature Physics* **2,** 856–861 (Dec. 2006).

97.Almeida, G. M. A. & Souza, A. M. C. Quantum transport with coupled cavities on an Apollonian network. *Phys. Rev. A* **87,** 033804 (3 Mar. 2013).

98.Zanardi, P. & Rasetti, M. Noiseless Quantum Codes. *Phys. Rev. Lett.* **79,** 3306–3309 (17 Oct. 1997).

99.Del Valle, E., Laussy, F. P. & Tejedor, C. Electrostatic control of quantum dot entanglement induced by coupling to external reservoirs. *EPL (Europhysics Letters)* **80,** 57001 (2007).

100.Manzano, G., Galve, F., Giorgi, G. L., Hernández-García, E. & Zambrini, R. Synchronization, quantum correlations and entanglement in oscillator networks. *Sci. Rep.* **3,** 1–6 (Mar. 2013).

101.Vollbrecht, K. G. H., Muschik, C. A. & Cirac, J. I. Entanglement Distillation by Dissipation and Continuous Quantum Repeaters. *Phys. Rev. Lett.* **107,** 120502 (12 Sept. 2011).

102.Krauter, H., Muschik, C. A., Jensen, K., *et al.* Entanglement Generated by Dissipation and Steady State Entanglement of Two Macroscopic Objects. *Phys. Rev. Lett.* **107,** 080503 (8 Aug. 2011).

103.Huelga, S. F., Rivas, Á. & Plenio, M. B. Non-Markovianity-Assisted Steady State Entanglement. *Phys. Rev. Lett.* **108,** 160402 (16 Apr. 2012).

104.Kast, D. & Ankerhold, J. Bipartite entanglement dynamics of two-level systems in sub-Ohmic reservoirs. *Phys. Rev. B* **90,** 100301 (10 Sept. 2014).

105.O'Brien, D., Settle, M. D., Karle, T., *et al.* Coupled photonic crystalheterostructure nanocavities. *Opt. Express* **15,** 1228–1233 (Feb. 2007).

106.Chalcraft, A. R. A., Lam, S., Jones, B. D., *et al.* Mode structure of coupled L3 photonic crystal cavities. *Opt. Express* **19,** 5670–5675 (Mar. 2011).

107.Witzany, M., Liu, T.-L., Shim, J.-B., *et al.* Strong mode coupling in InP quantum dot-based GaInP microdisk cavity dimers. *New Journal of Physics* **15,** 013060 (2013).

108.Tufarelli, T., Ciccarello, F. & Kim, M. S. Dynamics of spontaneous emission in a single-end photonic waveguide. *Phys. Rev. A* **87,** 013820 (1 Jan. 2013).

109.Grimsmo, A., Parkins, A. & Skagerstam, B.-S. Rapid Steady State Convergence for Quantum Systems Using Time-Delayed Feedback Control. *New Journal of Physics* **16,** 065004 (2014).

110.Lounis, B. & Orrit, M. Single-photon sources. *Reports on Progress in Physics* **68,** 1129 (2005).

111.Oxborrow, M. & Sinclair, A. G. Single-photon sources. *Contemporary Physics* **46,** 173–206 (2005).

112.Michler, P., Kiraz, A., Becher, C., *et al.* A Quantum Dot Single-Photon Turnstile Device. *Science* **290,** 2282–2285 (2000).

113. *Single Semiconductor Quantum Dots* (ed Michler, P.) 197–200 (Springer, New York, 2009).

114. Peaudecerf, B., Sayrin, C., Zhou, X., *et al.* Quantum feedback experiments stabilizing Fock states of light in a cavity. *Phys. Rev. A* **87,** 042320 (4 Apr. 2013).

115. Walls, D. & Milburn, G. *Quantum Optics* (Springer Berlin Heidelberg, 2008).

116. Kirchmair, G., Vlastakis, B., Leghtas, Z., *et al.* Observation of quantum state collapse and revival due to the single-photon Kerr effect. *Nature* **495.** 10.1038/nature11902, 205–209 (Mar. 2013).

117. Hein, S. M., Schulze, F., Carmele, A. & Knorr, A. Optical Feedback-Enhanced Photon Entanglement from a Biexciton Cascade. *Phys. Rev. Lett.* **113,** 027401 (2 July 2014).

118. Hein, S. M., Schulze, F., Naumann, N. L., Carmele, A. & Knorr, A. *Feedback-Enhanced Entanglement of Photons from a Biexciton Cascade* in *CLEO: QELS_Fundamental Science* (2014), FF1A–8.

119. Hein, S. M., Schulze, F., Carmele, A. & Knorr, A. *Photon pairs from a biexciton cascade with feedback-controlled polarization entanglement* in *SPIE OPTO* (2015), 93570W–93570W.

120. Edamatsu, K. Entangled Photons: Generation, Observation, and Characterization. *Jpn. J. Appl. Phys* **46,** 7175–7187 (2007).

121. Ekert, A. K. Quantum cryptography based on Bell's theorem. *Phys. Rev. Lett.* **67,** 661–663 (6 Aug. 1991).

122. Zhang, Z., Tengner, M., Zhong, T., Wong, F. N. C. & Shapiro, J. H. Entanglement's Benefit Survives an Entanglement-Breaking Channel. *Phys. Rev. Lett.* **111,** 010501 (1 July 2013).

123. Kwiat, P. G., Mattle, K., Weinfurter, H., *et al.* New High-Intensity Source of Polarization-Entangled Photon Pairs. *Phys. Rev. Lett.* **75,** 4337–4341 (24 Dec. 1995).

124. Benson, O., Santori, C., Pelton, M. & Yamamoto, Y. Regulated and Entangled Photons from a Single Quantum Dot. *Phys. Rev. Lett.* **84,** 2513–2516 (11 Mar. 2000).

125. Gywat, O., Burkard, G. & Loss, D. Biexcitons in coupled quantum dots as a source of entangled photons. *Phys. Rev. B* **65,** 205329 (20 May 2002).

126. Fattal, D., Inoue, K., Vučković, J., *et al.* Entanglement Formation and Violation of Bell's Inequality with a Semiconductor Single Photon Source. *Phys. Rev. Lett.* **92,** 037903 (3 Jan. 2004).

127. Stevenson, R. M., Young, R. J., Atkinson, P., *et al.* A semiconductor source of triggered entangled photon pairs. *Nature* **439,** 179–182 (Jan. 2006).

128. Callsen, G., Carmele, A., Hönig, G., *et al.* Steering photon statistics in single quantum dots: From one- to two-photon emission. *Phys. Rev. B* **87,** 245314 (24 June 2013).

129. Gammon, D., Snow, E. S., Shanabrook, B. V., Katzer, D. S. & Park, D. Fine Structure Splitting in the Optical Spectra of Single GaAs Quantum Dots. *Phys. Rev. Lett.* **76,** 3005–3008 (16 Apr. 1996).

130. Hafenbrak, R., Ulrich, S. M., Michler, P., *et al.* Triggered polarization-entangled photon pairs from a single quantum dot up to 30K. *New Journal of Physics* **9,** 315 (2007).

131. Ellis, D. J. P., Stevenson, R. M., Young, R. J., *et al.* Control of fine-structure splitting of individual InAs quantum dots by rapid thermal annealing. *Applied Physics Letters* **90,** 011907 (2007).

132.Stock, E., Warming, T., Ostapenko, I., *et al.* Single-photon emission from InGaAs quantum dots grown on (111) GaAs. *Applied Physics Letters* **96,** 093112 (2010).

133.Wang, J., Gong, M., Guo, G.-C. & He, L. Eliminating the fine structure splitting of excitons in self-assembled InAs/GaAs quantum dots via combined stresses. *Applied Physics Letters* **101,** 063114 (2012).

134.Gerardot, B. D., Seidl, S., Dalgarno, P. A., *et al.* Manipulating exciton fine structure in quantum dots with a lateral electric field. *Applied Physics Letters* **90,** 041101 (2007).

135.Stevenson, R. M., Hudson, A. J., Bennett, A. J., *et al.* Evolution of Entanglement Between Distinguishable Light States. *Phys. Rev. Lett.* **101,** 170501 (17 Oct. 2008).

136.Akopian, N., Lindner, N. H., Poem, E., *et al.* Entangled Photon Pairs from Semiconductor Quantum Dots. *Phys. Rev. Lett.* **96,** 130501 (13 Apr. 2006).

137.Avron, J. E., Bisker, G., Gershoni, D., *et al.* Entanglement on Demand through Time Reordering. *Phys. Rev. Lett.* **100,** 120501 (12 Mar. 2008).

138.Troiani, F. & Tejedor, C. Entangled photon pairs from a quantum-dot cascade decay: The effect of time reordering. *Phys. Rev. B* **78,** 155305 (15 Oct. 2008).

139.Seliger, M., Hohenester, U. & Pfanner, G. Entangled photons from quantum dot devices: efficiency of post-selection. *physica status solidi (b)* **246,** 289–292 (2009).

140.Pathak, P. K. & Hughes, S. Cavity-assisted fast generation of entangled photon pairs through the biexciton-exciton cascade. *Phys. Rev. B* **80,** 155325 (15 Oct. 2009).

141.Pathak, P. K. & Hughes, S. Generation of entangled photon pairs from a single quantum dot embedded in a planar photonic-crystal cavity. *Phys. Rev. B* **79,** 205416 (20 May 2009).

142.Stace, T. M., Milburn, G. J. & Barnes, C. H. W. Entangled two-photon source using biexciton emission of an asymmetric quantum dot in a cavity. *Phys. Rev. B* **67,** 085317 (8 Feb. 2003).

143.Troiani, F., Perea, J. I. & Tejedor, C. Cavity-assisted generation of entangled photon pairs by a quantum-dot cascade decay. *Phys. Rev. B* **74,** 235310 (23 Dec. 2006).

144.Carmele, A. & Knorr, A. Analytical solution of the quantum-state tomography of the biexciton cascade in semiconductor quantum dots: Pure dephasing does not affect entanglement. *Phys. Rev. B* **84,** 075328 (7 Aug. 2011).

145.Dousse, A., Suffczynski, J., Beveratos, A., *et al.* Ultrabright source of entangled photon pairs. *Nature* **466,** 217–220 (July 2010).

146.Johne, R., Gippius, N. A. & Malpuech, G. Entangled photons from a strongly coupled quantum dot-cavity system. *Phys. Rev. B* **79,** 155317 (15 Apr. 2009).

147.Schumacher, S., Förstner, J., Zrenner, A., *et al.* Cavity-assisted emission of polarization-entangled photons from biexcitons in quantum dots with fine-structure splitting. *Opt. Express* **20,** 5335–5342 (Feb. 2012).

148.Hoi, I. C., Kockum, A. F., Tornberg, L., *et al.* Probing the quantum vacuum with an artificial atom in front of a mirror. arXiv: 1410.8840 (2014).

149.Hoi, I.-C., Kockum, A. F., Tornberg, L., *et al.* Probing the quantum vacuum with an artificial atom in front of a mirror. *Nat. Phys.* **(advance online publication)** (Sept. 2015).

150.Rodt, S., Heitz, R., Schliwa, A., *et al.* Repulsive exciton-exciton interaction in quantum dots. *Phys. Rev. B* **68,** 035331 (3 July 2003).

151.Hudson, A. J., Stevenson, R. M., Bennett, A. J., *et al.* Coherence of an Entangled Exciton-Photon State. *Phys. Rev. Lett.* **99,** 266802 (26 Dec. 2007).

152.Carmele, A., Milde, F., Dachner, M.-R., *et al.* Formation dynamics of an entangled photon pair: A temperature-dependent analysis. *Phys. Rev. B* **81,** 195319 (19 May 2010).

153.Hohenester, U., Pfanner, G. & Seliger, M. Phonon-Assisted Decoherence in the Production of Polarization-Entangled Photons in a Single Semiconductor Quantum Dot. *Phys. Rev. Lett.* **99,** 047402 (4 July 2007).

154.Mitra, A. & Vyas, R. Entanglement and bistability in coupled quantum dots inside a driven cavity. *Phys. Rev. A* **81,** 012329 (1 Jan. 2010).

155.Shiau, H.-H., Mitra, A. & Vyas, R. Time evolution of entanglement and bistability of two coupled quantum dots in a driven cavity. *Journal of Modern Optics* **60,** 1273–1280 (2013).

156.Savage, C. M. & Carmichael, H. J. Single atom optical bistability. *Quantum Electronics, IEEE Journal of* **24,** 1495–1498 (1988).

157.Schwartz, M. E., Martin, L., Aron, C., *et al. Toward Resource-Efficient Deterministic Entanglement in 3D Superconducting Qubits* in *APS Meeting Abstracts* (Mar. 2015), 39008.

158.Zurek, W. H. Decoherence, einselection, and the quantum origins of the classical. *Rev. Mod. Phys.* **75,** 715–775 (3 May 2003).

159.Blais, A., Huang, R.-S., Wallraff, A., Girvin, S. M. & Schoelkopf, R. J. Cavity quantum electrodynamics for superconducting electrical circuits: An architecture for quantum computation. *Phys. Rev. A* **69,** 062320 (6 June 2004).

160.You, J. Q. & Nori, F. Atomic physics and quantum optics using superconducting circuits. *Nature* **474.** 10.1038/nature10122, 589–597 (June 2011).

161.Governale, M., Grifoni, M. & Schön, G. Decoherence and dephasing in coupled Josephson-junction qubits. *Chemical Physics* **268,** 273–283 (2001).

162.Shnirman, A., Makhlin, Y. & Schön, G. Noise and decoherence in quantum two-level systems. *Physica Scripta* **2002,** 147 (2002).

163.Dür, W., Vidal, G. & Cirac, J. I. Three qubits can be entangled in two inequivalent ways. *Phys. Rev. A* **62,** 062314 (6 Nov. 2000).

164.Bouwmeester, D., Pan, J.-W., Daniell, M., Weinfurter, H. & Zeilinger, A. Observation of Three-Photon Greenberger-Horne-Zeilinger Entanglement. *Phys. Rev. Lett.* **82,** 1345–1349 (7 Feb. 1999).

165.Purcell, E. M. Spontaneous Emission Probabilities at Radio Frequencies, in: Proceedings of the American Physical Society. *Phys. Rev.* **69,** 674–674 (11-12 June 1946).